

# Local Vulnerabilities and Global Robustness of Coupled Dynamical Systems on Complex Networks

Présentée le 6 février 2020

à la Faculté des sciences de base  
Chaire de théorie de la matière condensée  
Programme doctoral en physique

pour l'obtention du grade de Docteur ès Sciences

par

**Melvyn Sandy TYLOO**

Acceptée sur proposition du jury

Prof. H. M. Rønnow, président du jury  
Prof. F. Mila, Prof. Ph. Jacquod, directeurs de thèse  
Prof. M. Barahona, rapporteur  
Prof. E. Mallada, rapporteur  
Prof. P. De Los Rios, rapporteur



*Veni, vidi, vici.*  
— Julius Caesar 47 BC.

*À ma mère et ma grand-mère.*



# Abstract

Coupled dynamical systems are omnipresent in everyday life. In general, interactions between individual elements composing the system are captured by complex networks. The latter greatly impact the way coupled systems are functioning and evolving in time. An important task in such a context, is to identify the most fragile components of a system in a fast and efficient manner. It is also highly desirable to have bounds on the amplitude and duration of perturbations that could potentially drive the system through a transition from one equilibrium to another. A paradigmatic model of coupled dynamical system is that of oscillatory networks. In these systems, a phenomenon known as *synchronization* where the individual elements start to behave coherently may occur if couplings are strong enough. We propose frameworks to assess vulnerabilities of such synchronous states to external perturbations. We consider transient excursions for both small-signal response and larger perturbations that can potentially drive the system out of its initial basin of attraction.

In the first part of this thesis, we investigate the robustness of complex network-coupled oscillators. We consider transient excursions following external perturbations. For ensemble averaged perturbations, quite remarkably we find that robustness of a network is given by a family of network descriptors that we called *generalized Kirchhoff indices* and which are defined from extensions of the resistance distance to arbitrary powers of the Laplacian matrix of the system. These indices allow an efficient and accurate assessment of the overall vulnerability of an oscillatory network and can be used to compare robustness of different networks. Moreover, a network can be made more robust by minimizing its Kirchhoff indices. Then for specific local perturbations, we show that local vulnerabilities are captured by *generalized resistance centralities* also defined from extensions of the resistance distance. Most fragile nodes are therefore identified as the least central according to resistance centralities. Based on the latter, rankings of the nodes from most to least vulnerable can be established. In summary, we find that both local vulnerabilities and global robustness are accurately evaluated with resistance centralities and Kirchhoff indices. Moreover, the framework that we define is rather general and may be useful to analyze other coupled dynamical systems.

In the second part, we focus on the effect of larger perturbations that eventually lead the system to an escape from its initial basin of attraction. We consider coupled oscillators subjected to noise with various amplitudes and correlation in time. To predict desynchronization and transitions between synchronous states, we propose a simple heuristic criterion based on the distance between the initial stable fixed point and the closest saddle point. Surprisingly, we find numerically that our criterion leads to rather accurate estimates for the survival proba-

## Abstract

---

bility and first escape time. Our criterion is general and may be applied to other dynamical systems.

**Keywords:** *coupled dynamical systems, complex networks, centralities, indices, robustness, vulnerability, key players problem, coupled oscillators, synchronization, transient dynamics, linear response theory, escape of the basin of attraction.*

# Résumé

Les systèmes dynamiques couplés sur des réseaux complexes sont omniprésents dans la vie de tous les jours. En général, les interactions entre les éléments individuels composant le système sont modélisées par des réseaux complexes. Ces derniers ont un impact important sur la façon de fonctionner et l'évolution temporelle des systèmes couplés. Dans ce contexte, une question importante est comment peut-on identifier la composante la plus fragile d'un système d'une manière efficace et rapide. Il est aussi souhaitable d'avoir des bornes sur l'amplitude et la durée de perturbations qui pourraient éventuellement conduire le système à une transition d'un équilibre à un autre. Un modèle emblématique de système dynamique couplé est celui des réseaux oscillants. Dans ces systèmes, il existe un phénomène appelé *synchronisation* où les éléments individuels commencent à évoluer de manière cohérente si les couplages sont suffisamment forts. Nous proposons des méthodes pour évaluer les vulnérabilités de tels états synchrones face à des perturbations externes. Nous considérons le transient induit par des perturbations faibles mais aussi des perturbations plus importantes qui peuvent potentiellement amener le système en-dehors de son bassin d'attraction initial.

Dans la première partie de cette thèse, nous investiguons la robustesse d'oscillateurs couplés sur des réseaux complexes. Nous considérons le transient suivant des perturbations externes. Pour des perturbations moyennées sur des ensembles, nous trouvons de manière remarquable que la robustesse d'un réseau est décrite par une famille d'indices de réseaux que nous appelons *indices de Kirchhoff généralisés* et qui sont obtenus à partir d'extensions de la distance résistive aux puissances de la matrice Laplacienne du système. Ces indices permettent une évaluation efficace et précise de la vulnérabilité globale d'un réseau d'oscillateurs et peuvent être utilisés pour comparer la robustesse de différents réseaux. De plus, un réseau peut être rendu plus robuste en minimisant ses indices de Kirchhoff généralisés. Ensuite pour des perturbations spécifiques locales, nous montrons que les vulnérabilités locales sont expliquées par des *centralités résistives généralisées* aussi définies à partir d'extensions de la distance résistive. Les noeuds les plus fragiles sont par conséquent identifiés comme les moins centraux par rapport aux centralités résistives. En utilisant ces dernières, des classements des noeuds du plus au moins vulnérables peuvent être établis. En résumé, nous trouvons qu'à la fois les vulnérabilités locales et la robustesse globale sont précisément évaluées à l'aide des centralités résistives et des indices de Kirchhoff. Les méthodes que nous proposons sont générales et peuvent donc être utiles pour l'analyse d'autres systèmes dynamiques couplés.

Dans la deuxième partie, nous nous concentrons sur l'effet de perturbations plus importantes qui mènent finalement le système à une sortie de son bassin d'attraction initial. Nous

## Résumé

---

considérons des oscillateurs couplés soumis à du bruit avec différents amplitude et temps de corrélation. Pour prédire la désynchronisation et les transitions entre états synchrones, nous proposons un critère heuristique simple basé sur la distance entre le point fixe stable initial et le point de selle le plus proche. Étonnamment, nous trouvons numériquement que notre critère permet des évaluations précises de la probabilité de survie ainsi que du temps de première sortie. Notre critère est formulé de manière générale et peut donc être appliqué à d'autres systèmes dynamiques.

**Mots clés :** *systèmes dynamiques couplés, réseaux complexes, centralités, indices, robustesse, vulnérabilité, problème des key players, oscillateurs couplés, synchronisation, dynamique du transient, théorie de la réponse linéaire, sortie du bassin d'attraction.*

# Contents

<b>Abstract (English/Français)</b>	<b>i</b>
<b>General Introduction</b>	<b>1</b>
<b>1 Preliminaries</b>	<b>9</b>
1.1 A survey about complex networks . . . . .	9
1.1.1 Laplacian . . . . .	10
1.1.2 Centralities and indices . . . . .	11
1.2 Coupled oscillators and related models . . . . .	15
1.2.1 Kuramoto oscillators . . . . .	15
1.2.2 Linear oscillators . . . . .	17
1.3 Linear response theory . . . . .	18
<b>2 Robustness of Synchrony in Complex Networks and Generalized Kirchhoff Indices</b>	<b>21</b>
2.1 Introduction . . . . .	22
2.2 Model and method . . . . .	23
2.3 Generalized Kirchhoff indices. . . . .	24
2.4 Dirac delta perturbation . . . . .	25
2.5 Box perturbation . . . . .	26
2.6 Noisy perturbation . . . . .	26
2.7 Numerical simulations . . . . .	27
2.8 Conclusion . . . . .	28
2.9 Appendix . . . . .	30
2.9.1 Generalized Kirchhoff indices . . . . .	30
2.9.2 Direct calculation of fragility measures . . . . .	31
2.9.3 Dirac delta perturbation . . . . .	31
2.9.4 Box perturbation . . . . .	32
2.9.5 Noisy perturbation . . . . .	32
2.9.6 Perturbations as Fourier series . . . . .	34
2.9.7 Kirchhoff indices and phase dynamics . . . . .	35
2.9.8 Beyond Kuramoto . . . . .	39
<b>3 Global Robustness vs. Local Vulnerabilities in Complex Synchronous Networks</b>	<b>41</b>
3.1 Introduction . . . . .	42

## Contents

---

3.2	Resistance Distances, Centralities and Kirchhoff Indices . . . . .	43
3.3	Synchronized oscillators under external perturbations . . . . .	45
3.3.1	The Kuramoto model with inertia and its linearization . . . . .	45
3.3.2	Performance Measures . . . . .	47
3.3.3	Quench Perturbation . . . . .	49
3.3.4	Specific Local Vulnerabilities . . . . .	50
3.3.5	Averaged Global Robustness . . . . .	51
3.4	Numerical Results . . . . .	52
3.4.1	Local Vulnerabilities and Resistance Centralities . . . . .	52
3.4.2	Global Robustness and Generalized Kirchhoff Indices . . . . .	58
3.4.3	Generalized Kirchhoff Indices in Small-World Networks . . . . .	58
3.4.4	Regular Networks . . . . .	60
3.5	Conclusion . . . . .	60
<b>4</b>	<b>The Key Player Problem in Complex Oscillator Networks and Electric Power Grids: Resistance Centralities Identify Local Vulnerabilities</b>	<b>63</b>
4.1	Introduction . . . . .	64
4.2	Results . . . . .	67
4.3	Discussion . . . . .	71
4.4	Conclusion . . . . .	77
4.5	Appendix . . . . .	80
4.5.1	Calculation of the Performance Measures . . . . .	80
4.5.2	Resistance Distances, Centralities and Kirchhoff Indices . . . . .	84
4.5.3	Numerical Comparison of LRank with WLRank . . . . .	85
<b>5</b>	<b>Noise-Induced Desynchronization and Stochastic Escape from Equilibrium in Com- plex Networks</b>	<b>87</b>
5.1	Introduction . . . . .	88
5.2	The Model . . . . .	90
5.3	Escape from the basin . . . . .	91
5.4	Numerical simulations . . . . .	92
5.5	Conclusion . . . . .	96
5.6	Appendix . . . . .	96
5.6.1	Details of Calculations for the variance of the angle displacements . . . . .	96
5.6.2	Method to determine escape times . . . . .	97
5.6.3	The four networks . . . . .	98
5.6.4	Finding 1-saddles . . . . .	101
5.6.5	Linearization Breakdown . . . . .	104
<b>6</b>	<b>Overall Conclusion and Outlook</b>	<b>105</b>
	<b>Acknowledgements</b>	<b>107</b>

<b>Bibliography</b>	<b>109</b>
<b>Curriculum Vitae</b>	<b>119</b>



# General Introduction

Coupled dynamical systems are widely used to model natural and man-made systems. Such realizations range from the prey-predator interaction of different species evolving in the same environment [58, 65], fireflies flashing together in unison [43] or individuals exchanging opinion on social networks [32], to quantum phase dynamics of superconducting islands connected by Josephson junctions [127, 64], interacting molecules leading to preferential proteins folding [15] and voltage phase dynamics of electrical power grids [13]. All these systems are made of individual elements with their own internal dynamics. The coupling between individual units is described by a network that may be regular or complex in structure, temporal or static during the interactions. Even for individual dynamics that are rather simple taken independently, various rich collective behaviors emerge from the coupling network's geometry and topology.

In this context, there is an ubiquitous phenomenon where every elements start to behave coherently known as *synchronization* [77]. Such collective motion occurs for example in electrical grids when all synchronous machines rotate at the same frequency [76] or in Josephson junctions arrays where quantum phases of each superconducting island synchronize with some permanent Josephson currents circulating between them [127]. Stability as well as transient dynamics of synchrony within noisy environment, faults or perturbations in the internal parameters greatly depend on the interaction network, namely how strong and how structured is the coupling. This is still true in opinion formation on social networks [97] or vehicular platoons [96, 54] moving along together for which similar collective behavior known as *consensus* may occur.

Robustness of synchronous states can be investigated from various perspectives. One could evaluate the size of their basin of attraction [128, 35] to estimate the range of initial conditions that lead to synchronous states, or assess first escape time and transitions between synchronous states due to noisy environment [38, 107, 108, 60, 122, 62]. From another point of view, one could consider transient dynamics induced by perturbations in the internal parameters of individual elements close to an initial stationary state [7, 54, 102, 93, 110] or changes in the structure of the coupling network [27, 30, 113, 29, 37]. All the above stability features are greatly impacted not only by the internal parameters of each individual elements but also by the way the latter interact with each other. For example, the same perturbation applied on two individual elements having very different connectivities or centralities will

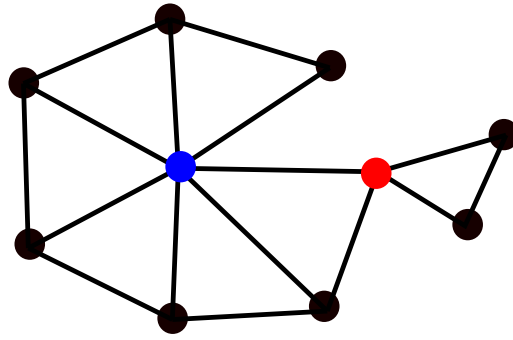


Figure 1 – Illustration of a complex network. The blue node is the most connected while the red one can potentially separate the network into two pieces if removed.

most probably lead to severally distinct responses of the overall coupled system.

In general, analyses shedding light on the interplay between coupled dynamics and network structure are highly desirable. Most of time it is a hard problem that leads to highly non trivial dependencies on the coupling network. Over the last decades, complex networks have witnessed an increasing interest. They have been investigated as dynamical systems on their own for example with preferential attachment algorithms [25] or as static objects. In that latter case, a question that has attracted much attention is that of the *key players* problem [5, 19, 112, 88]. These key players may be elements of the network which, once removed, lead to the biggest changes in the network according to some specific features. For example, in the network shown in Fig. 1, if one is interested in separating the network into two independent pieces, then the red node should be removed and is thus the key player. But if one wants to remove the most connected element, then the blue one is the key player. To identify such nodes, graph theoretic centralities have been defined mostly based solely on the network structure or considering random processes [16]. However, coupled dynamical systems are not random processes but deterministic systems satisfying physical conservation laws. For such systems, key players may be elements that, once removed, impact the stability at most, or once perturbed, drive the system through the largest transient excursion from its stationary state. That latter case is illustrated in Fig. 2, where Kuramoto oscillators [see Eq. (1.18)] coupled on the complex network shown in inset are taken at a stationary state. Then one applies the same perturbation on two different oscillators (red nodes). Even if both oscillators have the same number of neighbors, i.e. same degree, the responses of the system are quite different. In bottom panel, oscillators' angles spread more and need more time to return to the initial stationary state after the perturbation compared to top panel. It is an appealing avenue to try to predict such distinct responses using formerly defined centralities. But how to choose the correct one? Obviously one could try to relate numerically graph theoretic metrics to dynamical responses. However following this procedure and assuming it succeeds, one does not have any insights about the intrinsic connections between the considered metric and the dynamical system. One may therefore miss some dependencies especially on the dynamical parameters of the system [19, 16, 63].

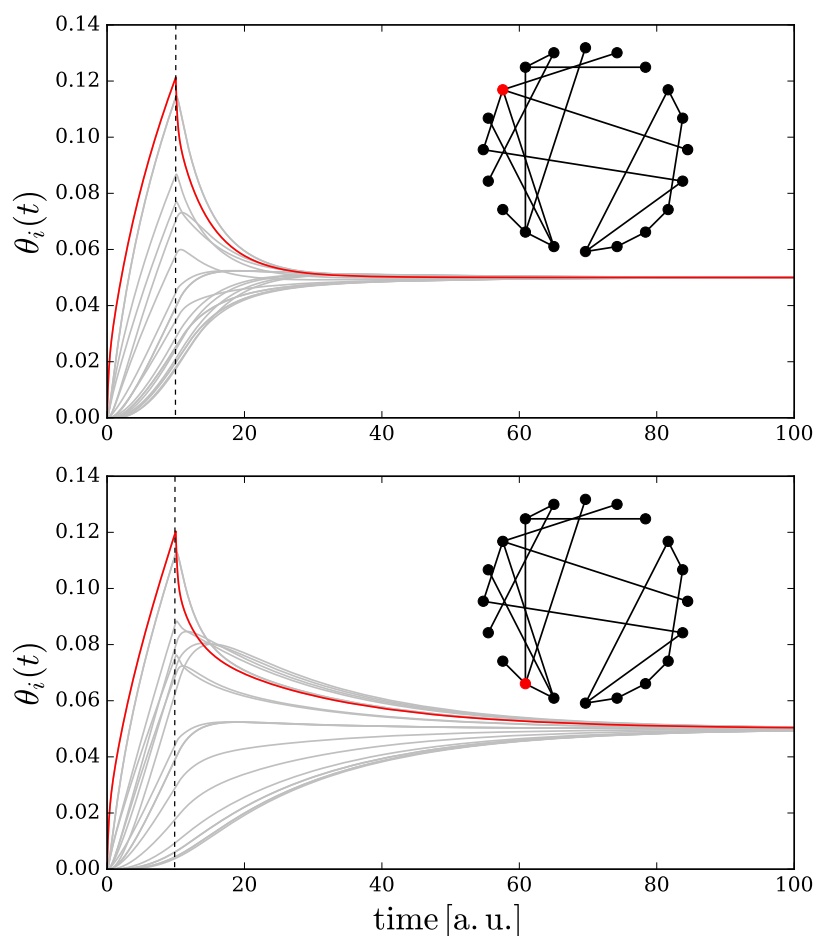


Figure 2 – Comparison between oscillators' response following a perturbation in the natural frequency of oscillators highlighted in red (with corresponding trajectories in red) that starts at 0 and ends at dashed lines. Both nodes in red have the same degree, however the responses are very different.

Indeed, the two very different behaviors shown in Fig. 2 may be non trivial functions of the local connectivities of the perturbed elements, of the global structure of the coupling network and of the spatial distributions of the dynamical parameters of the oscillators. Some effects of the dynamical parameters are illustrated in Fig. 3 where the time-evolution of the winding number  $q$  is recorded for oscillators subjected to noise and coupled on a cyclic network. Different values of  $q$  correspond to different synchronous state. One clearly sees that first escape time and the frequency of transitions between fixed points are functions of the correlation time of the noise and the dynamical parameters of the oscillators, namely in this case their inertia (see caption of Fig. 3).

It is thus often a complicated task to connect analytically dynamics of coupled systems to intuitive features of the coupling network. Related questions about the interplay between complex networks and coupled dynamical systems have attracted an increasing interest over the last

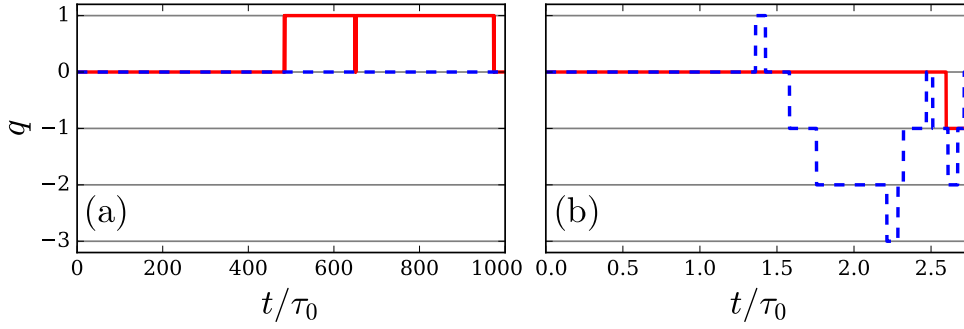


Figure 3 – Time-evolution of the winding number  $q$  of coupled oscillators on a cyclic network subject to noise in their internal parameters, namely their natural frequencies. Different values of  $q$  indicate different stable fixed points. Solid red lines correspond to inertialess oscillators while dashed blue lines correspond to oscillators with inertia. From panel (a) to (b), the correlation time  $\tau_0$  of the noise is increased.

decades that paved the way to some well-known results. Among them for example the relation between epidemic threshold and degree distribution [95], diffusion on complex networks and communicability [44] and synchronizability of oscillators and small-worldness [10].

## Research Objectives

As presented in the introduction, coupled dynamical systems on complex network impact various fields of research. For most of them, a rather simple and central question is how robust are such systems to external perturbations. In particular, this is a relevant question for complex oscillatory networks. These coupled systems are characterized by synchronous states where every elements evolve coherently at the same frequency. Many results on coupled oscillators focused on the synchronizability of different network topologies and the range of initial conditions or internal parameters allowing such synchronization. Properties of synchrony can be investigated from various angles. For example, synchronization can be optimal from its linear stability [99], the range of oscillators parameters that allows synchronization [10, 26, 132], the size of the basin of attraction around stable fixed points [128, 35], desynchronization and transitions between synchronous states that may occur due to noise [38, 60, 107] or how disturbances spread across the network [69, 129]. Here we propose to investigate robustness from the reaction of the system to external perturbations. As illustrated in Fig. 2, the response of coupled oscillators obviously depends on which element is attacked. However the different behaviors observed in Fig. 2 seem non trivially intricate with the network structure as simple local properties like the degree fails to predict such distinct responses. Moreover, inhomogeneities in the internal parameters of individual elements may also play a role and affect the system's response. In this context, a central task is to determine the implications of each system's component in the final response. In particular, two questions of prime importance arise: (i) how to identify the most vulnerable components of a coupled system and (ii) how the overall stability of the system relates to the structure of the coupling network. Answers to these

questions may have many potential applications. For example, in an electrical power network, which edge should be added to improve the global robustness of the synchronous states or in a social network which agent has the greatest influence on the general opinion. The resulting network description should provide an efficient and intuitive framework to understand how an initial input perturbation is related to an output response.

## Main Contributions

We first considered small-signal response of complex network-coupled oscillators. More precisely, we investigated transient regimes following perturbations that leave the dynamics close to the initial stable fixed point. Quite surprisingly, we found that the global robustness is captured by a family of new network indices which we called *generalized Kirchhoff indices*  $Kf_p$ . They provide an accurate and efficient assessment of the robustness of synchronous networks against ensemble averaged perturbations. Moreover they are easily obtained from the eigenvalues of the Laplacian of the coupling network weighted by angles differences at the initial fixed point. Interestingly generalized Kirchhoff indices can be interpreted as the sum of all *generalized resistance distances*  $\Omega_{ij}^{(p)}$  in the network as,

$$Kf_p = \sum_{i < j} \Omega_{ij}^{(p)}. \quad (1)$$

Resistance distances  $\Omega_{ij}^{(p)}$  are complex network distances. In particular for  $p = 1$ , one recovers the resistance distance originally defined in Ref. [71]. Then  $\Omega_{ij}^{(1)}$  has an intuitive meaning. It corresponds to the effective resistance between node  $i$  and  $j$  in a new network where one puts a resistor on each edge with resistance given by the inverse of the edge weight in the original network. Therefore resistance distance account for all existing path between two nodes. Interestingly, we found that, to improve the global robustness of coupled oscillators, one should minimize resistance distances, and thus minimize generalized Kirchhoff indices Eq. (1). The latter are non trivial functions of the coupling network and allow an accurate evaluation of network robustness as shown in Fig. 4 where  $Kf_1$  and  $Kf_2$  are calculated for cyclic networks with nearest and  $q^{\text{th}}$ - neighbors coupling. For example, even if networks with  $q = 17$  and  $q = 18$  may look similar, their Kirchhoff indices and thus their robustness are quite different. In summary, robustness of different networks can be compared through their set of Kirchoff indices. Then we found that local vulnerabilities are directly connected to combinations of  $Kf_p$ 's and new centralities that we called *generalized resistance centralities*,  $C_p(i)$ . The latter are straightforwardly defined as closeness centralities from resistance distances as,

$$C_p(i) = \left[ n^{-1} \sum_j \Omega_{ij}^{(p)} \right]^{-1}. \quad (2)$$

Quite remarkably, most fragile nodes within a network are identified as least central ones according to resistance centralities. As an example, Fig. 5 shows resistance centralities  $C_1(i)$

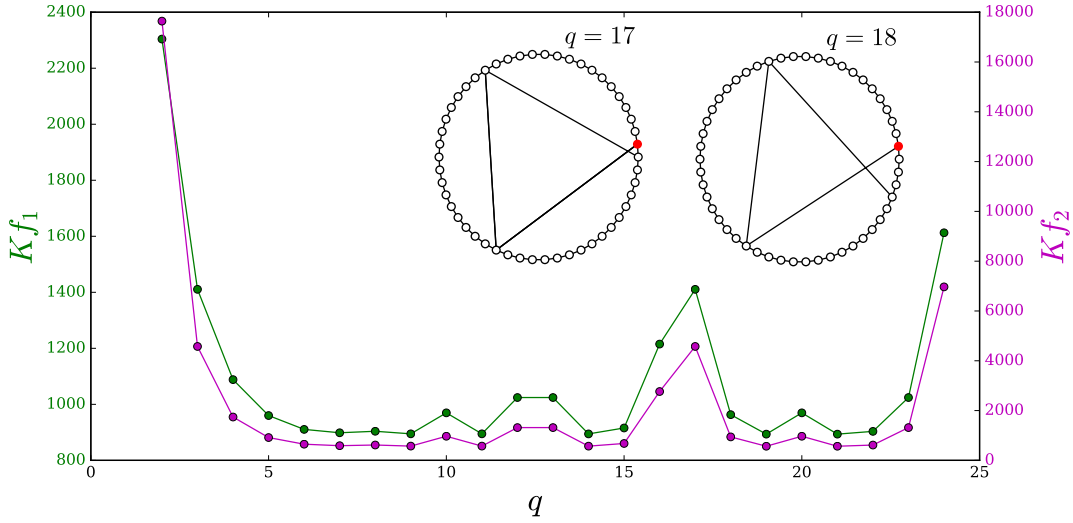


Figure 4 –  $Kf_1$  (green) and  $Kf_2$  (violet) for a cyclic graph with  $n = 50$  with nearest and  $q^{\text{th}}$ -neighbor coupling,  $a_{i,i\pm 1} = a_{i,i\pm q} = a_0$ . The inset sketches the model for  $q = 17, 18$  and illustrates one path involving  $q^{\text{th}}$ -range interactions starting from node in red.

and  $C_2(i)$  for the network shown in insets of Fig. 2.

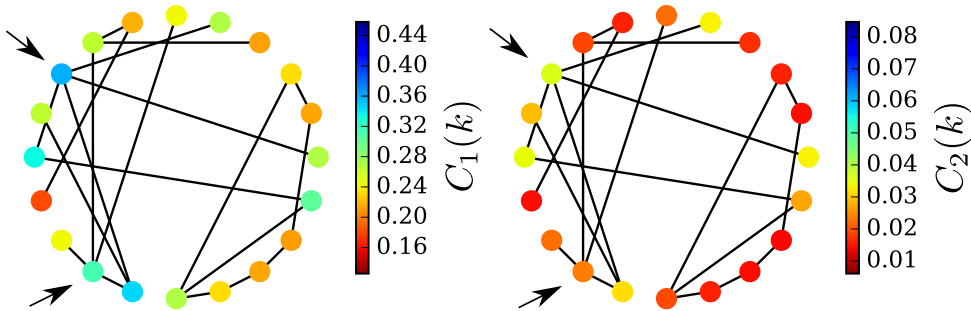


Figure 5 – Resistance centralities  $C_1(i)$  and  $C_2(i)$  defined in Eq. (2). Nodes pointed with arrows correspond to the perturbed nodes in Fig. 2.

One clearly sees that the node that induced that largest transient (bottom panel of Fig. 2) has lowest centralities  $C_1(i)$  and  $C_2(i)$  compared to the other one (top panel of Fig. 2). These centralities can also be used to build rankings of the nodes from most to least vulnerable, which are particularly useful to analyze local vulnerabilities in large scale networks. Moreover, for both global robustness and local vulnerabilities, we clarified the role of dynamical parameters, showing that inertia only has a limited effect on system’s excursion from synchronous state.

Second we went beyond weak perturbations and investigated desynchronization and transitions between synchronous states induced by larger perturbations as illustrated in Fig. 3. More precisely, we considered coupled oscillators within noisy internal parameters. Rather sur-

prisingly, based on a heuristic argument comparing standard deviations of oscillators' angles and the distance between the initial stable fixed point and the closest saddle point, we found estimates of the survival probability and first escape time that satisfactorily fits numerical simulations. Moreover we found that, increasing oscillators' inertia tend to facilitate escape from the initial basin of attraction.

In both cases of weak and large perturbation, the frameworks that we defined are rather general and thus may be used to analyze other types of coupled dynamical systems.

My research on vulnerabilities of coupled dynamical systems led to publications in peer-reviewed journals and preprints listed below.

- M. Tyloo, T. Coletta, P. Jacquod, Robustness of Synchrony in Complex Networks and Generalized Kirchhoff Indices, *Physical Review Letters* 120(8):084101 (2018). *Chapter 2 in the present thesis.*
- M. Tyloo, P. Jacquod, Global Robustness vs. Local Vulnerabilities in Complex Synchronous Networks, *Physical Review E* 100(3):032303 (2019). *Chapter 3*
- M. Tyloo, L. Pagnier, P. Jacquod, The Key Player Problem in Complex Oscillator Networks and Electric Power Grids: Resistance Centralities Identify Local Vulnerabilities, *Science Advances* 5(11):eaaw8359 (2019). *Chapter 4*
- M. Tyloo, R. Delabays, P. Jacquod, Noise-Induced Desynchronization and Stochastic Escape from Equilibrium in Complex Networks, *Physical Review E* 99(6):062213 (2019). *Chapter 5*
- F. Baumann, I. M. Sokolov, M. Tyloo, The Role of Active Leaders in Opinion Formation on Social Networks, *arXiv:1910.01897* (2019) submitted.
- R. Delabays, M. Tyloo, P. Jacquod, Rate of change of frequency under line contingencies in high voltage electric power networks with uncertainties, *Chaos* 29:103130 (2019).
- R. Delabays, M. Tyloo, P. Jacquod, The Size of the Sync Basin Revisited, *Chaos* 27:103109 (2017).

The forthcoming chapters are made from selected publications closely related to the question of global robustness and local vulnerabilities in complex network-coupled systems.

In preliminary chapter 1 we give some technical details about notions then used in the other chapters. Chapter 2 considers first-order oscillators and establish the relation between global robustness and Kirchhoff indices. Chapter 3 investigates more deeply the trade-off between local vulnerabilities and global robustness for second-order oscillators and the role of dynamical parameters. Chapter 4 focuses on local vulnerabilities of second-order oscillators and establish nodal rankings. Chapter 5 considers transitions between synchronous states

## **Introduction**

---

induced by a noisy environment and gives an estimate of the survival probability as well as first escape time. Finally chapter 6 gives a general conclusion and possible extensions of the presented results.

# 1 Preliminaries

In this preliminary chapter, we detail the mathematical tools used in the following chapters. In the first section we discuss definition and some properties of complex networks. In the second section we give a brief overview of coupled oscillators and related models. Finally in the third section we give details about linear response theory and its range of validity.

## A survey about complex networks

A complex network is a mathematical object, also called graph, that describes how some individual units are connected together. More precisely it is made of a set of vertices<sup>1</sup>  $\mathfrak{V} = \{1, \dots, n\}$  which is a collection of indices, and a set of edges  $\mathfrak{E} \subset \mathfrak{V} \times \mathfrak{V}$ . The number of nodes is  $n = |\mathfrak{V}|$  and the number of edges  $l = |\mathfrak{E}|$ . Each edge  $e(i, j) \in \mathfrak{E}$  is defined by a source node  $i$  and a target node  $j$  that are connected by  $e$  as well as a weight  $w(e)$ . There are at least two standard way to encode how the nodes are connected together by the edges and thus describe complex networks. The first one is via the *adjacency matrix*  $A \in \mathbb{R}^{n \times n}$  defined as,

$$a_{ij} = \begin{cases} w(e), & \text{if } e(i, j) \in \mathfrak{E}, \\ 0, & \text{otherwise.} \end{cases} \quad (1.1)$$

For undirected networks, the matrix elements of  $A$  satisfy  $a_{ij} = a_{ji}$ . In the following, we consider undirected networks and give details about directed networks in footnotes. The second way to describe a network is via the *incidence matrix*  $B \in \mathbb{R}^{n \times l}$  defined as,

$$b_{ie} = \begin{cases} \sqrt{w(e)}, & \text{if node } i \text{ is one end of edge } e, \\ 0, & \text{otherwise.} \end{cases} \quad (1.2)$$

---

<sup>1</sup>Also referred to as *nodes*.

From the adjacency matrix, one obtains the degree diagonal matrix  $K$  as,<sup>2</sup>

$$k_{ij} = \begin{cases} \sum_{k=1}^n a_{ik}, & \text{if } i = j, \\ 0, & \text{otherwise.} \end{cases} \quad (1.3)$$

Each element  $k_{ii}$  is then the weighted number of edges that are connected to node  $i$ . Note that the distribution of  $k_{ii}$  can be useful to characterize the homogeneity/regularity of a network. Finally, using  $A$  and  $K$ , one defines the *Laplacian* matrix as  $\mathbb{L} = K - A$ , which reads elementwise,

$$\mathbb{L}_{ij} = \begin{cases} -a_{ij}, & \text{if } i \neq j, \\ \sum_{k=1}^n a_{ik}, & \text{if } i = j. \end{cases} \quad (1.4)$$

Note that for undirected networks with positive edge weights, the Laplacian is also expressible as  $\mathbb{L} = B'B'^T$  where  $B'$  is the oriented<sup>3</sup> version of the incidence matrix Eq. (1.2). Many important properties of complex networks can be deduced from the above defined matrices. Some of them are briefly discussed below. The Laplacian is the matrix defining the coupling of many coupled dynamical systems in which we are interested. We thus give an extended description of its properties.

## Laplacian

Following its definition Eq. (1.4), the Laplacian satisfies  $\sum_j \mathbb{L}_{ij} = 0 \forall i$  and is thus a matrix of rank  $n-1$ . Moreover as  $\mathbb{L} = B'B'^T$ , the eigenvalues of the Laplacian are real<sup>4</sup> and satisfy  $0 = \lambda_1 \leq \lambda_2 \leq \dots \leq \lambda_n$ . If the network is connected, by the vanishing row/column sum property of the Laplacian, the eigenvector associated to  $\lambda_1 = 0$  is given by  $\mathbf{u}_1 = (1, 1, \dots, 1)/\sqrt{n}$ .<sup>5</sup> Disconnected networks can be identified by counting the number of vanishing eigenvalues. For example, if a network is made of two distinct disconnected subspaces of nodes  $\mathfrak{V}_1, \mathfrak{V}_2 \subset \mathfrak{V}$ , one can always separate the components of the eigenvectors accordingly and define  $\mathbf{u}_1, \mathbf{u}_2$  such that,

$$u_{\alpha,i} = \begin{cases} 1/\sqrt{n_\alpha}, & \text{if } i \in \mathfrak{V}_\alpha, \\ 0, & \text{otherwise,} \end{cases} \quad (1.5)$$

with  $n_\alpha = |\mathfrak{V}_\alpha|$  and  $\alpha = 1, 2$ . Then both  $\mathbf{u}_1$  and  $\mathbf{u}_2$  have associated eigenvalues that are vanishing, respectively  $\lambda_1 = 0$  and  $\lambda_2 = 0$ . The same argument holds true for more than two disconnected subspaces of nodes. Therefore, the number of independent connected components of a network is given by the degeneracy of the vanishing eigenvalue.

In case of a connected network, by orthogonality, eigenvectors with non-vanishing eigenvalues

---

<sup>2</sup>For a directed network, one has for each node *in*- and *out*- degrees defined as  $k_{out}(i) = \sum_{j=1}^n a_{ij}$  and  $k_{in}(i) = \sum_{j=1}^n a_{ji}$ .

<sup>3</sup>To get the oriented version we simply add a minus sign to one of the two non-vanishing matrix elements in each column of incidence matrix Eq. (1.2).

<sup>4</sup>In case of a directed network, the eigenvalues might have an imaginary part.

<sup>5</sup>We also refer to this eigenvector as the *constant vector*.

satisfy the relation,  $\sum_{i=1}^n u_{\alpha,i} = 0 \forall \alpha \geq 2$ . The main outcome of these relations is that if  $\mathbb{L}$  is applied to a vector  $\mathbf{x} \in \mathbb{R}^n$ , the component along the constant vector i.e.  $(\mathbf{u}_1 \cdot \mathbf{x}) \mathbf{u}_1$  has no effect as  $\mathbb{L} \mathbf{u}_1 = \mathbf{0}$ . Physically then, if the coupling of a dynamical system is given by a product of  $\mathbb{L}$  times a vector  $\mathbf{x} \in \mathbb{R}^n$  of nodal degrees of freedom, it implies that its entire dynamics as well as its steady states are invariant to constant shifts of  $\mathbf{x}$  as,

$$\mathbb{L} \mathbf{x} = \mathbb{L} (\mathbf{x} + c \mathbf{u}_1), \quad c \in \mathbb{R}. \quad (1.6)$$

Therefore one may only consider components orthogonal to  $\mathbf{u}_1$ , namely  $x_i \rightarrow x_i - n^{-1} \sum_{j=1}^n x_j$ . The eigenvector  $\mathbf{u}_2$  associated to the second smallest eigenvalue  $\lambda_2$  is called the *Fiedler mode* of the network [46]. The sign of its components gives a partition of the nodes into two connected subgroups which minimizes the sum of weights of required edges to remove to separate the network into two distinct pieces [114]. Because of the vanishing eigenvalue  $\lambda_1 = 0$ , the Laplacian matrix is not invertible. Nevertheless, one can still define its pseudo inverse denoted  $\mathbb{L}^\dagger$  which reads,

$$\mathbb{L}^\dagger_{ij} = \sum_{\alpha \geq 2} \frac{u_{\alpha,i} u_{\alpha,j}}{\lambda_\alpha} = [(\mathbb{L} + n \mathbf{u}_1^T \mathbf{u}_1)^{-1}]_{ij} - [\mathbf{u}_1^T \mathbf{u}_1]_{ij}, \quad (1.7)$$

where in the sum, the index corresponding to the vanishing eigenvalue has been omitted.

From a more intuitive perspective, the Laplacian of the network is often encountered in coupled dynamical systems because it relates to differences between degrees of freedom or properties of connected nodes. More precisely, if  $\mathbf{x} \in \mathbb{R}^n$  is a vector of nodal degrees of freedom/properties one has,

$$\sum_{j=1}^n \mathbb{L}_{ij} x_j = - \sum_{j=1}^n a_{ij} (x_i - x_j), \quad i = 1, \dots, n. \quad (1.8)$$

Therefore, the  $i^{\text{th}}$  component of Eq. (1.8) is simply the sum of the differences between  $x_i$  and its connected components  $x_j$  weighted by adjacency matrix elements  $a_{ij}$ . Such coupled systems have gauge invariance with respect to constant shifts of  $\mathbf{x}$  along  $\mathbf{u}_1$ . Dynamics based on the minimization/maximization of these differences is at the core of many models in fields as various as coupled oscillators [67, 89, 77], consensus algorithms [66, 90], opinion dynamics [98, 97, 12], diffusion [95, 89] or epidemic spreading [50] on complex networks.

### Centralities and indices

Many metrics have been defined over the years to compare the properties of different networks or within one network properties of different nodes [45]. Here we give a quick review of some of them that are used in the following chapters. We first review local descriptors usually called *centralities* focusing on nodal properties and then move to global network descriptors often called *network indices*. A good overview of these notions is given in Ref. [16].

One possibility to define a centrality is by using a distance metric. In that case, there are two common ways to define a centrality. The first one is the *closeness centrality* that reads for node  $i$ ,

$$\mathcal{C}^c(i, d) = \left[ n^{-1} \sum_{j=1}^n d(i, j) \right]^{-1}, \quad (1.9)$$

where  $d(i, k)$  is some distance metric going from node  $i$  to  $k$ . In words, it is simply the inverse of the average distance between  $i$  and the other nodes of the network. Now if  $C(i, d)$  is large (small), it means that node  $i$  is central (peripheral) in the network according to the distance  $d$ . The only failing of closeness centrality is that if a node  $j$  is not reachable from node  $i$  then  $d(i, j) = \infty$  and thus  $\mathcal{C}^c$  diverges. To take into account such problems one may replace arithmetic average by harmonic mean. This defines the *harmonic centrality* that reads,

$$\mathcal{C}^h(i, d) = n^{-1} \sum_{j \neq i} d^{-1}(i, j). \quad (1.10)$$

Centralities may also be defined without distances. For example, one can characterize nodes according to their degree Eq. (1.3) or their local clustering coefficient (see 1.1.2). Another possibility is to consider the spectral characteristics of the nodes by looking at the eigenvectors and eigenvalues of the adjacency or Laplacian matrices. Finally, based on any centrality, one can establish a ranking of the nodes. Obviously, all these locally defined centralities can be averaged over all nodes such that they may then be used as global indices describing the network as a whole.

The next paragraphs briefly discuss these known centralities, indices or ranking that appear in the following chapters.

### Geodesic distance

While looking at the connectivity of a network, one intuitive feature to say whether or not two nodes are close to each other is the *geodesic distance*  $g(i, j)$ . It corresponds to the shortest path between two nodes and is standardly obtained out of the powers of the adjacency matrix of the network. For a general weighted network, the geodesic distance between node  $i$  and  $j$  reads,

$$g(i, j) = \min_{\text{all } \langle i \rightarrow j \rangle} \left[ \sum_{e \in \langle i \rightarrow j \rangle} w(e) \right], \quad (1.11)$$

where  $\langle i \rightarrow j \rangle$  denotes a path from  $i$  to  $j$ . Summing over all geodesic distances in the network yields the average geodesic distance,

$$L = \frac{2}{n(n-1)} \sum_{i < j} g(i, j). \quad (1.12)$$

Index  $L$ , also called *characteristic path length*, measures how close nodes are within a network. Geodesic distance is a very intuitive metric to measure how far nodes are from each other. However, it only accounts for the shortest path and does not even take into account multiplicity of such paths that may occur. For example, a fluid flowing from one node to another will not only use the shortest path but all existing ones as well. In the results presented below, we consider the *resistance distance* which accounts for all existing paths between nodes.

### Clustering coefficient

A network property that one may want to evaluate is the clustering. More precisely, whether a network forms one large component with long range couplings or is made of small groups of highly connected nodes. To measure such property of a network, one can define the *clustering coefficient*  $cl(i)$  [126]. The idea behind clustering coefficient is to see how well connected are the neighbors of a node  $i$ . If node  $i$  has  $k_{ii}$  neighbors then there can be at most  $\frac{k_{ii}(k_{ii}-1)}{2}$  edges connecting them together. The clustering coefficient of  $i$  is defined as,

$$cl(i) = \frac{2k'}{k_{ii}(k_{ii}-1)}, \quad (1.13)$$

where  $k'$  is the actual number of edges connecting together the neighbors of  $i$ . Therefore, nodes being part of a highly connected cluster have  $cl$  close to 1. Again one can define the average clustering of a network as,

$$Cl = n^{-1} \sum_{i=1}^n cl(i). \quad (1.14)$$

It has been shown that starting from an initial regular cycle network and gradually rewiring edges leads to *small-world* networks with the interesting property to have a low average geodesic distance  $l$  while keeping a high clustering coefficient  $Cl$  [126]. This is illustrated in Fig. 1.1, where small-world networks correspond to rewiring probabilities around 0.01. Investigation on such networks have demonstrated that they exhibit enhanced synchronization properties [10].

### PageRank

One of the most famous ranking of nodes in complex networks is probably the *PageRank* [23]. It is defined from the row stochastic adjacency matrix  $\bar{A}$ ,

$$\bar{a}_{ij} = \begin{cases} \frac{a_{ij}}{k_{ii}}, & \text{if } i \neq j, \\ 0, & \text{if } i = j. \end{cases} \quad (1.15)$$

Then one can define a new matrix as, [16]

$$G = \alpha \bar{A} + (1 - \alpha) \mathbf{1}^T \mathbf{v}, \quad (1.16)$$

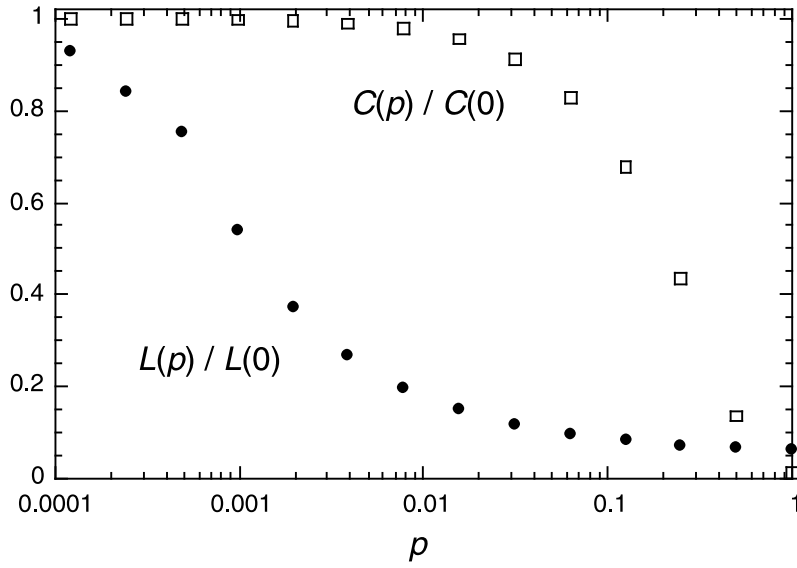


Figure 1.1 – Clustering coefficient  $Cl$  (denoted  $C$  on the figure) and characteristic path length  $L$  for networks obtained from a rewiring procedure that starts from an initial regular cyclic network with  $n = 1000$  nodes and 1<sup>st</sup>- to 5<sup>th</sup>-nearest neighbors coupling. Then each edge is rewired with a probability  $p$ .  $Cl$  and  $L$  have been averaged over 20 realizations. *Figure taken from Ref. [126].*

where  $\alpha \in [0, 1)$  and  $\mathbf{v}$  is a distribution. By Perron-Fröbenius theorem,  $G$  has a left dominant eigenvector  $\mathbf{p}$  whose components are all positive. Therefore  $\mathbf{p}$  can be interpreted as a probability distribution. The PageRank is then given by ordering the components of  $\mathbf{p}$ . It gives a ranking of the nodes according to the frequency at which they are visited during a random walk on the network. The second term in Eq. (1.16) allows the random walker to jump with a probability  $(1 - \alpha)$  to any node at each step. The main advantage of PageRank is its rather low computational cost even for large networks. Indeed, from the row stochastic property of  $G$ , the eigenvalue corresponding to  $\mathbf{p}$  is equal to 1. Therefore  $\mathbf{p}$  can be obtained by applying  $G$  many times on any starting distribution  $\mathbf{w}$  as,

$$\mathbf{p} = \lim_{N \rightarrow \infty} G^N \mathbf{w}. \tag{1.17}$$

The computational efficiency of this ranking has been exploited by *Google* web search engine to order large number of referenced sites.

To summarize, most complex network metrics have been defined from coupling structure or by considering random processes evolving on them. However, coupled dynamical systems usually have to satisfy conservation laws dictated by the physics governing the system. It is thus often complicated to connect analytically, complex network metrics that have intuitive meaning to coupled dynamical systems. Some well-known results where such connection has been established for epidemic spreading and diffusion on complex networks are given by

Refs. [95, 44].

## Coupled oscillators and related models

### Kuramoto oscillators

The most famous model of coupled oscillators is that of *Kuramoto* [77] and reads,

$$\dot{\theta}_i = P_i - \sum_{j=1}^n a_{ij} \sin(\theta_i - \theta_j), \quad i = 1, \dots, n. \quad (1.18)$$

These coupled differential equations describe a set of  $n$  oscillators, each of them having as degree of freedom a compact angle coordinate  $\theta_i \in (-\pi, \pi]$  and an internal parameter called *natural frequency*<sup>6</sup>  $P_i$ . The coupling is given by the elements of the adjacency matrix  $a_{ij}$ . Originally, Kuramoto introduced his model with a homogeneous all-to-all interaction network, i.e.  $a_{ij} = K/n$  and showed that above a critical coupling strength  $K > K_c$ , a finite fraction of the oscillators synchronize with  $\dot{\theta}_i - \dot{\theta}_j = 0$  [77]. For even larger values of  $K$ , all oscillators evolve in synchrony with  $\dot{\theta}_i = \dot{\theta}_j \forall i, j$ . Such synchronous state is called *phase-locking state*.<sup>7</sup> Synchronization is also achievable with oscillators coupled on complex networks provided that the coupling is large enough compared to the width of distribution of  $P_i$ 's [67, 39].

A phase-locking state  $\boldsymbol{\theta}^{(0)}$  of Eq. (1.18) satisfies,

$$P_i = \sum_{j=1}^n a_{ij} \sin(\theta_i^{(0)} - \theta_j^{(0)}), \quad i = 1, \dots, n. \quad (1.19)$$

The existence and number of different synchronous states as well as their characteristics strongly depend on the coupling network and the distribution of  $P_i$ 's. It has been shown for planar networks that each stable fixed point can be identified by the *winding vector*  $\mathbf{q}(\boldsymbol{\theta}^{(0)})$  describing the loop flows on each cycle of the network [73, 42, 68, 34]. For a network made of a single cycle, the *winding number* reads,

$$q(\boldsymbol{\theta}^{(0)}) = (2\pi)^{-1} \sum_{i=1}^n \left| \theta_i^{(0)} - \theta_{i+1}^{(0)} \right|_{[-\pi, \pi]}, \quad (1.20)$$

where  $\left| \theta_i^{(0)} - \theta_{i+1}^{(0)} \right|_{[-\pi, \pi]}$  means angle differences taken module  $2\pi$  in the interval  $(-\pi, \pi]$ . Fig. 1.2 illustrates a stable fixed point for a meshed network with non zero winding vector. A numerical procedure to find such synchronous states is given in Ref. [35].

The linear stability of  $\boldsymbol{\theta}^{(0)}$  can be analyzed by calculating the Jacobian matrix<sup>8</sup>  $\mathcal{J}(\boldsymbol{\theta}^{(0)})$  of

<sup>6</sup>The reason of such a name is that in a completely decoupled system, from Eq. (1.18) each oscillator rotates at its natural frequency i.e.  $\dot{\theta}_i = P_i$ .

<sup>7</sup>We refer to such a state as *stable fixed point*, *steady* or *stationnary* or *synchronous state* or *equilibrium*.

<sup>8</sup>Also called *stability matrix*.

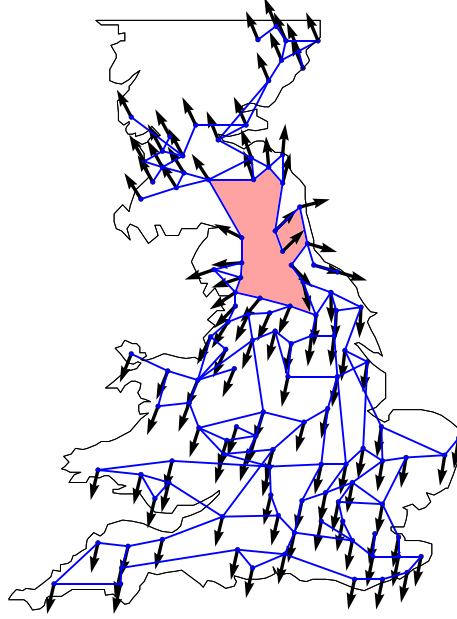


Figure 1.2 – Example of a stable fixed point of Eq. (1.18) with identical natural frequencies  $P_i = 0 \forall i$  defined on a meshed network (model of the UK AC transmission grid [84, 35]). The fixed point is characterized by a non zero winding number  $q = 1$  on the large cycle highlighted in red. *Figure adapted from Ref. [35].*

Eq. (1.18) that is,

$$[\mathcal{J}(\boldsymbol{\theta}^{(0)})]_{ij} = \begin{cases} a_{ij} \cos(\theta_i^{(0)} - \theta_j^{(0)}), & \text{if } i \neq j, \\ -\sum_{k=1}^n a_{ik} \cos(\theta_i^{(0)} - \theta_k^{(0)}), & \text{if } i = j. \end{cases} \quad (1.21)$$

One should note that  $\mathcal{J}(\boldsymbol{\theta}^{(0)})$  defined in Eq. (1.21) satisfies all the properties of a Laplacian matrix, i.e  $\sum_j [\mathcal{J}(\boldsymbol{\theta}^{(0)})]_{ij} = \sum_i [\mathcal{J}(\boldsymbol{\theta}^{(0)})]_{ij} = 0$ . Moreover, it has been shown that if  $|\theta_i^{(0)} - \theta_j^{(0)}| < \pi/2 \forall i, j$  then the eigenvalues of  $\mathcal{J}(\boldsymbol{\theta}^{(0)})$  are all non-positive and thus  $\boldsymbol{\theta}^{(0)}$  is a stable fixed point of Eq. (1.18) [35]. In the following chapters, whenever we consider a stable fixed point, it means that the eigenvalues of its corresponding stability matrix are all negative.

To investigate the transient behavior of the system near its synchronous state, one can linearize the dynamics of Eq. (1.18) around  $\boldsymbol{\theta}^{(0)}$ . Doing so, the initial non-linear oscillators are reduced to linear oscillators evolving on a new network whose edge weights are given by minus the stability matrix, namely  $a_{ij} \cos(\theta_i - \theta_j)$  instead of  $a_{ij}$ . As it is a linear system, it is analytically solvable. Some details are given in the next section.

The Kuramoto model can be extended to massive oscillators by adding a second-order time derivative to Eq. (1.18) that yields,

$$m_i \ddot{\theta}_i + d_i \dot{\theta}_i = P_i - \sum_{j=1}^n a_{ij} \sin(\theta_i - \theta_j), \quad i = 1, \dots, n. \quad (1.22)$$

Now each oscillator has two additional dynamical parameters, namely an inertia  $m_i$  and a damping  $d_i$ . One feature modelled by introducing inertia is non instantaneous response of the frequency to perturbations. Obviously, the synchronous states of Eq. (1.22) are the same as Eq. (1.18). Beside being paradigmatic models for synchronization for neuronal or Josephson junctions networks, one physical realization of Eqs. (1.18), (1.22) that has attracted an increasing interest over the last decade are high voltage power networks [104]. In that case,  $\theta_i$ 's are phases of the complex voltage and natural frequencies are injected ( $P_i > 0$ ) or consumed ( $P_i < 0$ ) power at each bus. Nodes are thus either loads ( $P_i < 0$ ) or generators ( $P_i > 0$ ). Usually loads do not have any inertia and thus their dynamics are governed by Eq. (1.18) while conventional generators have inertia with a dynamics therefore given by Eq. (1.22). Such mix of first- and second-order Kuramoto oscillators describes the dynamics of high voltage power grids in the lossless line approximation<sup>9</sup>, on short time scales, where variations in voltage amplitudes are neglected as they fluctuate on longer time scales [13, 39, 83].

### Linear oscillators

Instead of the non-linear sine coupling of Eq. (1.18), one can consider linear coupled oscillators with continuous degrees of freedom  $x_i \in \mathbb{R} \forall i$ , whose dynamics takes the simple form,

$$\dot{x}_i = P_i - \sum_{j=1}^n a_{ij} (x_i - x_j), \quad i = 1, \dots, n. \quad (1.23)$$

Note that the second term on the right-hand side of Eq. (1.23) is the product of the Laplacian of the network times  $\mathbf{x}$ . Thus Eq. (1.23) reads in a vectorial form,

$$\dot{\mathbf{x}} = \mathbf{P} - \mathbb{L}\mathbf{x}. \quad (1.24)$$

The solution of Eq. (1.24) is simply obtained from eigenvalues  $\lambda_\alpha$  and eigenvectors  $\mathbf{u}_\alpha$  of  $\mathbb{L}$  as,

$$\mathbf{x}(t) = \sum_{\alpha} \left[ (\mathbf{x}(t=0) \cdot \mathbf{u}_\alpha) e^{-\lambda_\alpha t} + e^{-\lambda_\alpha t} \int_0^t e^{\lambda_\alpha t'} \mathbf{P}(t') \cdot \mathbf{u}_\alpha dt' \right] \mathbf{u}_\alpha, \quad (1.25)$$

where we take into account a possible time-dependence of the natural frequencies  $\mathbf{P}$ . Steady states solution  $\mathbf{x}^{(0)}$  of Eq. (1.23) is obtain using the pseudo inverse of  $\mathbb{L}$  as,

$$\mathbf{x}^{(0)} = \mathbb{L}^\dagger \mathbf{P}. \quad (1.26)$$

With  $P_i = 0 \forall i$ , Eq. (1.23) corresponds to a first order consensus model [103].

---

<sup>9</sup>The real part of the admittance, namely the conductance of the lines is neglected. This is a justified approximation for high voltage power networks for which conductance is typically ten times smaller than susceptance.

## Linear response theory

When subject to modification or perturbation of internal parameters or degrees of freedom, a dynamical system enters a transient regime. Depending on the strength of the perturbation, one should differentiate small-signal response where the system stays close to its initial fixed point from larger perturbations that eventually lead to escape from the initial basin of attraction. In the case of small-signal response, the transient behavior of the system can be approximated by its *linear response*. We give details and illustrations of the linear response of Eq. (1.18) taken at a fixed point  $\boldsymbol{\theta}^{(0)}$  for  $\mathbf{P}^{(0)}$  to an additive perturbation in the natural frequencies. More precisely one has  $\mathbf{P}(t) = \mathbf{P}^{(0)} + \delta\mathbf{P}(t)$  that makes angles become time-dependent as  $\boldsymbol{\theta}(t) = \boldsymbol{\theta}^{(0)} + \delta\boldsymbol{\theta}(t)$ . Equation (1.18) then becomes,

$$\delta\dot{\theta}_i(t) = P_i^{(0)} + \delta P_i(t) - \sum_{j=1}^n a_{ij} \sin\left[\theta_i^{(0)} + \delta\theta_i(t) - \theta_j^{(0)} - \delta\theta_j(t)\right], \quad i = 1, \dots, n. \quad (1.27)$$

The linear response is given by Taylor expanding the last term in the right hand side of Eq. (1.27) that yields,

$$\delta\dot{\theta}_i(t) \cong \delta P_i(t) - \sum_{j=1}^n a_{ij} \cos\left(\theta_i^{(0)} - \theta_j^{(0)}\right) [\delta\theta_i(t) - \delta\theta_j(t)], \quad i = 1, \dots, n, \quad (1.28)$$

where we used Eq. (1.19). Now that the time-dependence occurs only in linear expression, one can rewrite Eq. (1.28) in a vectorial form as,

$$\delta\dot{\boldsymbol{\theta}} = \delta\mathbf{P}(t) - \mathbb{L}(\boldsymbol{\theta}^{(0)})\delta\boldsymbol{\theta}. \quad (1.29)$$

The linear response is equivalent to Eq. (1.24) with coupling strength given by  $\mathbb{L}(\boldsymbol{\theta}^{(0)})_{ij} = a_{ij} \cos\left(\theta_i^{(0)} - \theta_j^{(0)}\right)$ . Therefore solution of Eq. (1.28) has a form similar to Eq. (1.30) as,

$$\delta\boldsymbol{\theta}(t) = \sum_{\alpha} \left[ e^{-\lambda_{\alpha} t} \int_0^t e^{\lambda_{\alpha} t'} \delta\mathbf{P}(t') \cdot \mathbf{u}_{\alpha} dt' \right] \mathbf{u}_{\alpha}, \quad (1.30)$$

where  $\lambda_{\alpha}$  and  $\mathbf{u}_{\alpha}$  are eigenvalues and eigenvectors respectively of  $\mathbb{L}(\boldsymbol{\theta}^{(0)})$ . Fig. 1.3 compares  $\delta\theta_i(t)$  numerically obtained by time-evolving Eq. (1.18) and the analytical expression for the response Eq. (1.30) for two consecutive quench perturbations,  $\delta P_1(t) = \delta P_0 \Theta(\tau_0 - t) - 2\delta P_0 \Theta(\tau_1 - t) \Theta(t - \tau_0)$  (see Eq (1.31)). To give a good illustration of the validity of the linearization, we chose natural frequencies  $\mathbf{P}^{(0)}$  such that angle differences at the stable fixed point are rather large (up to  $45^\circ$ ). One can remark that even for a perturbation with large amplitude  $\delta P_0 = 0.1 a_0$ , linear response still gives a fair approximation of oscillators response even if one notice some discrepancies when  $\delta\theta_i(t)$  becomes large.

The analytical expression for the response of the system to  $\delta P_1(t) = \delta P_0 \Theta(\tau_0 - t) - 2\delta P_0 \Theta(\tau_1 -$

$t)\Theta(t - \tau_0)$  is obtained from Eq. (1.30) as,

$$\delta\theta_i(t) = \begin{cases} \delta P_0 t + \sum_{\alpha \geq 2} \frac{\delta P_0 u_{\alpha,i} u_{\alpha,j}}{\lambda_\alpha} (1 - e^{-\lambda_\alpha t}), & t < \tau_0, \\ 3\delta P_0 \tau_0 - 2\delta P_0 t + \sum_{\alpha \geq 2} \frac{\delta P_0 u_{\alpha,i} u_{\alpha,j}}{\lambda_\alpha} (3e^{-\lambda_\alpha(t-\tau_0)} - e^{-\lambda_\alpha t} - 2), & \tau_0 < t < \tau_1, \\ \delta P_0 (3\tau_0 - 2\tau_1) + \sum_{\alpha \geq 2} \frac{\delta P_0 u_{\alpha,i} u_{\alpha,j}}{\lambda_\alpha} (3e^{-\lambda_\alpha(t-\tau_0)} - e^{-\lambda_\alpha t} - 2e^{-\lambda_\alpha(t-\tau_1)}), & \tau_1 < t. \end{cases} \quad (1.31)$$

Note that other tools are standardly used to analyze system's responses such as observability Gramians [119] or transfer functions [93].

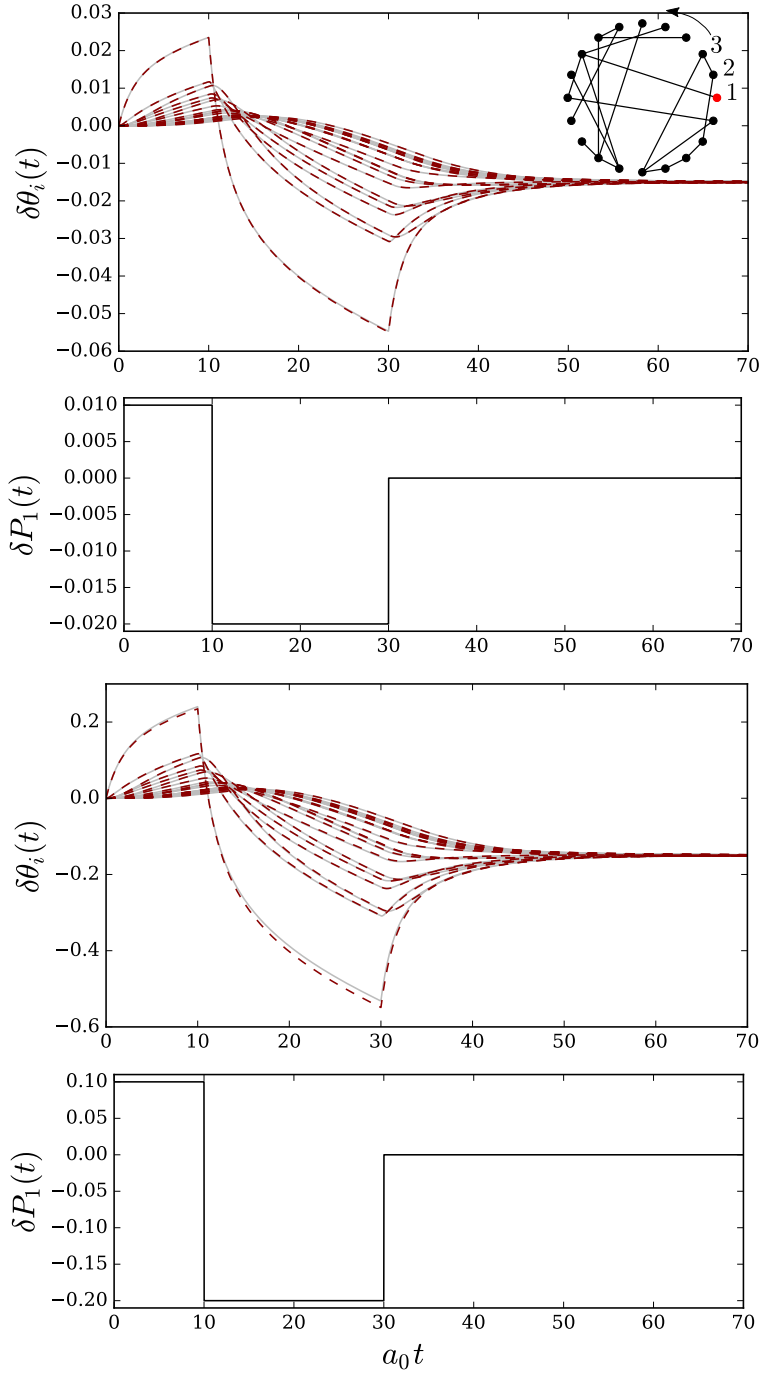


Figure 1.3 – Comparison between oscillators response numerically obtained (grey solid lines) and the analytical expression Eq. (1.31) (red dashed lines) for perturbation shown in lower panels (second and fourth rows) applied on node 1 depicted in inset, i.e  $\delta P_1(t) = \delta P_0\Theta(\tau_0 - t) - 2\delta P_0\Theta(\tau_1 - t)\Theta(t - \tau_0)$ . The amplitude of the perturbation has been multiplied by ten in the bottom panels compared the top ones. The coupling among oscillators is homogeneous with  $a_{ij} = a_0$ , and the natural frequencies  $\mathbf{P}^{(0)}$  are uniformly distributed in the interval  $a_0[-0.75, 0.75]$ .

## **2 Robustness of Synchrony in Complex Networks and Generalized Kirchhoff Indices**

*Chapter 2 is a postprint version of a letter published as:*

M. Tyloo, T. Coletta, P. Jacquod, *Physical Review Letters* 120(8):084101 (2018) [121].

## Chapter 2. Robustness of Synchrony in Complex Networks and Generalized Kirchhoff Indices

---

In network theory, a question of prime importance is how to assess network vulnerability in a fast and reliable manner. With this issue in mind, we investigate the response to external perturbations of coupled dynamical systems on complex networks. We find that for specific, non-averaged perturbations, the response of synchronous states depends on the eigenvalues of the stability matrix of the unperturbed dynamics, as well as on its eigenmodes via their overlap with the perturbation vector. Once averaged over properly defined ensembles of perturbations, the response is given by new graph topological indices, which we introduce as *generalized Kirchhoff indices*. These findings allow for a fast and reliable method for assessing the specific or average vulnerability of a network against changing operational conditions, faults or external attacks.

### Introduction

From social to natural sciences, communication technology to electrical engineering, information sciences to cybernetics, graph theory profoundly impacts many fields of human knowledge [9]. Graphs allow for a convenient modelization of complex systems where their structure defines the couplings between the system's individual components, each of them with its own internal dynamics. The resulting coupled differential equations determine the system dynamics and its steady-state solutions. Of particular interest is to predict the behavior of the system when it is perturbed away from steady-state, for instance when an electric power plant goes offline in an operating power grid or when a line is cut and information has to be redirected in a communication network. An issue of key importance for network security is how to assess fast and reliably a network's vulnerability. This is not an easy task: network vulnerability depends on both the system dynamics and the network topology and geometry. It is highly desirable to identify a set of easily computed descriptors that characterize network vulnerability [45]. In this manuscript we propose a new family of network descriptors in a two-step approach. We investigate the sensitivity against external perturbations of synchronous states of coupled dynamical systems on complex networks. First, we quantify this sensitivity using performance measures recently introduced in the context of electric power grids [7, 119, 102]. Second, by direct calculation of these performance measures, we identify a new class of easily computed topological indices that generally characterize synchrony robustness/fragility under ensemble-averaged perturbations.

Synchronization is ubiquitous [117] in systems of coupled dynamical systems. It follows from the interplay between the internal dynamics of the individual systems and the coupling between them [77, 105, 3, 100]. Optimization of synchronization has been investigated from various angles. The synchronous state can be optimal from the point of view of linear stability [99], the range of parameters that allow synchronization [10, 26, 132], the value that an order parameter takes at synchrony [111] or the volume of the basin of attraction around a stable synchronous fixed point [128, 86, 35]. Here we extend these investigations by asking what makes synchronous states more or less fragile against external perturbations. The answer is surprisingly simple and applies to a large variety of perturbations and of fragility performance

measures – synchrony fragility depends on a family of topological indices, which generalize the Kirchhoff index introduced in Ref. [71].

## Model and method

Our analysis focuses on the Kuramoto model [77]

$$\dot{\theta}_i = P_i - \sum_j a_{ij} \sin(\theta_i - \theta_j), \quad i = 1, \dots, n, \quad (2.1)$$

though our results are more general and apply to a wider class of coupled dynamical systems (see 2.9.8). Eq. (2.1) models the behavior of a set of  $n$  harmonic oscillators, each with its angle coordinate  $\theta_i$  and its natural frequency  $P_i$ , coupled to one another with couplings defined by the weighted adjacency matrix  $a_{ij} \geq 0$ . Kuramoto originally considered identical all-to-all coupling,  $a_{ij} \equiv K/n$  [77]. It was found that for  $K > K_c$ , a finite number of oscillators synchronize, with  $\dot{\theta}_i - \dot{\theta}_j = 0$ . This type of frequency synchronization also occurs for nonhomogeneous couplings  $b_{ij}$  defined on a complex network [40], the case of interest here. Without loss of generality we set  $\sum_i P_i = 0$ , for which the frequency synchronous state has  $\dot{\theta}_i \equiv 0, \forall i$ <sup>1</sup>.

We consider a stable fixed-point solution  $\boldsymbol{\theta}^{(0)} = (\theta_1^{(0)}, \dots, \theta_n^{(0)})$  to Eq. (2.1) with unperturbed natural frequencies  $\mathbf{P}^{(0)}$ . We then subject this state to a time-dependent perturbation  $\mathbf{P}(t) = \mathbf{P}^{(0)} + \delta\mathbf{P}(t)$ , so that angles become time-dependent,  $\boldsymbol{\theta}(t) = \boldsymbol{\theta}^{(0)} + \delta\boldsymbol{\theta}(t)$ . Linearizing the dynamics of Eq. (2.1) about  $\boldsymbol{\theta}^{(0)}$ , one obtains

$$\delta\dot{\boldsymbol{\theta}} = \delta\mathbf{P} - \mathbb{L}(\boldsymbol{\theta}^{(0)}) \delta\boldsymbol{\theta}, \quad (2.2)$$

where we introduced the weighted Laplacian matrix  $\mathbb{L}(\boldsymbol{\theta}^{(0)})$  with matrix elements

$$\mathbb{L}_{ij} = \begin{cases} -a_{ij} \cos(\theta_i^{(0)} - \theta_j^{(0)}), & i \neq j, \\ \sum_k a_{ik} \cos(\theta_i^{(0)} - \theta_k^{(0)}), & i = j. \end{cases} \quad (2.3)$$

This Laplacian is minus the stability matrix of the linearized dynamics, and since we consider a stable synchronous state, it is positive semidefinite, with a single eigenvalue  $\lambda_1 = 0$  with eigenvector  $\mathbf{u}_1 = (1, 1, 1, \dots, 1)/\sqrt{n}$ , and  $\lambda_i > 0, i = 2, 3, \dots, n$ .

The first term on the right-hand side of Eq. (2.2) perturbs angles away from the synchronous state. To assess the magnitude of this excursion in the spirit of Refs. [7, 119, 102] we consider

<sup>1</sup>For systems with  $\sum_i P_i = n\Omega \neq 0$ , this is equivalently achieved by considering the system in a rotating frame with  $\theta_i(t) \rightarrow \theta_i(t) + \Omega t$ .

## Chapter 2. Robustness of Synchrony in Complex Networks and Generalized Kirchhoff Indices

---

two fragility performance measures

$$\mathcal{P}_1(T) = \sum_i \int_0^T |\delta\theta_i(t) - \Delta(t)|^2 dt, \quad (2.4a)$$

$$\mathcal{P}_2(T) = \sum_i \int_0^T |\delta\dot{\theta}_i(t) - \dot{\Delta}(t)|^2 dt. \quad (2.4b)$$

Because synchronous states are defined modulo any homogeneous angle shift, the transformation  $\theta_i^{(0)} \rightarrow \theta_i^{(0)} + C$  does not change the synchronous state. Accordingly, only angle shifts with  $\sum_i \delta\theta_i(t) = 0$  matter, which is incorporated in the definitions of  $\mathcal{P}_{1,2}$  by subtracting averages  $\Delta(t) = n^{-1} \sum_j \delta\theta_j(t)$  and  $\dot{\Delta}(t) = n^{-1} \sum_j \delta\dot{\theta}_j(t)$ . An alternative procedure is to restrict oneself to perturbations orthogonal to  $\mathbf{u}_1$  [7, 119, 102]. Either procedure ensures, together with the non-negativity of  $\mathbb{L}$ , that  $\mathcal{P}_{1,2} < \infty$ , even when  $T \rightarrow \infty$ , if the perturbation is short and weak enough that it leaves the dynamics inside the basin of attraction of  $\boldsymbol{\theta}^{(0)}$ . Low values for  $\mathcal{P}_{1,2}^\infty \equiv \mathcal{P}_{1,2}(T \rightarrow \infty)$  indicate then that the system absorbs the perturbation with little fluctuations, while large values indicate a temporary fragmentation of the system into independent pieces –  $\mathcal{P}_{1,2}^\infty$  measures the coherence of the synchronous state [7].

We expand angle deviations over the eigenstates  $\mathbf{u}_\alpha$  of  $\mathbb{L}$ ,  $\delta\boldsymbol{\theta}(t) = \sum_\alpha c_\alpha(t) \mathbf{u}_\alpha$ , and rewrite Eq. (2.2) as

$$\dot{c}_\alpha(t) = \delta\mathbf{P}(t) \cdot \mathbf{u}_\alpha - \lambda_\alpha c_\alpha(t), \quad (2.5)$$

whose general solution reads

$$c_\alpha(t) = e^{-\lambda_\alpha t} c_\alpha(0) + e^{-\lambda_\alpha t} \int_0^t dt' e^{\lambda_\alpha t'} \delta\mathbf{P}(t') \cdot \mathbf{u}_\alpha. \quad (2.6)$$

Being interested in perturbations  $\delta\mathbf{P}$  that start at  $t = 0$ , when the system is in the synchronous state with  $\delta\boldsymbol{\theta}(0) = 0$ , we set  $c_\alpha(0) \equiv 0$ . The performance measures of Eqs. (2.4) are given by  $\mathcal{P}_1(T) = \sum_{\alpha \geq 2} \int_0^T c_\alpha^2(t) dt$  and  $\mathcal{P}_2(T) = \sum_{\alpha \geq 2} \int_0^T \dot{c}_\alpha^2(t) dt$ . We next introduce generalized Kirchhoff indices in terms of which we express  $\mathcal{P}_{1,2}$  for three different classes of perturbations  $\delta\mathbf{P}(t)$ .

### Generalized Kirchhoff indices.

The Kirchhoff index originally followed from the definition of the resistance distance in a graph [71]. To a connected graph, one associates an electrical network where each edge is a resistor given by the inverse edge weight in the original graph. The resistance distance is the resistance  $\Omega_{ij}^{(1)}$ <sup>2</sup> between any two nodes  $i$  and  $j$  on the electrical network. The Kirchhoff index is then defined as [71]

$$Kf_1 \equiv \sum_{i < j} \Omega_{ij}^{(1)}, \quad (2.7)$$

---

<sup>2</sup>Superscript notation  $\Omega_{ij}^{(1)}$  will become clear in chapter 3.

where the sum runs over all pairs of nodes in the graph. For a graph with Laplacian  $\mathbb{L}$ , it has been shown that  $Kf_1$  is given by the spectrum  $\{\lambda_\alpha\}$  of  $\mathbb{L}$  as [133, 56, 29]

$$Kf_1 = n \sum_{\alpha \geq 2} \lambda_\alpha^{-1}. \quad (2.8)$$

Up to a normalization prefactor,  $Kf_1$  gives the mean resistance distance  $\overline{\Omega}$  over the whole graph. Intuitively, one expects the dynamics of a complex system to depend not only on  $\overline{\Omega^{(1)}}$ , but on the full set  $\{\Omega_{ij}^{(1)}\}$ . Higher moments of  $\{\Omega_{ij}^{(1)}\}$  are encoded in generalized Kirchhoff indices  $Kf_p$  (see 2.9.1) which we define as

$$Kf_p = n \sum_{\alpha \geq 2} \lambda_\alpha^{-p}, \quad (2.9)$$

for integers  $p$ . Below we show that  $\mathcal{P}_{1,2}$  can be expressed as linear combinations of the  $Kf_p$ 's corresponding to  $\mathbb{L}$  in Eq. (2.3). We note that, continued to  $p \in \mathbb{C}$ ,  $Kf_p$  is known as the *spectral zeta function* of  $\mathbb{L}$  [125].

### Dirac delta perturbation

We first consider  $\delta \mathbf{P}(t) = \delta \mathbf{P}_0 \tau_0 \delta(t)$  with the Dirac delta-function  $\delta(t)$ . Because the perturbation is limited in time, the limit  $T \rightarrow \infty$  can be taken in Eqs. (2.4). One obtains (see 2.9.3)

$$\mathcal{P}_1^\infty = \sum_{\alpha} \frac{(\delta \mathbf{P}_0 \cdot \mathbf{u}_\alpha)^2 \tau_0^2}{2} \lambda_\alpha^{-1}, \quad (2.10a)$$

$$\mathcal{P}_2^\infty = \sum_{\alpha} \frac{(\delta \mathbf{P}_0 \cdot \mathbf{u}_\alpha)^2 \tau_0^2}{2} \lambda_\alpha. \quad (2.10b)$$

Both performance measures depend on the scalar product of the perturbation  $\delta \mathbf{P}_0$  with the eigenmodes  $\mathbf{u}_\alpha$  of  $\mathbb{L}$ . Such scalar products occur also when analyzing propagation of disturbances on networks [69]. To get more insight on the typical network response, we define an ensemble of perturbation vectors with  $\langle \delta P_{0i} \delta P_{0j} \rangle = \delta_{ij} \langle \delta P_0^2 \rangle^3$ . Averaging over that ensemble gives

$$\langle \mathcal{P}_1^\infty \rangle = \frac{\langle \delta P_0^2 \rangle \tau_0^2}{2n} Kf_1, \quad (2.11a)$$

$$\langle \mathcal{P}_2^\infty \rangle = \frac{\langle \delta P_0^2 \rangle \tau_0^2}{2n} Kf_{-1}. \quad (2.11b)$$

The network structure determines the performance measures via the spectrum of the weighted Laplacian of Eq. (2.3). The latter depends on the network structure – its topology and edge weights, as well as the internal dynamics of the oscillators, which modifies the edge weights

---

<sup>3</sup>The choice  $\delta \mathbf{P}_0 = (0, 0, \dots, 0, \Delta_j, 0, \dots)$  is equivalent to the averaging procedure used in the approach to performance measures used in Refs.[7, 119].

## Chapter 2. Robustness of Synchrony in Complex Networks and Generalized Kirchhoff Indices

via angle differences  $\theta_i^{(0)} - \theta_j^{(0)}$  determined by  $\mathbf{P}^{(0)}$ . The way all these ingredients determine average network fragility is however simply encoded in  $Kf_{-1}$  and  $Kf_1$ . We note that Eq. (2.11a) appeared in slightly different, but equivalent form in Ref. [7].

### Box perturbation

Next, we go beyond the  $\delta$ -perturbations discussed so far [7, 119, 102] and consider a perturbation that is extended, but still limited in time,  $\delta\mathbf{P}(t) = \delta\mathbf{P}_0 \Theta(t) \Theta(\tau_0 - t)$ ,<sup>4</sup> with the Heaviside function  $\Theta(t) = 0, t < 0$  and  $\Theta(t) = 1, t > 0$ . Here also, the limit  $T \rightarrow \infty$  can be taken in Eqs. (2.4). One obtains (see 2.9.4)

$$\mathcal{P}_1^\infty = \sum_{\alpha \geq 2} \frac{(\delta\mathbf{P}_0 \cdot \mathbf{u}_\alpha)^2}{\lambda_\alpha^3} (\lambda_\alpha \tau_0 - 1 + e^{-\lambda_\alpha \tau_0}), \quad (2.12a)$$

$$\mathcal{P}_2^\infty = \sum_{\alpha \geq 2} \frac{(\delta\mathbf{P}_0 \cdot \mathbf{u}_\alpha)^2}{\lambda_\alpha} (1 - e^{-\lambda_\alpha \tau_0}). \quad (2.12b)$$

As in Eqs. (2.10), both performance measures depend on  $\delta\mathbf{P}_0 \cdot \mathbf{u}_\alpha$ . After averaging over the same ensemble of perturbation vectors as above, Eq. (2.12) becomes (see Supplemental Material)

$$\langle \mathcal{P}_1^\infty \rangle = \langle \delta P_0^2 \rangle \sum_{\alpha \geq 2} \frac{\lambda_\alpha \tau_0 - 1 + e^{-\lambda_\alpha \tau_0}}{\lambda_\alpha^3} \simeq \begin{cases} \langle \delta P_0^2 \rangle \tau_0^2 Kf_1 / 2n, & \lambda_\alpha \tau_0 \ll 1, \forall \alpha, \\ \langle \delta P_0^2 \rangle \tau_0 Kf_2 / n, & \lambda_\alpha \tau_0 \gg 1, \forall \alpha. \end{cases} \quad (2.13a)$$

$$\langle \mathcal{P}_2^\infty \rangle = \langle \delta P_0^2 \rangle \sum_{\alpha \geq 2} \frac{1 - e^{-\lambda_\alpha \tau_0}}{\lambda_\alpha} \simeq \begin{cases} \langle \delta P_0^2 \rangle \tau_0 Kf_0 / n, & \lambda_\alpha \tau_0 \ll 1, \forall \alpha, \\ \langle \delta P_0^2 \rangle Kf_1 / n, & \lambda_\alpha \tau_0 \gg 1, \forall \alpha. \end{cases} \quad (2.13b)$$

Compared to Dirac delta perturbations,  $\langle \mathcal{P}_1^\infty \rangle$  now depends on  $Kf_2$  when  $\tau_0$  is the longest time scale. This is so, because time-extended perturbations scatter through the network before they are damped by  $\perp$ . Accordingly, they depend on details of the network contained in higher moments of the distribution of resistance distances, hence on a generalized Kirchhoff index of higher order.

### Noisy perturbation

We finally consider fluctuating perturbations characterized by zero average and second moment  $\overline{\delta P_i(t_1) \delta P_j(t_2)} = \delta_{ij} \delta P_{0i}^2 \exp[-|t_1 - t_2|/\tau_0]$  correlated over a typical time scale  $\tau_0$ . Because this perturbation is not limited in time, we consider  $\mathcal{P}_{1,2}(T)$  at finite but large  $T$ . Keeping only the leading order term in  $T$ , we have (see 2.9.5)

$$\overline{\mathcal{P}_1}(T) = T \sum_{\alpha} \frac{\sum_{i \in N_n} \delta P_{0i}^2 u_{\alpha,i}^2}{\lambda_\alpha (\lambda_\alpha + \tau_0^{-1})} + \mathcal{O}(T^0), \quad (2.14a)$$

$$\overline{\mathcal{P}_2}(T) = (T/\tau_0) \sum_{\alpha} \frac{\sum_{i \in N_n} \delta P_{0i}^2 u_{\alpha,i}^2}{\lambda_\alpha + \tau_0^{-1}} + \mathcal{O}(T^0). \quad (2.14b)$$

<sup>4</sup>We also refer to such perturbation as *quench perturbation*.

The response is determined by the overlap of the perturbation vector with the eigenmodes of  $\mathbb{L}$ . The noise amplitude  $\delta P_{0i}^2$  is localized on the set  $N_n$  of noisy nodes. Averaging over an ensemble of perturbations defined by all permutations of the noisy nodes over all nodes (see 2.9.5),  $\langle \mathcal{P}_{1,2} \rangle$  is given by Eqs. (2.14) with  $\sum_i \delta P_{0i}^2 u_{\alpha,i}^2 \rightarrow \langle \delta P_0^2 \rangle$ . If  $\tau_0^{-1}$  lies inside the spectrum of  $\mathbb{L}$ ,  $\mathcal{P}_{1,2}$  are functions of the spectrum of  $\mathbb{L}$  and the inverse correlation time  $\tau_0^{-1}$ . If, on the other hand,  $\tau_0^{-1}$  lies outside the spectrum of  $\mathbb{L}$ , averaged measures are directly expressible as infinite sums over generalized Kirchhoff indices,  $\langle \mathcal{P}_{1,2} \rangle = n^{-1} \langle \delta P_0^2 \rangle T \sum_{m=0}^{\infty} C_{1,2}^{(m)}$  with

$$C_1^{(m)} = \begin{cases} (-1)^m \tau_0^{-(m+1)} Kf_{-m+1}, & \lambda_\alpha \tau_0 < 1, \\ (-1)^m \tau_0^{-m} Kf_{m+2}, & \lambda_\alpha \tau_0 > 1, \end{cases} \quad (2.15a)$$

$$C_2^{(m)} = \begin{cases} (-1)^m \tau_0^m Kf_{-m}, & \lambda_\alpha \tau_0 < 1, \\ (-1)^m \tau_0^{-(m+1)} Kf_{m+1}, & \lambda_\alpha \tau_0 > 1. \end{cases} \quad (2.15b)$$

## Numerical simulations

To confirm our results numerically, we focus on  $\mathcal{P}_1$  for both box and noisy perturbations, varying their time scale  $\tau_0$ . We consider Eq. (2.1) with two types of networks, (i) small-world networks, where a cycle graph with constant coupling  $a_{ij} = a_0$  for any node  $i$  to its 4 nearest neighbors undergoes random rewiring with probability  $p_r \in [0, 1]$  [126]<sup>5</sup>, and (ii) simple cyclic networks where each node is coupled to its nearest- and  $q^{\text{th}}$ -neighbors with a constant coupling  $a_{i,i\pm 1} = a_{i,i\pm q} = a_0$  (see inset in Fig. 2.2). In both cases, we fix the number of nodes to  $n = 50$ . In all cases, the unperturbed natural frequencies vanish,  $P_i^{(0)} = 0$ . The box perturbation has  $\delta \mathbf{P}_0 = (0, 0, \dots, \delta P_{0i_1}, 0, \dots, \delta P_{0i_2}, 0, \dots)$  with  $\delta P_{0i_1} = -\delta P_{0i_2} = 0.01 a_0$ , and averaging is performed over all pairs of nodes  $(i_1, i_2)$ . The noisy perturbation acts on all nodes, and we construct noise sequences  $P_i(t)$  satisfying  $\overline{\delta P_i(t_1) \delta P_j(t_2)} = \delta_{ij} \delta P_{0i}^2 \exp[-|t_1 - t_2|/\tau_0]$  using the method described in Ref. [48], with  $\delta P_{0i} = 0.01 a_0$ .

The theory is numerically confirmed for small-world networks in Fig. 2.1, where  $\mathcal{P}_1$  decreases monotonously as the rewiring probability  $p$  increases, in complete agreement with the predictions of Eqs. (2.13a) and (2.14a) (colored solid lines). This is qualitatively understood as follows. As  $p_r$  increases and more network edges are rewired, more couplings with longer range appear in the network, which stiffens the synchronous state. Fig. 2.1 shows that the resulting decrease in fragility of synchrony occurs already with  $p_r \simeq 0.1 - 0.2$ , where only few long-range couplings exist in the network – true small-world networks [126]. Earlier works showed that small-world networks have larger range of parameters over which synchrony prevails, compared to random networks [10]. Fig. 2.1 shows that, additionally, synchronous states in small-world networks are more robust than in regular networks.

Further insight into synchrony fragility is obtained when considering our cyclic graph model with nearest- and  $q^{\text{th}}$ -neighbor coupling. If the range of the coupling were the only ingredient

<sup>5</sup>Small-world networks roughly correspond to a  $p \simeq 0.1$  rewiring probability. Here we refer to the rewiring model defined in Ref. [126] as "small-world networks" for any  $p \in [0, 1]$  by some abuse of language.

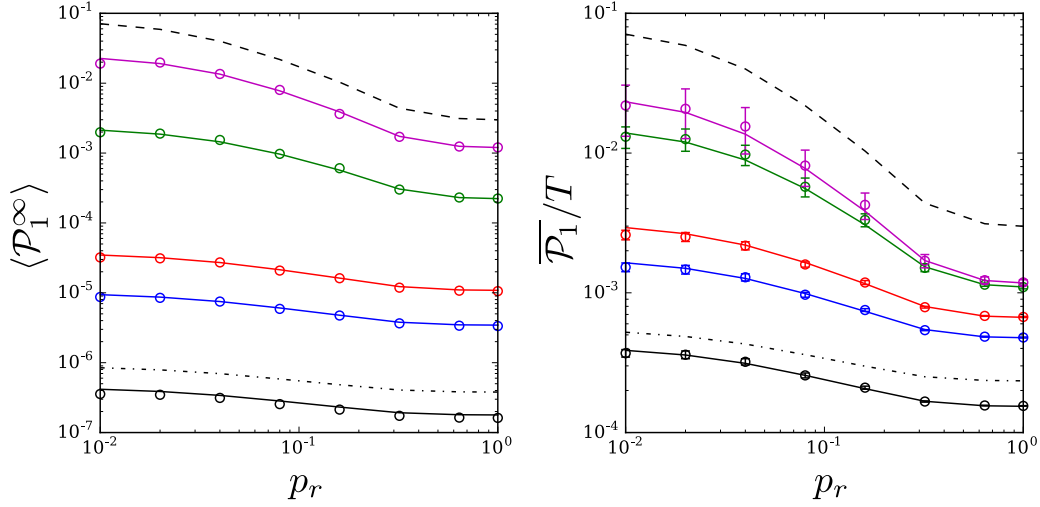


Figure 2.1 – Performance measure  $\langle \mathcal{P}_1^\infty \rangle$  (for box perturbation, left panel) and  $\overline{\mathcal{P}_1}/T$  (for noisy perturbation, right panel) for the small-world model with  $n = 50$  nodes as a function of the rewiring probability  $p_r$  [126] and with  $\tau_0 = 0.1/a_0$  (black),  $0.5/a_0$  (blue),  $1/a_0$  (red),  $10/a_0$  (green) and  $50/a_0$  (violet). Solid lines give Eqs. (2.13a) (left) and (2.14a) (right) calculated numerically over an ensemble of networks obtained from 20 different rewirings. The dotted-dashed lines give  $Kf_1$  and the dashed lines  $Kf_2$ , both vertically shifted. In the right panel,  $\overline{\mathcal{P}_1}(T)$  is averaged over  $T' \in [T - 200/a_0, T + 200/a_0]$  with  $T = 800/a_0$ , and error bars give the standard deviation of numerically obtained values with 10 different noise sequences.

determining the fragility of the synchronous state, then one would observe a monotonous decrease of  $\mathcal{P}_1$  as a function of  $q$ . Fig. 2.2 shows numerical results for the cyclic graphs and five values of  $\tau_0$  ranging from  $\lambda_\alpha \tau_0 \lesssim 1$  to  $\lambda_\alpha \tau_0 \gtrsim 1, \forall \alpha$ . Analytical results of Eqs. (2.13a) and (2.14a), in particular, the crossover from  $\langle \mathcal{P}_1^\infty \rangle \sim Kf_1$  to  $\langle \mathcal{P}_1^\infty \rangle \sim Kf_2$  predicted in Eq. (2.13a) when  $\tau_0$  increases, are clearly confirmed. Particularly remarkable is that  $Kf_1$  and  $Kf_2$  are not monotonous in the coupling range  $q$  (see 2.9.7), which is clearly reflected in the behavior of  $\langle \mathcal{P}_1^\infty \rangle$ . This unambiguously demonstrates that average fragility of synchrony does not depend trivially on the range of the couplings between oscillators, but is entirely determined by generalized Kirchhoff indices.

## Conclusion

Using both performance measures defined in Eqs. (2.4), we have expressed synchrony fragility in terms of the weighted Laplacian matrix  $\mathbb{L}$  of the system's network. We have first shown that the response to specific perturbations is determined by both the spectrum of  $\mathbb{L}$  and its eigenmodes  $\mathbf{u}_\alpha$  through their scalar product  $\delta \mathbf{P}_0 \cdot \mathbf{u}_\alpha$  with the perturbation vector. Eqs. (2.10), (2.12) and (2.14) clearly indicate that perturbations overlapping with the eigenmodes with smallest Lyapunov exponents have the largest impact on the synchronous state. The most vulnerable nodes are accordingly identified as the nodes carrying these eigenmodes. Second, we considered performance measures averaged over ergodic ensembles of perturbations. In

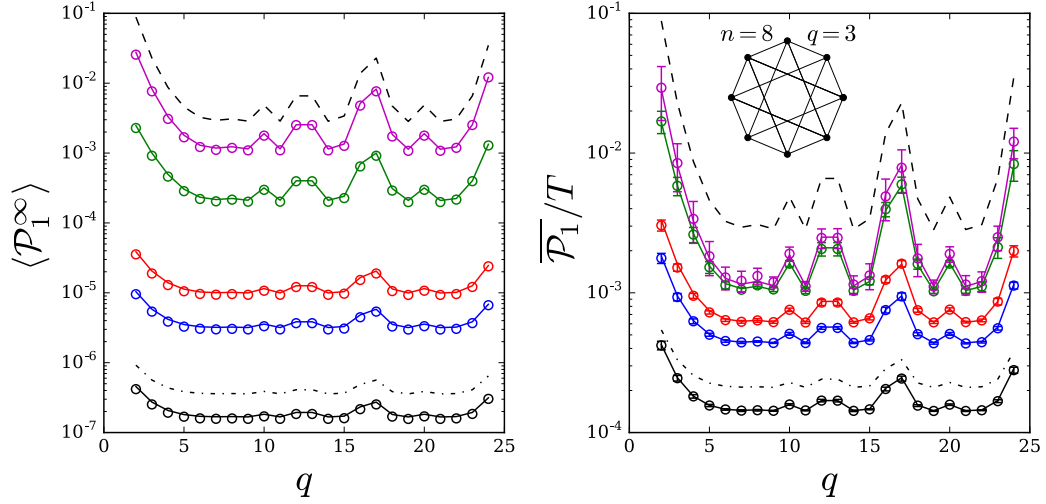


Figure 2.2 – Performance measure  $\langle \mathcal{P}_1^\infty \rangle$  (for box perturbation, left panel) and  $\overline{\mathcal{P}_1}/T$  (for noisy perturbation, right panel) for the cyclic graph with  $n = 50$  nodes with nearest- and  $q^{\text{th}}$ -neighbor coupling,  $a_{i,i\pm 1} = b_{i,i\pm q} = a_0$ , as a function of  $q$  and with  $\tau_0 = 0.1/a_0$  (black),  $0.5/a_0$  (blue),  $1/a_0$  (red),  $10/a_0$  (green) and  $50/a_0$  (violet). Solid lines give Eqs. (2.13a) (left) and (2.14a) (right). The dotted-dashed lines give  $Kf_1$  and the dashed lines  $Kf_2$ , both vertically shifted. In the right panel,  $\overline{\mathcal{P}_1}(T)$  is averaged over  $T' \in [T - 200/a_0, T + 200/a_0]$  with  $T = 800/a_0$ , and error bars give the standard deviation of numerically obtained values with 10 different realizations of noisy perturbations. The inset sketches the model for  $n = 8$  and  $q = 3$ .

this case, they depend on  $\mathbb{L}$  only through generalized Kirchhoff indices, which we introduced in Eq. (2.9). The latter are both spectral and topological in nature, as they can be re-expressed in terms of the resistance distances in the virtual network defined by  $\mathbb{L}$  (see 2.9.1). A network's average/global fragility can therefore be easily quantified by a direct calculation of generalized Kirchhoff indices. This is a computationally easy task, requiring in most instances to determine few of the smallest eigenvalues of  $\mathbb{L}$ , and that, for a given system, can be done for few typical fixed points once and for all. Our findings are rather general and generalized Kirchhoff indices naturally characterize the fragility of synchronous states for many coupled dynamical systems, beyond the Kuramoto model considered here as well as for other types of perturbation not discussed here (see 2.9.8).

Two extensions of this work should be considered in priority. First, our approach has been based on the implicit assumption that the perturbation is sufficiently weak that the system stays close to its initial state. Criteria for acute vulnerability should account for the breakdown of this assumption and quantify the perturbation threshold above which networks either lose synchrony or change their synchronous state. Second, synchrony fragility for second-order systems with inertia should be considered, investigating in particular more closely the case of electric power grids under the influence of fluctuating power injections [131]. Work along those lines is in progress.

## Appendix

### Generalized Kirchhoff indices

For a complex graph determined by its Laplacian matrix  $\mathbb{L}$ , we introduce a family of graph invariants

$$Kf_p = n \sum_{\alpha \geq 2} \lambda_\alpha^{-p}, \quad (2.16)$$

where  $\lambda_\alpha$  is an eigenvalue of  $\mathbb{L}$ . We call them *generalized Kirchhoff indices* because the Kirchhoff index introduced in Ref. [71] can be expressed as [133, 56]

$$Kf_1 = n \sum_{\alpha \geq 2} \lambda_\alpha^{-1}. \quad (2.17)$$

We show that, just like the original Kirchhoff index  $Kf_1$ , generalized Kirchhoff indices can be expressed as functions of the resistance distances between any pair of nodes  $(i, j)$  in the network. The network's Laplacian matrix  $\mathbb{L}$  has one zero eigenvalue. We therefore define the matrix  $\Gamma$

$$\Gamma = \mathbb{L} + \mathbf{u}_1 \mathbf{u}_1^\top, \quad (2.18)$$

in terms of which the resistance distance  $\Omega_{ij}^{(1)}$  between nodes  $i$  and  $j$  is defined as [71]

$$\Omega_{ij}^{(1)} = \Gamma_{ii}^{-1} + \Gamma_{jj}^{-1} - \Gamma_{ij}^{-1} - \Gamma_{ji}^{-1}. \quad (2.19)$$

This can be rewritten in terms of the eigenvectors of  $\mathbb{L}$  as [28]

$$\Omega_{ij}^{(1)} = \sum_{\alpha \geq 2} \frac{(u_{\alpha,i} - u_{\alpha,j})^2}{\lambda_\alpha}, \quad (2.20)$$

where the zero mode corresponding to  $\lambda_1 = 0$  is omitted in the sum. We show that  $Kf_1$  and  $Kf_2$  can be rewritten in terms of resistance distances. For  $Kf_1$ , one has

$$\sum_{i < j} \Omega_{ij}^{(1)} = \frac{1}{2} \sum_{i,j} \sum_{\alpha \geq 2} \frac{(u_{\alpha,i} - u_{\alpha,j})^2}{\lambda_\alpha} = Kf_1, \quad (2.21)$$

because the eigenvectors  $\alpha \geq 2$  of  $\mathbb{L}$  satisfy  $\sum_i u_{\alpha,i} = 0$  and  $\sum_i u_{\alpha,i}^2 = 1$ . To express  $Kf_2$ , higher moments of the distribution of resistance distances are needed. One has,

$$\sum_{i,j} \Omega_{ij}^{(1)2} = \sum_{i,j;\alpha,\beta \geq 2} \frac{(u_{\alpha,i} - u_{\alpha,j})^2 (u_{\beta,i} - u_{\beta,j})^2}{\lambda_\alpha \lambda_\beta} = 2n \sum_{i;\alpha,\beta \geq 2} \frac{u_{\alpha,i}^2 u_{\beta,i}^2}{\lambda_\alpha \lambda_\beta} + \frac{2(Kf_1)^2}{n^2} + \frac{4Kf_2}{n}, \quad (2.22)$$

$$\sum_{i,j,k} \Omega_{ij}^{(1)} \Omega_{jk}^{(1)} = \sum_{i,j,k;\alpha,\beta \geq 2} \frac{(u_{\alpha,i} - u_{\alpha,j})^2 (u_{\beta,j} - u_{\beta,k})^2}{\lambda_\alpha \lambda_\beta} = \frac{3(Kf_1)^2}{n} + n^2 \sum_{i;\alpha,\beta \geq 2} \frac{u_{\alpha,i}^2 u_{\beta,i}^2}{\lambda_\alpha \lambda_\beta}. \quad (2.23)$$

Combining the latter two equations, one has

$$\frac{n}{4} \left( \sum_{i,j} \Omega_{ij}^{(1)2} \right) - \frac{1}{2} \left( \sum_{i,j,k} \Omega_{ij}^{(1)} \Omega_{jk}^{(1)} \right) + \frac{(Kf_1)^2}{n} = Kf_2. \quad (2.24)$$

For  $p \geq 3$ , it is possible though algebraically tedious to show that  $Kf_p$  can be expressed in a similar way in terms of higher moments of resistance distances.

### Direct calculation of fragility measures

The fragility performance measures introduced in Eqs. (2.4) of the main text can be rewritten in terms of the coefficients of the expansion  $\delta\boldsymbol{\theta}(t) = \sum_{\alpha} c_{\alpha}(t)\mathbf{u}_{\alpha}$  of angle displacements over the eigenvectors  $\mathbf{u}_{\alpha}$  of  $\mathbb{L}$ . One has

$$\mathcal{P}_1(T) = \sum_{\alpha \geq 2} \int_0^T c_{\alpha}^2(t) dt, \quad \mathcal{P}_2(T) = \sum_{\alpha \geq 2} \int_0^T \dot{c}_{\alpha}^2(t) dt. \quad (2.25)$$

The coefficients  $c_{\alpha}(t)$  are solutions of

$$c_{\alpha}(t) = e^{-\lambda_{\alpha}t} c_{\alpha}(0) + e^{-\lambda_{\alpha}t} \int_0^t dt' e^{\lambda_{\alpha}t'} \delta\mathbf{P}(t') \cdot \mathbf{u}_{\alpha}, \quad (2.26)$$

and in our case where the perturbation starts at  $t = 0$ ,  $c_{\alpha}(0) = 0$ . We treat sequentially, and in some additional details, the three perturbations considered in the main text.

### Dirac delta perturbation

We first consider  $\delta\mathbf{P}(t) = \delta\mathbf{P}_0\tau_0\delta(t)$ . Inserting it into Eq. (2.26) one obtains,

$$c_{\alpha}(t) = (\delta\mathbf{P}_0 \cdot \mathbf{u}_{\alpha})\tau_0 e^{-\lambda_{\alpha}t}. \quad (2.27)$$

This directly gives

$$\mathcal{P}_1(T) = \sum_{\alpha \geq 2} \frac{(\delta\mathbf{P}_0 \cdot \mathbf{u}_{\alpha})^2 \tau_0^2}{2\lambda_{\alpha}} (1 - e^{-2\lambda_{\alpha}T}), \quad \mathcal{P}_2(T) = \sum_{\alpha \geq 2} \frac{(\delta\mathbf{P}_0 \cdot \mathbf{u}_{\alpha})^2 \tau_0^2}{2} \lambda_{\alpha} (1 - e^{-2\lambda_{\alpha}T}). \quad (2.28)$$

Taking the limit  $\lambda_{\alpha}T \gg 1$ , one obtains Eqs. (10a,b) of the main text,

$$\mathcal{P}_1(T \rightarrow \infty) = \mathcal{P}_1^{\infty} = \frac{\tau_0^2}{2} \sum_{\alpha \geq 2} \frac{(\delta\mathbf{P}_0 \cdot \mathbf{u}_{\alpha})^2}{\lambda_{\alpha}}, \quad (2.29a)$$

$$\mathcal{P}_2(T \rightarrow \infty) = \mathcal{P}_2^{\infty} = \frac{\tau_0^2}{2} \sum_{\alpha \geq 2} (\delta\mathbf{P}_0 \cdot \mathbf{u}_{\alpha})^2 \lambda_{\alpha}. \quad (2.29b)$$

Averaging over the ensemble of perturbation vectors defined by  $\langle \delta P_{0i} \rangle = 0$ ,  $\langle \delta P_{0i} \delta P_{0j} \rangle = \delta_{ij} \langle \delta P_0^2 \rangle$ , we have  $\langle (\delta\mathbf{P}_0 \cdot \mathbf{u}_{\alpha})^2 \rangle = \sum_{i,j} \langle \delta P_{0i} \delta P_{0j} \rangle \mathbf{u}_{\alpha,i} \mathbf{u}_{\alpha,j} = \langle \delta P_0^2 \rangle$ ,  $\forall \alpha$ . The averaged fragility

## Chapter 2. Robustness of Synchrony in Complex Networks and Generalized Kirchhoff Indices

---

measures become,

$$\langle \mathcal{P}_1^\infty \rangle = \frac{\langle \delta P_0^2 \rangle \tau_0^2}{2} \sum_{\alpha \geq 2} \frac{1}{\lambda_\alpha} = \frac{\langle \delta P_0^2 \rangle \tau_0^2}{2n} Kf_1, \quad (2.30a)$$

$$\langle \mathcal{P}_2^\infty \rangle = \frac{\langle \delta P_0^2 \rangle \tau_0^2}{2} \sum_{\alpha \geq 2} \lambda_\alpha = \frac{\langle \delta P_0^2 \rangle \tau_0^2}{2n} Kf_{-1}, \quad (2.30b)$$

just as in Eqs. (2.11) in the main text.

### Box perturbation

We next consider  $\delta \mathbf{P}(t) = \delta \mathbf{P}_0 \Theta(t) \Theta(\tau_0 - t)$ . Eq. (2.26) with  $c_\alpha(0) = 0$  now gives,

$$c_\alpha(t) = \begin{cases} (\delta \mathbf{P}_0 \cdot \mathbf{u}_\alpha)(1 - e^{-\lambda_\alpha t}) / \lambda_\alpha, & t \leq \tau_0, \\ (\delta \mathbf{P}_0 \cdot \mathbf{u}_\alpha)(e^{\lambda_\alpha(\tau_0 - t)} - e^{-\lambda_\alpha t}) / \lambda_\alpha, & t > \tau_0. \end{cases} \quad (2.31)$$

Eqs. (2.25) become

$$\mathcal{P}_1(T) = \sum_{\alpha \geq 2} \frac{(\delta \mathbf{P}_0 \cdot \mathbf{u}_\alpha)^2}{\lambda_\alpha^3} \left( \lambda_\alpha \tau_0 - 1 + e^{-\lambda_\alpha \tau_0} - \frac{e^{2\lambda_\alpha(\tau_0 - T)}}{2} + e^{\lambda_\alpha(\tau_0 - T)} - \frac{e^{-2\lambda_\alpha T}}{2} \right), \quad (2.32a)$$

$$\mathcal{P}_2(T) = \sum_{\alpha \geq 2} \frac{(\delta \mathbf{P}_0 \cdot \mathbf{u}_\alpha)^2}{\lambda_\alpha} \left( 1 - e^{-\lambda_\alpha \tau_0} - \frac{e^{2\lambda_\alpha(\tau_0 - T)}}{2} + e^{\lambda_\alpha(\tau_0 - 2T)} - \frac{e^{-2\lambda_\alpha T}}{2} \right). \quad (2.32b)$$

Taking the limit  $\lambda_\alpha T \gg 1$ , one recovers Eqs. (2.12) in the main text,

$$\mathcal{P}_1^\infty = \sum_{\alpha \geq 2} \frac{(\delta \mathbf{P}_0 \cdot \mathbf{u}_\alpha)^2}{\lambda_\alpha^3} (\lambda_\alpha \tau_0 - 1 + e^{-\lambda_\alpha \tau_0}), \quad (2.33a)$$

$$\mathcal{P}_2^\infty = \sum_{\alpha \geq 2} \frac{(\delta \mathbf{P}_0 \cdot \mathbf{u}_\alpha)^2}{\lambda_\alpha} (1 - e^{-\lambda_\alpha \tau_0}). \quad (2.33b)$$

Following the same averaging procedure as for the  $\delta$ -perturbation, one finally recovers Eqs. (2.13) in the main text,

$$\langle \mathcal{P}_1^\infty \rangle = \langle \delta P_0^2 \rangle \sum_{\alpha \geq 2} \frac{1}{\lambda_\alpha^3} (\lambda_\alpha \tau_0 - 1 + e^{-\lambda_\alpha \tau_0}), \quad (2.34a)$$

$$\langle \mathcal{P}_2^\infty \rangle = \langle \delta P_0^2 \rangle \sum_{\alpha \geq 2} \frac{1}{\lambda_\alpha} (1 - e^{-\lambda_\alpha \tau_0}). \quad (2.34b)$$

The asymptotic behaviors for  $\lambda_\alpha \tau_0 \ll 1$  and  $\lambda_\alpha \tau_0 \gg 1$  are easily computed via a Taylor-expansion.

### Noisy perturbation

We finally consider fluctuating perturbations characterized by zero average  $\overline{\delta P_{0i}} = 0$ , and second moments  $\overline{\delta P_i(t_1) \delta P_j(t_2)} = \delta_{ij} \delta P_{0i}^2 \exp[-\tau_0^{-1} |t_1 - t_2|]$  correlated over a typical time

scale  $\tau_0$ . With this ensemble average, one obtains,

$$\begin{aligned}
 \overline{\mathcal{P}}_1(T) &= \sum_{\alpha \geq 2} \int_0^T \overline{c_\alpha^2(t)} dt \\
 &= \sum_{\alpha \geq 2} \int_0^T e^{-2\lambda_\alpha t} \int_0^t \int_0^t e^{\lambda_\alpha(t_1+t_2)} \overline{\delta \mathbf{P}(t_1) \cdot \mathbf{u}_\alpha \delta \mathbf{P}(t_2) \cdot \mathbf{u}_\alpha} dt_1 dt_2 dt \\
 &= \sum_{\alpha \geq 2} \sum_i (\delta P_{0i} u_{\alpha,i})^2 \int_0^T e^{-2\lambda_\alpha t} \int_0^t \int_0^t e^{\lambda_\alpha(t_1+t_2)} e^{-|t_1-t_2|/\tau_0} dt_1 dt_2 dt \\
 &= \sum_{\alpha \geq 2} \sum_i (\delta P_{0i} u_{\alpha,i})^2 \left[ \frac{T}{\lambda_\alpha(\lambda_\alpha + \tau_0^{-1})} + \frac{1 - e^{-2\lambda_\alpha T}}{2\lambda_\alpha^2(\lambda_\alpha - \tau_0^{-1})} + \frac{2(e^{-(\lambda_\alpha + \tau_0^{-1})T} - 1)}{(\lambda_\alpha + \tau_0^{-1})(\lambda_\alpha^2 - \tau_0^{-2})} \right].
 \end{aligned}$$

To calculate  $\overline{\mathcal{P}}_2$  we note that,

$$\overline{\hat{c}_\alpha^2(t)} = \lambda_\alpha^2 \overline{c_\alpha^2(t)} + \overline{(\delta \mathbf{P}(t) \cdot \mathbf{u}_\alpha)^2} - 2\lambda_\alpha e^{-\lambda_\alpha t} \int_0^t e^{\lambda_\alpha t'} \overline{\delta \mathbf{P}(t') \cdot \mathbf{u}_\alpha \delta \mathbf{P}(t) \cdot \mathbf{u}_\alpha} dt'. \quad (2.35)$$

One obtains, after some algebra

$$\overline{\mathcal{P}}_2(T) = \sum_{\alpha \geq 2} \sum_i (\delta P_{0i} u_{\alpha,i})^2 \left[ \frac{T}{\tau_0(\lambda_\alpha + \tau_0^{-1})} + \frac{1 - e^{-2\lambda_\alpha T}}{2(\lambda_\alpha - \tau_0^{-1})} + \frac{2\lambda_\alpha \tau_0^{-1} (e^{-(\lambda_\alpha + \tau_0^{-1})T} - 1)}{(\lambda_\alpha + \tau_0^{-1})(\lambda_\alpha^2 - \tau_0^{-2})} \right].$$

For  $\lambda_\alpha T \gg 1$ , one recovers Eqs. (eq:c12noisy) in the main text,

$$\overline{\mathcal{P}}_1(T) = \sum_{\alpha \geq 2} \sum_i (\delta P_{0i} u_{\alpha,i})^2 \frac{T}{\lambda_\alpha(\lambda_\alpha + \tau_0^{-1})} + \mathcal{O}(T^0), \quad (2.36)$$

$$\overline{\mathcal{P}}_2(T) = \sum_{\alpha \geq 2} \sum_i (\delta P_{0i} u_{\alpha,i})^2 \frac{\tau_0^{-1} T}{(\lambda_\alpha + \tau_0^{-1})} + \mathcal{O}(T^0). \quad (2.37)$$

Averaging over all permutations,  $\sigma$ , of the components of  $\delta \mathbf{P}_0 = (\delta P_{01}, \dots, \delta P_{0n})$ , one has the following identity,

$$\frac{1}{n!} \sum_\sigma \sum_i (\delta P_{0\sigma(i)} u_{\alpha,i})^2 = \frac{(n-1)!}{n!} \left( \sum_i \delta P_{0i}^2 \right) \left( \sum_j u_{\alpha,j}^2 \right) = \frac{(\delta P_0)^2}{n} \equiv \langle \delta P_0^2 \rangle. \quad (2.38)$$

We finally obtain the leading-order contribution in  $T$ ,

$$\langle \mathcal{P}_1 \rangle(T) = \langle \delta P_0^2 \rangle \sum_{\alpha \geq 2} \frac{T}{\lambda_\alpha(\lambda_\alpha + \tau_0^{-1})} + \mathcal{O}(T^0), \quad (2.39)$$

$$\langle \mathcal{P}_2 \rangle(T) = \langle \delta P_0^2 \rangle \sum_{\alpha \geq 2} \frac{\tau_0^{-1} T}{(\lambda_\alpha + \tau_0^{-1})} + \mathcal{O}(T^0), \quad (2.40)$$

which can be Taylor-expanded in geometric series when either  $\lambda_\alpha \tau_0 > 1$  or  $\lambda_\alpha \tau_0 < 1$ ,  $\forall \alpha$  to obtain  $\langle \mathcal{P}_{1,2} \rangle = n^{-1} \langle \delta P_0^2 \rangle T \sum_{m=0}^{\infty} C_{1,2}^{(m)}$ . One easily recovers the coefficients  $P_{1,2}^{(m)}$  given in

## Chapter 2. Robustness of Synchrony in Complex Networks and Generalized Kirchhoff Indices

---

Eqs. (2.15) in the main text. Note that, when  $\lambda_\alpha \tau_0 \ll 1$ ,

$$\langle \mathcal{P}_1 \rangle(T) \simeq \frac{T \langle \delta P_0^2 \rangle}{n} P_1^{(0)} = \frac{T \langle \delta P_0^2 \rangle \tau_0}{n} K f_1, \quad (2.41)$$

$$\langle \mathcal{P}_2 \rangle(T) \simeq \frac{T \langle \delta P_0^2 \rangle}{n} P_2^{(0)} = \frac{T \langle \delta P_0^2 \rangle}{n} K f_0. \quad (2.42)$$

For  $\lambda_\alpha \tau_0 \gg 1$ , one obtains,

$$\langle \mathcal{P}_1 \rangle(T) \simeq \frac{T \langle \delta P_0^2 \rangle}{n} P_1^{(0)} = \frac{T \langle \delta P_0^2 \rangle}{n} K f_2, \quad (2.43)$$

$$\langle \mathcal{P}_2 \rangle(T) \simeq \frac{T \langle \delta P_0^2 \rangle}{n} P_2^{(0)} = \frac{T \langle \delta P_0^2 \rangle}{\tau_0 n} K f_1. \quad (2.44)$$

### Perturbations as Fourier series

From Eq. (2.6) in the main text, it is clear that, with  $c_\alpha(0) = 0$ ,  $\mathcal{P}_{1,2}$  will always be a sum over eigenmodes of  $\mathbb{L}$  labeled  $\alpha$ , and that each term in that sum contains a factor  $(\delta \mathbf{P} \cdot \mathbf{u}_\alpha)^2$ , regardless of the choice of perturbation. Our first main conclusion, that the response of the synchronous state under specific, nonaveraged perturbation depends on the spectrum of  $\mathbb{L}$  and on the overlap of its eigenmodes with the perturbation vector is therefore rather general.

Our approach can moreover be extended to any perturbation that can be expanded in a Fourier series,

$$\delta \mathbf{P}(t) = \sum_f \left( \delta \mathbf{P}_f^+ \exp[2\pi i f t / \tau_0] + \delta \mathbf{P}_f^- \exp[-2\pi i f t / \tau_0] \right). \quad (2.45)$$

The condition that the components of the perturbation vector are real,  $\delta P_i \in \mathbb{R}$ , gives either  $\delta P_{f,i}^+ = \delta P_{f,i}^- \in \mathbb{R}$  or  $\delta P_{f,i}^+ = -\delta P_{f,i}^- \in i\mathbb{R}$ . Because  $\delta \mathbf{P}(t=0) = 0$ , we consider only the latter case in what follows. Eq. (6) in the main text gives

$$c_\alpha(t) = \exp[-\lambda_\alpha t] \sum_{f,i} u_{\alpha,i} \delta P_{f,i}(t) \left( \frac{e^{(\lambda_\alpha + 2\pi i f / \tau_0)t} - 1}{\lambda_\alpha + 2\pi i f / \tau_0} - \frac{e^{(\lambda_\alpha - 2\pi i f / \tau_0)t} - 1}{\lambda_\alpha - 2\pi i f / \tau_0} \right). \quad (2.46)$$

In the long time limit we obtain

$$c_\alpha(t \rightarrow \infty) = \sum_{f,i} u_{\alpha,i} |\delta P_{f,i}(t)| \frac{(4\pi f / \tau_0) \cos(2\pi f t / \tau_0) - 2\lambda_\alpha \sin(2\pi f t / \tau_0)}{\lambda_\alpha^2 + 4\pi^2 f^2 / \tau_0^2} \quad (2.47)$$

To get the average of the performance measure  $\mathcal{P}_1$ , we square this expressions, average it over an homogeneous ensemble of perturbation as in the main text and sum over  $\alpha$ . For a sufficiently long duration of perturbation, integrating over time gives the dominant contribution to the fragility performance measures (under the assumption that  $T$  is large, but shorter than

the duration of the perturbation)

$$\mathcal{P}_1(T) \simeq \frac{T \tau_0^2}{2} \sum_{\alpha, f} \langle \delta \mathbf{P}_{f,0}^2 \rangle \frac{4\lambda_\alpha^2 \tau_0^2 + 16\pi^2 f^2}{(\lambda_\alpha^2 \tau_0^2 + 4\pi^2 f^2)^2}. \quad (2.48)$$

For each Fourier harmonics, the denominator can be Taylor-expanded, depending on whether  $\lambda_\alpha \tau_0 > 2\pi f$  or  $\lambda_\alpha \tau_0 < 2\pi f$ . When  $2\pi f / \tau_0$  lies outside the spectrum of the Laplacian, Eq. (2.48) allows to express  $\mathcal{P}_1(T)$  as a sum over even-order generalized Kirchhoff indices.

## Kirchhoff indices and phase dynamics

### Kirchhoff indices in the cycle model with nearest and $q^{\text{th}}$ -neighbor coupling

The eigenvalues  $\lambda_\alpha$  of the Laplacian of our model with uniform nearest and  $q^{\text{th}}$ -neighbor coupling are obtained by a Fourier transformation and are given by,

$$\lambda_\alpha = 4 - 2 \cos(k_\alpha) - 2 \cos(k_\alpha q), \quad \alpha = 1, \dots, n, \quad (2.49)$$

where  $k_\alpha = \frac{2\pi(\alpha-1)}{n}$ . Then one obtains,

$$Kf_1 = n \sum_{\alpha \geq 2} \frac{1}{4 - 2 \cos(k_\alpha) - 2 \cos(k_\alpha q)}. \quad (2.50)$$

The dependence of the denominator of Eq. (2.50) with  $q$  makes it is clear that  $Kf_1$  is a non monotonous function of  $q$ . This is shown in Fig. 2.3 for  $n = 50$ . As mentioned in the main text, two seemingly similar choices of long range interactions may lead to large differences of the Kirchhoff index. This translates into large variations of the network's average resistance distance, which can be understood topologically in terms of the commensurability of the  $q^{\text{th}}$ -neighbor coupling with the number  $n$  of nodes in the network. Since the resistance distance between any two nodes accounts for all paths between them, one may expect that  $q^{\text{th}}$ -neighbor couplings provide short, alternative paths between nodes, effectively bringing them closer to each other. This is however not always the case. In fact, if  $n$  is a small integer multiple of  $q$ , or nearly so, paths involving multiple  $q$ -range hops, starting from a given node, come back to the initial node or close to it. Such paths only allow to reach nodes in the close vicinity of the starting node and do not reduce significantly the resistance distance between many nodes close to the original one. In contrast, without commensurability between  $q$  and  $n$ , the resistance distance between most of the nodes to the original one is reduced.

This is illustrated in Fig. 2.3 which plots  $Kf_1$  and  $Kf_2$  as a function of  $q$  for  $n = 50$ . As expected peaks are present for  $q = 10, 17$  and  $24$  such that  $n/q$  is a small integer or close to a small integer. The insets of Fig. 2.3 sketch how despite these long range interactions some portions of the network keep the same geodesic distance to the red node 1.

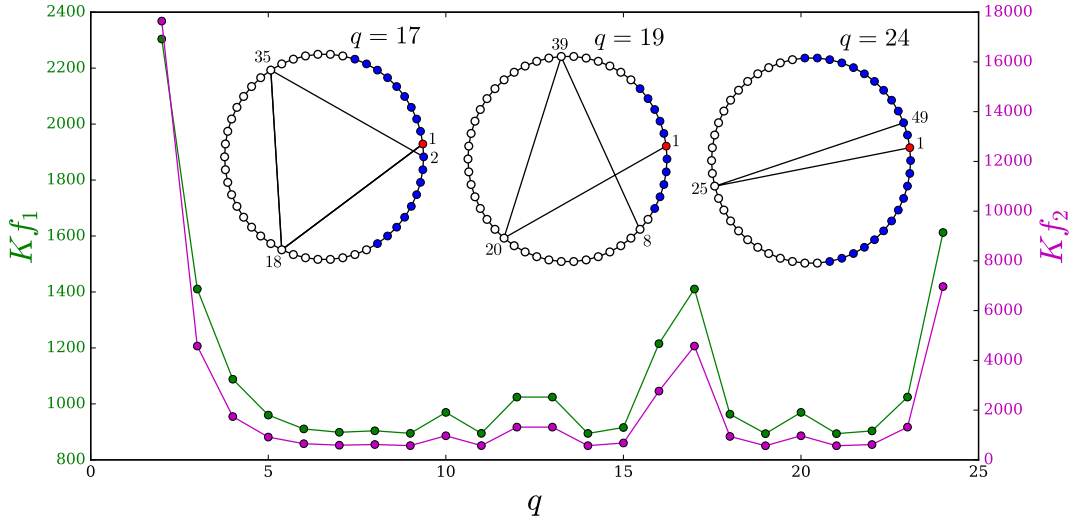


Figure 2.3 –  $Kf_1$  (green) and  $Kf_2$  (violet) for a cyclic graph with  $n = 50$  with nearest and  $q^{\text{th}}$ -neighbor coupling,  $a_{i,i\pm 1} = a_{i,i\pm q} = a_0$ . The inset sketches the model for  $q = 17$ ,  $19$ , and  $24$  and illustrates one path involving  $q^{\text{th}}$ -range interactions starting from node 1 (red). The addition of  $q^{\text{th}}$ -neighbor interactions does not reduce the geodesic distance between the reference node (red) and the set of nodes colored in blue.

### Influence on the phase dynamics

The two seemingly similar cycle models with  $n = 50$ , nearest- and  $q^{\text{th}}$ -neighbor coupling with  $q = 17$  and  $q = 19$  considered in Fig. 2 in the main text nevertheless behave strikingly differently under an external perturbation. This is so, because they have very different generalized Kirchhoff indices  $Kf_1$  and  $Kf_2$ . To illustrate this behavioral discrepancy, Fig. 2.4 compares the phase dynamics for the box perturbation for these two graphs. The left panel is for the cyclic graph with  $q = 17$ , which has a fragility performance measure  $\mathcal{P}_1$  bigger than for the cyclic graph with  $q = 19$  in the right panel. Clearly the angle deviations on the left panel spread more and take more time to return to the initial fixed point after the perturbation than on the right panel. From Eq. (13b) in the main text,  $\langle \mathcal{P}_1^\infty \rangle$  is proportional to  $Kf_2$  in the corresponding limit  $\lambda_\alpha \tau_0 \gg 1 \forall \alpha$ . The numerically obtained values (indicated in Fig. 2.4) of  $\mathcal{P}_1$  follow that trend, though not exactly, as expected for this single realization of perturbation.

### $\lambda_2$ vs. Generalized Kirchhoff indices

Here we show that the generalized Kirchhoff indices give more information on the fragility of synchronous states than the smallest Lyapunov exponent,  $\lambda_2$ . We compare star and cycle graphs with the same number of nodes. In both cases the eigenvalues of the Laplacian matrix can be calculated analytically. The spectrum of the Laplacian of a star graph with  $n$  nodes is  $\{0, 1, n\}$ , with the eigenvalue 1 having multiplicity  $n - 2$ , thus  $\lambda_2 = 1$ ,  $Kf_1 = (n - 1)^2$ , and  $Kf_2 = (n^3 - 2n^2 - 1)/n$ . The spectrum of the Laplacian of a cycle graph with only nearest neighbor

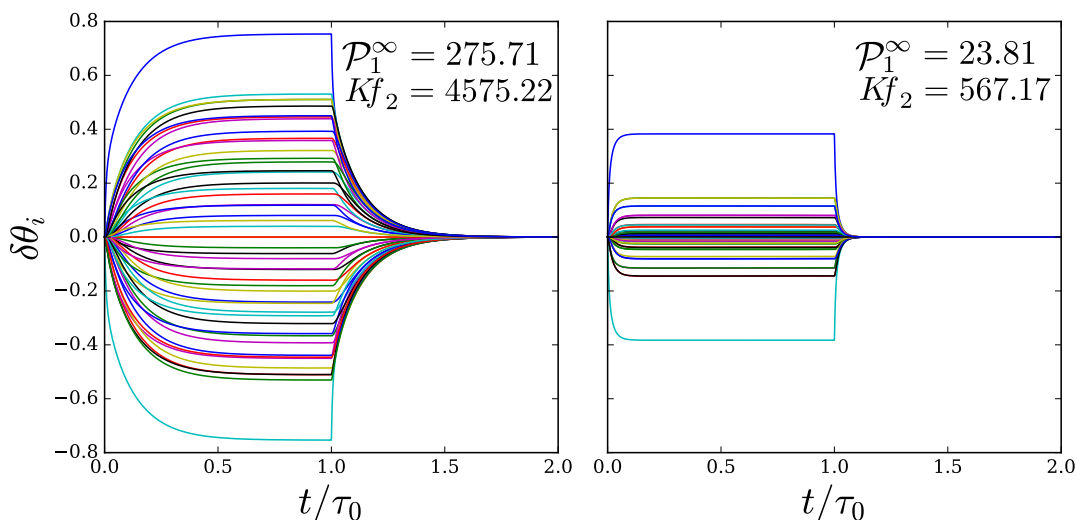


Figure 2.4 – Phases  $\delta\theta_i$  for the cyclic graph with  $n = 50$  with nearest and  $q^{\text{th}}$ -neighbor coupling,  $a_{i,i\pm 1} = a_{i,i\pm q} = a_0$  with  $q = 17$  (left panel) and  $q = 19$  (right panel), as a function of the normalized time  $t/\tau_0$ , for a box perturbation with  $\tau_0 = 50/a_0$  and perturbation vector with non zero components  $\delta P_{0,1} = a_0$ ,  $\delta P_{0,11} = -a_0$ .

coupling is  $\lambda_\alpha = 2[1 - \cos(2\pi(\alpha - 1)/n)]$ , with  $\alpha = 1, \dots, n$ . One has,  $\lambda_2 = 2[1 - \cos(2\pi/n)]$ ,  $Kf_1 = n(n^2 - 1)/12$ , and  $Kf_2 = n(n^2 - 1)(n^2 + 11)/720$ . The density of eigenvalues approaching zero increases with  $n$  in the cycle graph, while in the star graph the Lyapunov exponents accumulate at a finite value as  $n$  increases (i.e.  $\lambda_2 = \lambda_3 = \dots = \lambda_{n-1} = 1$ ). Thus we expect a crossover in the vulnerability of these two network topologies as  $n$  is increased. Fig. 2.5 shows  $\lambda_2$  (left panel), and the performance measure  $\mathcal{P}_1$  in both the limits  $\lambda_\alpha \tau_0 \ll 1$  (center panel) and  $\lambda_\alpha \tau_0 \gg 1$  (right panel) as a function of the number of nodes. For  $n < 6$ , the cycle network has a larger  $\lambda_2$  and a smaller  $\mathcal{P}_1$  compared to the star network which means that the largest contribution to  $Kf_1$  and  $Kf_2$  comes from  $\lambda_2^{-1}$ . However, for  $6 > n > 8$ , both  $Kf_1$  and  $Kf_2$  are not dominated by  $\lambda_2^{-1}$ , therefore the cycle network is less fragile under an external perturbation than the star network even though it has a smaller  $\lambda_2$ . For  $n = 8$  and  $n = 9$ , the cycle network is less fragile against short time perturbation but more fragile against long time perturbation compared to the star network. This reflects the fact that for those values,  $Kf_1$  is smaller for the cycle than for the star network, while the relation is opposite for  $Kf_2$  [see the corresponding relation between  $\mathcal{P}_1$  and generalized Kirchhoff indices in Eq. (2.13a)].

We apply the same analysis to small-world graphs, which are obtained from a  $n = 20$  cycle network with first and second nearest neighbor couplings, which are rewired [126]. Fig. 2.6 shows three graphs obtained with this procedure, which have different relations between  $\lambda_2$  and their generalized Kirchhoff indices  $Kf_1$  and  $Kf_2$ . Graph 1 has a smaller  $\lambda_2$  but smaller  $Kf_1$  or  $Kf_2$  compared to graph 2, while graph 3 has a smaller  $\lambda_2$ , similar  $Kf_1$  and larger  $Kf_2$  compared to graph 2. These relations are reflected by the performance measures  $\mathcal{P}_1$  for box perturbations presented in Table 2.1.

## Chapter 2. Robustness of Synchrony in Complex Networks and Generalized Kirchhoff Indices

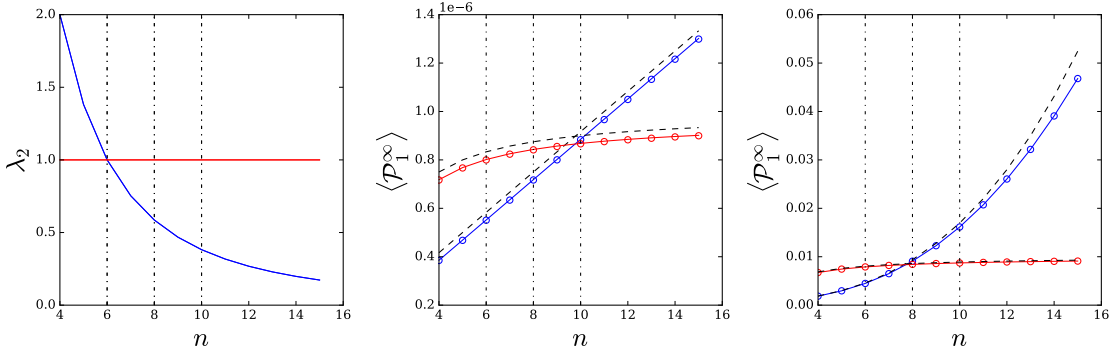


Figure 2.5 –  $\lambda_2$  (left panel) and performance measure  $\langle \mathcal{P}_1^\infty \rangle$  for a box perturbation with  $\tau_0 = 50/a_0$  (center panel) and  $\tau_0 = 0.1/a_0$  (right panel) as a function of the number of nodes for the star network (red) and the cyclic network (blue). Solid lines give Eq. (2.13a). The dashed lines give the two limits of Eq. (2.13a) :  $\lambda_\alpha \tau_0 \ll 1$  (center panel) and  $\lambda_\alpha \tau_0 \gg 1$  (right panel)

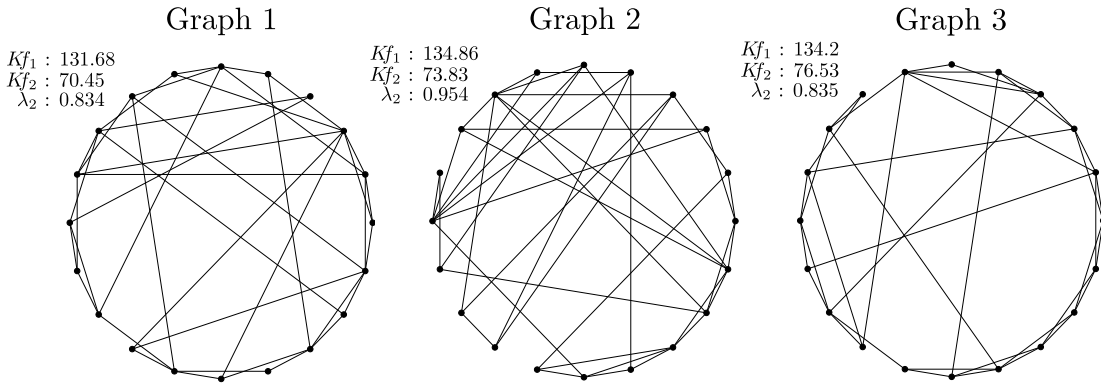


Figure 2.6 – Starting from a homogeneous cyclic network with first and second nearest neighbor couplings and size  $n = 20$ , graphs 1, 2 and 3 have been obtained after rewiring some randomly chosen edges.

Graph	1	2	3
$\lambda_2$	0.834	0.954	0.835
$\lambda_\alpha \tau_0 \ll 1 : \langle \mathcal{P}_1^\infty \rangle \propto Kf_1$	3.16e-7	3.24e-7	3.22e-7
$\lambda_\alpha \tau_0 \gg 1 : \langle \mathcal{P}_1^\infty \rangle \propto Kf_2$	1.83e-3	1.91e-3	1.98e-3

Table 2.1 –  $\lambda_2$ , performance measure  $\langle \mathcal{P}_1^\infty \rangle$  obtained numerically in the two limits :  $\lambda_\alpha \tau_0 \ll 1$  ( $\tau_0 = 0.1/a_0$ ),  $\lambda_\alpha \tau_0 \gg 1$  ( $\tau_0 = 50/a_0$ ).

### Beyond Kuramoto

Instead of the Kuramoto model defined by Eq. (2.1), one may consider other models of coupled dynamical systems. Two extensions have to be differentiated. First, one may consider different coupling than the sine-coupling in the Kuramoto model. This is straightforwardly included in our approach and leads only to a differently weighted Laplacian matrix, giving, for a fixed network, a different Lyapunov spectrum and different eigenmodes  $\mathbf{u}_\alpha$ , but leaving all expressions for the performance measures unchanged. Second, one may consider dynamical systems with more internal degrees of freedom, such as the one considered by Pecora and Carroll [99]

$$\dot{\mathbf{x}} = \mathbf{P}(\mathbf{x}) + \mathbb{B} \otimes \mathbf{H}(\mathbf{x}), \quad (2.51)$$

with  $\mathbf{x} = (\mathbf{x}_1, \mathbf{x}_2, \dots, \mathbf{x}_n)$ ,  $\mathbf{P}(\mathbf{x}) = (\mathbf{f}(\mathbf{x}_1), \mathbf{f}(\mathbf{x}_2), \dots, \mathbf{f}(\mathbf{x}_n))$ ,  $\mathbb{B}$  the Laplacian matrix of the graph considered and  $\mathbf{H}$  a function defining the coupling between adjacent dynamical systems with coordinates  $\mathbf{x}_i \in \mathbb{R}^d$ . Our approach assumes the existence of a synchronous state with  $\mathbf{x}_1^{(0)} = \mathbf{x}_2^{(0)} = \dots = \mathbf{x}_n^{(0)}$ . Linearizing about the synchronous state with  $\mathbf{x} = \mathbf{x}^{(0)} + \delta\mathbf{x}$  and considering a perturbation gives, instead of Eq. (2.2),

$$\delta\dot{\mathbf{x}} = \delta\mathbf{P} + [\mathbb{1} \otimes D\mathbf{P}(\mathbf{x}^{(0)}) + \mathbb{B} \otimes D\mathbf{H}(\mathbf{x}^{(0)})] \delta\mathbf{x}, \quad (2.52)$$

where  $D\mathbf{P}$  and  $D\mathbf{H}$  are Jacobian matrices. The first term on the right-hand side is similar to the perturbation considered above, and the third one is a generalization of the Laplacian term in Eq. (2.2), where the network Laplacian is extended to take account of additional nodal degrees of freedom. The new second term occurs because  $\mathbf{P}$  now depends on internal degrees of freedom  $\mathbf{x}$  (it does not in the Kuramoto model). The formula given for the performance need now to be evaluated with the eigenvalues  $\Lambda_{\alpha,l}$  and eigenmodes  $\mathbf{U}_{\alpha,l}$  of  $[\mathbb{1} \otimes D\mathbf{P}(\mathbf{x}^{(0)}) + \mathbb{B} \otimes D\mathbf{H}(\mathbf{x}^{(0)})]$ ,  $l = 1, 2, \dots, d$ .



# **3 Global Robustness vs. Local Vulnerabilities in Complex Synchronous Networks**

*Chapter 3 is a postprint version of an article published as:  
M. Tyloo, P. Jacquod, *Physical Review E*, 100(3):032303 (2019) [120].*

### Chapter 3. Global Robustness vs. Local Vulnerabilities in Complex Synchronous Networks

---

In complex network-coupled dynamical systems, two questions of central importance are how to identify the most vulnerable components and how to devise a network making the overall system more robust to external perturbations. To address these two questions, we investigate the response of complex networks of coupled oscillators to local perturbations. We quantify the magnitude of the resulting excursion away from the unperturbed synchronous state through quadratic performance measures in the angle or frequency deviations. We find that the most fragile oscillators in a given network are identified by centralities constructed from network resistance distances. Further defining the global robustness of the system from the average response over ensembles of homogeneously distributed perturbations, we find that it is given by a family of topological indices known as generalized Kirchhoff indices. Both resistance centralities and Kirchhoff indices are obtained from a spectral decomposition of the stability matrix of the unperturbed dynamics and can be expressed in terms of resistance distances. We investigate the properties of these topological indices in small-world and regular networks. In the case of oscillators with homogeneous inertia and damping coefficients, we find that inertia only has small effects on robustness of coupled oscillators. Numerical results illustrate the validity of the theory.

## Introduction

Complex networks are widely used to model nature- as well as man-made coupled dynamical systems [104]. Physical realizations of such systems range from microscopic Josephson junction arrays [127] and interacting molecules in chemical reactions [78, 77] to macroscopic high voltage electric power grids [13] and communication or social networks [115, 9]. Individual elements are represented by nodes in a complex network, which have internal parameters and degrees of freedom. The latter are governed by differential equations that depend on both the internal dynamics of the individual elements and the coupling to the adjacent nodes. Two central questions are (i) how to identify nodes, which, once attacked, perturbed or removed, have the most dramatic effect on the overall dynamics of the coupled system and (ii) how to devise a coupling network guaranteeing robustness of the system against random external perturbations. Attempts to answer such questions are often based on complex network theory, numerically relating dynamical effects to graph-theoretic metrics. This approach has been often criticized, e.g. in Refs. [19, 16, 63], because (i) it gives no *a priori* criterion for which metric should be considered in which situation and (ii) it does not directly incorporate the intrinsic dynamics of the network-coupled system.

Here we propose an altogether different analytical approach. First, we use robustness performance measures that quantify the excursion during the transient dynamics following a perturbation. Second, we spectrally decompose the coupling matrix to calculate the response of the system to some external perturbations. Third, by direct calculation, we relate the obtained analytical expressions for performance measures (i) to local centralities when analyzing local vulnerabilities, and (ii) to global topological indices when assessing global robustness of the networked system. Following these steps, we identify a new class of local and global

topological indices that characterize robustness of synchrony of complex network-coupled oscillators. Our method builds up on investigations of consensus algorithms [7, 54], electric power systems [102, 93, 110] and coupled oscillators systems [121, 123]. Already implicitly present in Refs. [54, 93, 110], the Kirchhoff index was first identified as a global robustness quantifier in our earlier work, Ref. [121]. Local vulnerabilities have been more recently connected to centralities related to the resistance distance [54, 123].

In this manuscript, we investigate vulnerabilities and global robustness of synchronous network-coupled oscillators. Frequency synchronization often occurs in such systems when the coupling between individual oscillators is strong enough that they start to oscillate at the same frequency, even when their natural frequency is not homogeneous [117, 100]. Frequency synchronization has attracted a large interest, in particular, the robustness of the synchronous state has been studied from a variety of points of view. One may for instance consider the linear stability of the synchronous state [99], the range of network parameters where synchrony occurs [10, 26, 132], the volume of the basin of attraction of the synchronous state [128, 86, 35], the influence of noise on the synchronous state, in particular how it can lead to desynchronization or drive the system to another synchronous state [38, 60, 107, 61, 122, 62], how disturbances spread across the network [69, 129, 94], or even how topological changes affect synchrony [30, 113, 29]. Here, we investigate the robustness of the synchronous state against external perturbations. For both local and ensemble-averaged perturbations on oscillators with identical dynamical parameters, we find that the robustness of the synchronous state is given by a new family of topological indices based on the resistance distance [71, 121, 123].

The manuscript is organized as follows. Section 3.2 recalls the definition of the resistance distance and generalizes it to graphs corresponding to powers of the Laplacian matrix. Section 3.3 describes our model of coupled oscillators, briefly discusses synchronized states and evaluates how they respond to external perturbations. Performance measures quantifying this response are also introduced and calculated for quench perturbations. Sections 3.4 numerically illustrates the theory on different graphs for local and global vulnerabilities. An analysis of Kirchhoff indices in both small-world and regular networks is also done. We conclude in Section 3.5.

## Resistance Distances, Centralities and Kirchhoff Indices

The resistance distance  $\Omega_{ij}^{(1)}$  is a graph-theoretic metric with an intuitive physical interpretation [71]. To any graph, one associates an electrical network of resistors whose capacities are given by the inverse of the edge weights. In this case,  $\Omega_{ij}^{(1)}$  is the effective resistance between  $i$  and  $j$ , i.e. the voltage that develops between  $i$  and  $j$  when a unit current is injected at  $i$  and collected at  $j$  with no injection nor collection at any other node. The resistance distance can be expressed with the network Laplacian matrix  $\mathbb{L}$  as

$$\Omega_{ij}^{(1)} = \mathbb{L}_{ii}^\dagger + \mathbb{L}_{jj}^\dagger - \mathbb{L}_{ij}^\dagger - \mathbb{L}_{ji}^\dagger, \quad (3.1)$$

### Chapter 3. Global Robustness vs. Local Vulnerabilities in Complex Synchronous Networks

---

where  $\mathbb{L}^\dagger$  is the Moore-Penrose pseudo inverse of  $\mathbb{L}$ . The resistance distance can be formulated in a convenient way using eigenvectors  $\mathbf{u}_\alpha$  and eigenvalues  $\lambda_\alpha$  of  $\mathbb{L}$ . It is given by [130, 29],

$$\Omega_{ij}^{(1)} = \sum_{\alpha \geq 2} \frac{(u_{\alpha,i} - u_{\alpha,j})^2}{\lambda_\alpha}, \quad (3.2)$$

where the zero-eigenvector of  $\mathbb{L}$  corresponding to  $\lambda_1 = 0$  is omitted in the sum. The resistance distance is a graph-theoretic distance metric because (i)  $\Omega_{ii}^{(1)} = 0, \forall i$ , (ii)  $\Omega_{ij} \geq 0 \forall i, j$ , and (iii)  $\Omega_{ij}^{(1)} + \Omega_{jk}^{(1)} \geq \Omega_{ik}^{(1)}, \forall i, j, k$  (triangle inequality) [71].

A measure of nodal centrality is given by the inverse of the average resistance distance from any node  $k$  to all other network nodes,

$$C_1(k) = \left[ n^{-1} \sum_j \Omega_{kj}^{(1)} \right]^{-1} = \left[ \sum_{\alpha \geq 2} \frac{u_{\alpha,k}^2}{\lambda_\alpha} + n^{-2} Kf_1 \right]^{-1}. \quad (3.3)$$

It is a closeness centrality in the usual sense [16], meaning in particular that large values of  $C_1(k)$  indicate nodes  $k$  that are central in the network according to the resistance distance  $\Omega_{ij}^{(1)}$ . The second term in bracket on the right-hand-side of Eq. (3.3) is a graph topological index known as the Kirchhoff index of the network and defined by [71],

$$Kf_1 = \sum_{i < j} \Omega_{ij}^{(1)} = n \sum_{\alpha \geq 2} \lambda_\alpha^{-1}, \quad (3.4)$$

where the second equality follows from Eq. (3.2) [121].

Until now we have introduced global topological indices and local centralities expressed through resistance distances of the original coupling network. In the upcoming sections, we show how resistance distances naturally come out when quantifying robustness of network-coupled oscillators, but that new distance metrics related to powers of the Laplacian matrix also emerge. We therefore generalize Eqs. (3.1)–(3.4) to quantities corresponding to the  $p^{\text{th}}$  power  $\mathbb{L}^p$  of the Laplacian matrix ( $p \in \mathbb{N}$ ). This matrix is still a Laplacian matrix, and the associated resistance distance is defined as

$$\Omega_{ij}^{(p)} = (\mathbb{L}^p)_{ii}^\dagger + (\mathbb{L}^p)_{jj}^\dagger - (\mathbb{L}^p)_{ij}^\dagger - (\mathbb{L}^p)_{ji}^\dagger. \quad (3.5)$$

Still using the eigenvectors and eigenvalues of  $\mathbb{L}$  we have,

$$\Omega_{ij}^{(p)} = \sum_{\alpha \geq 2} \frac{(u_{\alpha,i} - u_{\alpha,j})^2}{\lambda_\alpha^p}. \quad (3.6)$$

One can easily check that  $\Omega_{ij}^{(p)}$  is still a graph-theoretic distance metric satisfying the properties mentioned between Eqs. (3.2) and (3.3). We finally have generalized resistance centralities

[123]

$$C_p(k) = \left[ n^{-1} \sum_j \Omega_{kj}^{(p)} \right]^{-1} = \left[ \sum_{\alpha \geq 2} \frac{u_{\alpha,k}^2}{\lambda_\alpha^p} + n^{-2} Kf_p \right]^{-1}, \quad (3.7)$$

and generalized Kirchhoff indices [121]

$$Kf_p = \sum_{i < j} \Omega_{ij}^{(p)} = n \sum_{\alpha \geq 2} \lambda_\alpha^{-p}. \quad (3.8)$$

We note that generalized resistance distances can in principle be expressed as function of  $\Omega_{ij}^{(1)}$ . For instance one has

$$Kf_2 = \frac{n}{4} \sum_{i,j} \Omega_{ij}^{(1)2} - \frac{1}{2} \sum_{i,j,k} \Omega_{ij}^{(1)} \Omega_{jk}^{(1)} + \frac{(Kf_1)^2}{n}. \quad (3.9)$$

Below we show how global robustness and local vulnerabilities quantified with performances measures can be expressed in terms of the resistance distance-based centralities and the generalized Kirchhoff indices just introduced.

## Synchronized oscillators under external perturbations

### The Kuramoto model with inertia and its linearization

We consider a set of network-coupled oscillators defined by the following set of coupled differential equations,

$$m_i \ddot{\theta}_i + d_i \dot{\theta}_i = P_i - \sum_j a_{ij} \sin(\theta_i - \theta_j). \quad (3.10)$$

Oscillators labeled  $i = 1, \dots, n$  sit on the  $n$  nodes of a weighted graph defined by the adjacency matrix with elements  $a_{ij} \geq 0$ . They have compact angle coordinates  $\theta_i \in (-\pi, \pi]$ , natural frequencies  $P_i / d_i$ <sup>1</sup> and inertia as well as damping parameters  $m_i$  and  $d_i$ . For  $m_i = 0$ , Eq. (3.10) gives the celebrated Kuramoto model on a complex network, for which it is known that when the couplings are sufficiently strong, a finite fraction of, or all oscillators synchronize, i.e. with  $\dot{\theta}_i - \dot{\theta}_j = 0$ , depending on the distribution of the natural frequencies [77, 100, 67, 2]. Here, we consider  $P_i$  defined on a bounded, real interval and set  $\sum_i P_i = 0$  without loss of generality, so that synchronous states have  $\dot{\theta}_i = 0, \forall i$ .

Eq. (3.10) is governed by three sets of time scales. The first one consists of the inverse natural frequencies  $d_i / P_i$ . The second one is given by ratios  $m_i / d_i$  and corresponds to the relaxation time of individual oscillators. Finally, the third one is given by the network relaxation times  $d_i / \lambda_\alpha$  defined by the damping parameters and the eigenvalues  $\lambda_\alpha$  of the weighted Laplacian

<sup>1</sup>By some abuse of language, we often refer to  $P_i$  as natural frequencies.

### Chapter 3. Global Robustness vs. Local Vulnerabilities in Complex Synchronous Networks

matrix defined in Eq. (5.3) below. The first of these sets essentially determines the synchronous state, together with the coupling network. Depending on the other two sets of time scales, perturbations are locally damped or they propagate across the network [121, 123, 94].

We consider a stable fixed-point solution  $\boldsymbol{\theta}^{(0)} = (\theta_1^{(0)}, \dots, \theta_n^{(0)})$  to Eq. (3.10) with unperturbed natural frequencies  $\mathbf{P}^{(0)}$ . We subject this state to a time-dependent perturbation  $\mathbf{P}(t) = \mathbf{P}^{(0)} + \delta\mathbf{P}(t)$ , which renders angles time-dependent,  $\boldsymbol{\theta}(t) = \boldsymbol{\theta}^{(0)} + \delta\boldsymbol{\theta}(t)$ . Linearizing the dynamics of Eq. (3.10) about  $\boldsymbol{\theta}^{(0)}$ , one obtains

$$\mathbf{M}\delta\ddot{\boldsymbol{\theta}} + \mathbf{D}\delta\dot{\boldsymbol{\theta}} = \delta\mathbf{P}(t) - \mathbb{L}(\{\theta_i^{(0)}\})\delta\boldsymbol{\theta}, \quad (3.11)$$

where we introduced inertia and damping matrices,  $\mathbf{M} = \text{diag}\{m_i\}$  and  $\mathbf{D} = \text{diag}\{d_i\}$ , respectively, and the weighted Laplacian matrix  $\mathbb{L}(\{\theta_i^{(0)}\})$  with matrix elements

$$\mathbb{L}_{ij} = \begin{cases} -a_{ij} \cos(\theta_i^{(0)} - \theta_j^{(0)}), & i \neq j, \\ \sum_k a_{ik} \cos(\theta_i^{(0)} - \theta_k^{(0)}), & i = j. \end{cases} \quad (3.12)$$

This Laplacian is minus the stability matrix of the linearized dynamics, and since we consider a stable synchronous state, it is positive semidefinite, with a single eigenvalue  $\lambda_1 = 0$  with eigenvector  $\mathbf{u}_1 = (1, 1, 1, \dots, 1)/\sqrt{n}$ , and  $\lambda_\alpha > 0$ ,  $\alpha = 2, 3, \dots, n$ . From here on, we order the Lyapunov exponents  $\lambda_\alpha$  in increasing order, i.e.  $\lambda_1 = 0 < \lambda_2 < \dots < \lambda_n$ .

Eq. (3.11) can be solved analytically through a spectral expansion if (i) both  $\mathbf{M}$  and  $\mathbf{D}$  commute with  $\mathbb{L}$  or (ii) if  $\mathbf{M}^{-1}\mathbf{D} = \gamma\mathbb{L}$ . In case (i), the spectral expansion is over the eigenmodes of  $\mathbb{L}$ , while in case (ii) it is over the eigenmodes of  $\mathbf{M}^{-1/2}\mathbb{L}\mathbf{M}^{-1/2}$  [93, 29]. Here, we focus on case (i) with  $m_i = m$ ,  $d_i = d \forall i$ .

Expanding the angle deviations over the eigenmodes of  $\mathbb{L}$  as  $\delta\boldsymbol{\theta}(t) = \sum_\alpha c_\alpha(t)\mathbf{u}_\alpha$ , Eq. (3.11) leads to a Langevin equation,

$$m \ddot{c}_\alpha(t) + d \dot{c}_\alpha(t) = \delta\mathbf{P}(t) \cdot \mathbf{u}_\alpha - \lambda_\alpha c_\alpha(t), \quad (3.13)$$

whose general solution reads

$$c_\alpha(t) = m^{-1} e^{-(\gamma + \Gamma_\alpha)t/2} \int_0^t e^{\Gamma_\alpha t_1} \int_0^{t_1} \delta\mathbf{P}(t_2) \cdot \mathbf{u}_\alpha e^{(\gamma - \Gamma_\alpha)t_2/2} dt_2 dt_1, \quad (3.14)$$

with  $\Gamma_\alpha = \sqrt{\gamma^2 - 4\lambda_\alpha/m}$  and  $\gamma = d/m$ . Similar expressions have been derived using the transfer function formalism [93, 55] or within linear response [84, 121, 69]. When  $\gamma^2 < 4\lambda_\alpha/m$ ,  $\Gamma_\alpha \in i\mathbb{R}$  and accordingly,  $|\Gamma_\alpha|$  corresponds to the angular frequency of oscillations along the eigenmode  $\mathbf{u}_\alpha$  of  $\mathbb{L}$ . When on the other hand  $\gamma^2 > 4\lambda_\alpha/m$ ,  $\Gamma_\alpha \in \mathbb{R}$  and gives an additional damping beyond  $\gamma$ . From Eq. (5.10), angle and frequency deviations can be calculated as  $\delta\boldsymbol{\theta}(t) = \sum_\alpha c_\alpha(t)\mathbf{u}_\alpha$ . The above described perturbation in the natural frequencies of Eq. (3.10) models physical disturbances that can occur e.g. when a magnetic field is applied to an array of coupled Josephson junctions [127] or when the injected or consumed powers change in a high voltage

electric power grid [13].

#### Performance Measures

The perturbation  $\delta \mathbf{P}(t)$  moves the oscillators angles and frequencies away from their value at synchrony and renders them time dependent. For not too strong, finite-time perturbations, they eventually relax to their synchronous values and to assess the magnitude of the excursion away from synchrony, we introduce the following quadratic performance measures

$$\mathcal{P}_1(T) = \sum_i \int_0^T |\delta \theta_i(t) - \Delta(t)|^2 dt, \quad (3.15a)$$

$$\mathcal{P}_2(T) = \sum_i \int_0^T |\delta \dot{\theta}_i(t) - \dot{\Delta}(t)|^2 dt. \quad (3.15b)$$

Fig. 3.1 shows the ratio between performance measure  $\mathcal{P}_1$ , defined in Eq. (3.15a), numerically obtained by perturbing each node of graphs (a) and (e) shown in the inset. Even if the average value of the performance measure is lower for graph (e), the latter can be more strongly sensitive to certain local perturbations. Below we show that specific local vulnerabilities and global averaged robustness are determined by nodal centralities and global topological indices (orange). Similar measures have been discussed in the context of consensus algorithms [7, 54], electric power systems [102, 93, 110] and coupled oscillators systems [121, 123]. The results we are about to present directly connect these performance measures to resistance-distance based centralities and Kirchhoff indices introduced in Section 3.2. While similar connections may have been inferred from some of these works (in particular Refs. [93, 110, 121]), to the best of our knowledge, it was first unambiguously stated in Ref. [123].

Because synchronous states are defined modulo any homogeneous angle shift, they are unaffected by the transformation  $\theta_i^{(0)} \rightarrow \theta_i^{(0)} + C$ . Accordingly, only angle shifts with  $\sum_i \delta \theta_i(t) = 0$  matter, which is incorporated in the definitions of  $\mathcal{P}_{1,2}$  by subtracting averages  $\Delta(t) = n^{-1} \sum_j \delta \theta_j(t)$  and  $\dot{\Delta}(t) = n^{-1} \sum_j \delta \dot{\theta}_j(t)$ . If the perturbation is not too strong and finite in time, both  $\mathcal{P}_1$  and  $\mathcal{P}_2$  are finite even for  $T \rightarrow \infty$ . Low values for  $\mathcal{P}_{1,2}^\infty \equiv \mathcal{P}_{1,2}(T \rightarrow \infty)$  indicate then that the system absorbs the perturbation with little fluctuations, while large values indicate a temporary fragmentation of the system into independent pieces – qualitatively speaking,  $\mathcal{P}_{1,2}^\infty$  measures the coherence of the synchronous state [7].

Using the spectral expansion with coefficients given in Eq. (5.10), the performance measures of Eqs. (3.15) read, in our case of homogeneous inertia and damping coefficients

$$\mathcal{P}_1(T) = \sum_{\alpha \geq 2} \int_0^T c_\alpha^2(t) dt, \quad (3.16a)$$

$$\mathcal{P}_2(T) = \sum_{\alpha \geq 2} \int_0^T \dot{c}_\alpha^2(t) dt. \quad (3.16b)$$

Performance measures depend on the perturbation vector  $\delta \mathbf{P}(t) = \delta \mathbf{P}_0 f(t)$ , which may have

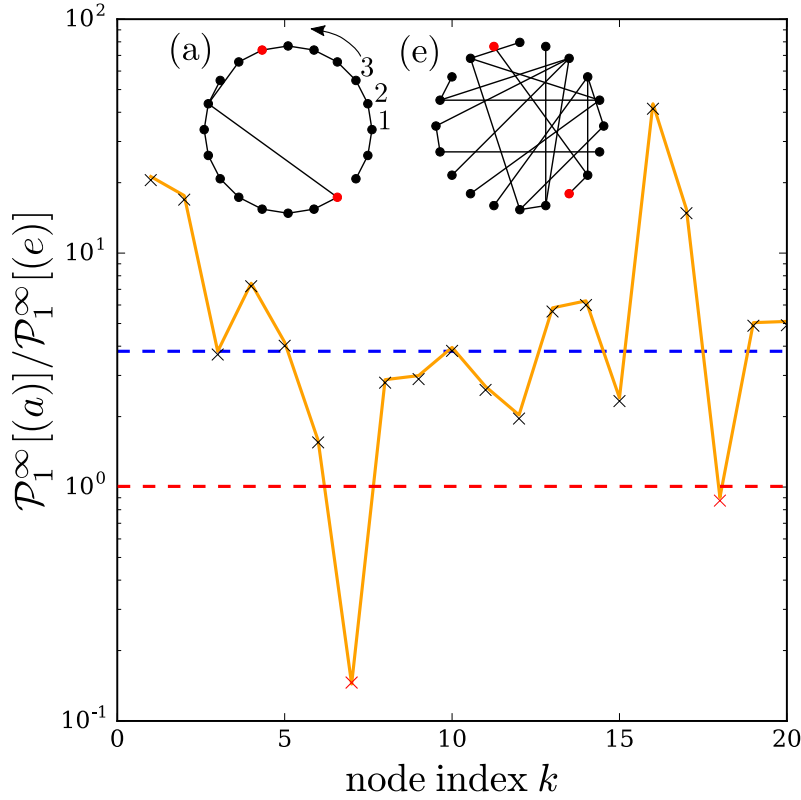


Figure 3.1 – Ratio of the performance measures  $\mathcal{P}_1$  for graph (a) vs. (e) of Fig. 3.2 (shown in the insets), for a quench perturbation of magnitude  $\delta P_0 = 0.01$  and duration  $\gamma\tau_0 = 500$  on node  $k = 1, 2, 3, \dots, 20$  (see text). On average, graph (e) is four times more robust to external perturbations than graph (a) (blue dashed line). However, some nodes of graph (a) can be more robust than those of graph (e) (red crosses correspond to quench perturbation applied on the red nodes shown in the inset). Both specific local vulnerabilities (crosses) and global averaged robustness (blue dashed lines) are well predicted by combinations of local centralities, and global topological indices (orange solid line, see text).

different time dependences  $f(t)$  – such as, for instance, noisy fluctuations or instantaneous, Dirac-delta perturbations – and different geographical dependences encoded in  $\delta \mathbf{P}_0$ . In this manuscript we consider quenches where  $f(t)$  vanishes outside some time interval, inside which it is constant but nonzero. In the next section we calculate performance measures for general perturbation vectors  $\delta \mathbf{P}_0$  for such quenches. As for geographical dependences, we then consider two cases of (i) nodal vulnerabilities, with local perturbations  $\delta \mathbf{P}_0 = (0, \dots, \delta P_{0,k}, \dots, 0)$  and (ii) global robustness, where performance measures are averaged over all possible locations  $k$  for the perturbation.

#### Quench Perturbation

We compute both performance measures  $\mathcal{P}_{1,2}$  for a quench perturbation  $\delta \mathbf{P}(t) = \delta \mathbf{P}_0 \Theta(t) \Theta(\tau_0 - t)$  with the Heaviside function  $\Theta(t)$  and a perturbation vector  $\delta \mathbf{P}_0$  encoding the geographical distribution of the perturbation. The duration  $\tau_0$  of the quench allows to explore the different time scales of the system and we show below that  $\mathcal{P}_{1,2}$  varies significantly depending on  $\tau_0$ . Using Eq. (5.10), Eqs.(3.15) give

$$\begin{aligned} \mathcal{P}_1^\infty &= \frac{m}{8\gamma} \sum_{\alpha \geq 2} \frac{(\delta \mathbf{P}_0 \cdot \mathbf{u}_\alpha)^2}{\Gamma_\alpha \lambda_\alpha^3} \left[ 2\Gamma_\alpha (4\gamma\tau_0\lambda_\alpha/m - 3\gamma^2 - \Gamma_\alpha^2) + (\gamma + \Gamma_\alpha)^3 e^{-\tau_0 \frac{(\gamma - \Gamma_\alpha)}{2}} - (\gamma - \Gamma_\alpha)^3 e^{-\tau_0 \frac{(\gamma + \Gamma_\alpha)}{2}} \right], \\ \mathcal{P}_2^\infty &= \frac{1}{2d} \sum_{\alpha \geq 2} \frac{(\delta \mathbf{P}_0 \cdot \mathbf{u}_\alpha)^2}{\Gamma_\alpha \lambda_\alpha} \left[ 2\Gamma_\alpha - (\gamma + \Gamma_\alpha) e^{-\frac{\tau_0(\gamma - \Gamma_\alpha)}{2}} + (\gamma - \Gamma_\alpha) e^{-\frac{\tau_0(\gamma + \Gamma_\alpha)}{2}} \right]. \end{aligned} \quad (3.17a)$$

It is easily checked that  $\mathcal{P}_{1,2}^\infty \in \mathbb{R}$  in both cases  $\gamma^2 > 4\lambda_\alpha/m$  (with  $\Gamma_\alpha \in \mathbb{R}$ ) and  $\gamma^2 < 4\lambda_\alpha/m$  (with  $\Gamma_\alpha \in i\mathbb{R}$ ).

Both performance measures are given by a spectral sum of terms corresponding to the eigenmodes of the network Laplacian matrix  $\mathbb{L}$ . Each term in this sum depends on the scalar product of the perturbation vector  $\delta \mathbf{P}_0$  with the eigenmodes  $\mathbf{u}_\alpha$  of  $\mathbb{L}$  times a mode-dependent factor. The latter is an almost always decreasing function of the eigenvalues  $\lambda_\alpha$ . Therefore, Eqs. (3.17) suggest that the largest excursion can be obtained by overlapping  $\delta \mathbf{P}_0$  with few of the lowest-lying eigenmodes of  $\mathbb{L}$ , in particular  $\mathbf{u}_2$ , the so-called Fiedler mode of the network [46].

To get more insight into Eqs. (3.17), we compute their two asymptotic limits of long and short  $\tau_0$ . For perturbations with very short duration i.e.  $\tau_0 \ll m/d$ ,  $(\gamma \pm \Gamma_\alpha)^{-1}$ , we have,

$$\mathcal{P}_1^\infty = \frac{\tau_0^2}{2d} \sum_{\alpha \geq 2} \frac{(\delta \mathbf{P}_0 \cdot \mathbf{u}_\alpha)^2}{\lambda_\alpha}, \quad (3.18a)$$

$$\mathcal{P}_2^\infty = \frac{\tau_0^2}{2md} \sum_{\alpha \geq 2} (\delta \mathbf{P}_0 \cdot \mathbf{u}_\alpha)^2. \quad (3.18b)$$

Each term in the sum over modes depends on  $\lambda_\alpha$  for  $\mathcal{P}_1^\infty$  but not for  $\mathcal{P}_2^\infty$ . Consequently,  $\mathcal{P}_1^\infty$  depends explicitly on the location of the perturbation, while there is no such dependence for  $\mathcal{P}_2^\infty$ , which depends only on the squared norm of the perturbation vector  $\delta \mathbf{P}_0$  orthogonal to  $\mathbf{u}_1$ . This reflects the fact that in the regime of short  $\tau_0$ , the perturbation does not act long enough to change the kinetic energy of inertiafull oscillators, which  $\mathcal{P}_2^\infty$  essentially measures. Consequently, the perturbation is quickly damped locally, with little dependence on its location in the situation we consider of homogeneously distributed inertia. We note that similar topology-independent results were obtained for instantaneous, Dirac-delta perturbations [6].

### Chapter 3. Global Robustness vs. Local Vulnerabilities in Complex Synchronous Networks

---

In the other limit  $\tau_0 \gg m/d$ ,  $(\gamma \pm \Gamma_\alpha)^{-1}$ , the performance measures read

$$\mathcal{P}_1^\infty = \tau_0 \sum_{\alpha \geq 2} \frac{(\delta \mathbf{P}_0 \cdot \mathbf{u}_\alpha)^2}{\lambda_\alpha^2}, \quad (3.19a)$$

$$\mathcal{P}_2^\infty = d^{-1} \sum_{\alpha \geq 2} \frac{(\delta \mathbf{P}_0 \cdot \mathbf{u}_\alpha)^2}{\lambda_\alpha}. \quad (3.19b)$$

In this case of a long-lasting perturbation, both  $\mathcal{P}_1^\infty$  and  $\mathcal{P}_2^\infty$  depend on the location of the perturbation. Furthermore, and perhaps more importantly, the inertia affects neither  $\mathcal{P}_1^\infty$  nor  $\mathcal{P}_2^\infty$ . This is so since, for long quenches, oscillators have the time to synchronize at a new frequency with zero angular acceleration before the perturbation is over. We further note that  $\tau_0$  no longer appears in  $\mathcal{P}_2^\infty$ , since the latter considers deviations orthogonal to  $\mathbf{u}_1$ . Consequently, the whole time spent by the oscillators at the new frequency does not contribute to  $\mathcal{P}_2^\infty$ . Most importantly, Eqs. (3.18) and (3.19) suggest that in both asymptotic limits of short and long perturbations,  $\mathcal{P}_{1,2}^\infty \propto \sum_{\alpha \geq 2} (\delta \mathbf{P}_0 \cdot \mathbf{u}_\alpha)^2 / \lambda_\alpha^p$  with  $p = 0, 1, 2$ . That result was already hinted at in Ref. [121] for inertialess oscillators and various types of perturbations. Below we show how this dependence leads to performance measures depending on the resistance distances, centralities and Kirchhoff indices introduced in Section 3.2.

Eqs. (3.17) and their asymptotic limits, Eqs. (3.18) and (3.19), give the performance measures  $\mathcal{P}_{1,2}^\infty$  for any perturbation vector  $\delta \mathbf{P}_0$ . We next discuss two important cases of (i) a single-node perturbation,  $\delta P_{0,i} = \delta P_0 \delta_{ik}$ , where large values of the node-dependent performance measures  $\mathcal{P}_{1,2}^\infty \rightarrow \mathcal{P}_{1,2}^\infty(k)$  identify local vulnerabilities and (ii) averaged perturbation over ensemble of homogeneously distributed perturbation vectors  $\delta \mathbf{P}_0$ , where large values of  $\mathcal{P}_{1,2}^\infty \rightarrow \langle \mathcal{P}_{1,2}^\infty \rangle$  indicate globally fragile networks.

#### Specific Local Vulnerabilities

To assess local vulnerabilities of the coupled oscillators, we apply a quench perturbation on a single node. The vulnerability of node  $k$  is then given by Eqs. (3.17) with the components of the perturbation vector given by  $\delta P_{0,i} = \delta P_0 \delta_{ik}$ . In the limit of short duration of perturbation,  $\tau_0 \ll m/d$ ,  $(\gamma \pm \Gamma_\alpha)^{-1}$ , one obtains

$$\mathcal{P}_1^\infty(k) = \frac{\delta P_0^2 \tau_0^2}{2d} \sum_{\alpha \geq 2} \frac{u_{\alpha,k}^2}{\lambda_\alpha} = \frac{\delta P_0^2 \tau_0^2}{2d} [C_1^{-1}(k) - n^{-2} Kf_1], \quad (3.20a)$$

$$\mathcal{P}_2^\infty(k) = \frac{\delta P_0^2 \tau_0^2}{2md} \sum_{\alpha \geq 2} u_{\alpha,k}^2 = \frac{\delta P_0^2 \tau_0^2}{2md} \frac{(n-1)}{n}, \quad (3.20b)$$

where the right-hand side of Eq. (3.20a) directly follows from Eq. (3.3). For a perturbation on node  $k$ ,  $\mathcal{P}_1^\infty(k)$  is expressed in terms of the centrality,  $C_1(k)$ , a local nodal descriptor, and the Kirchhoff index  $Kf_1$ , a global network descriptor. Consequently, the most vulnerable nodes in a given network, according to  $\mathcal{P}_1^\infty(k)$ , are identified by their resistance-distance based centrality  $C_1(k)$ .

### 3.3. Synchronized oscillators under external perturbations

In the other limit of long perturbations,  $\tau_0 \gg m/d$ ,  $(\gamma \pm \Gamma_\alpha)^{-1}$ , Eqs. (3.19) give

$$\mathcal{P}_1^\infty(k) = \delta P_0^2 \tau_0 \sum_{\alpha \geq 2} \frac{u_{\alpha,k}^2}{\lambda_\alpha^2} = \delta P_0^2 \tau_0 [C_2^{-1}(k) - n^{-2} Kf_2], \quad (3.21a)$$

$$\mathcal{P}_2^\infty(k) = \frac{\delta P_0^2}{d} \sum_{\alpha \geq 2} \frac{u_{\alpha,k}^2}{\lambda_\alpha} = \frac{\delta P_0^2}{d} [C_1^{-1}(k) - n^{-2} Kf_1]. \quad (3.21b)$$

This time  $\mathcal{P}_1^\infty$  is given by the higher order centrality  $C_2(k)$  and Kirchhoff index  $Kf_2$ .

When considering a given, fixed network, Eqs. (3.20) and (3.21) show that perturbations on the most central nodes – as measured by either centrality  $C_1(k)$  or  $C_2(k)$  – give the smallest overall responses, except when considering  $\mathcal{P}_2^\infty(k)$  for a short-time perturbation. In that latter case, the response is homogeneous and perturbing any node leads to the same performance measure  $\mathcal{P}_2^\infty(k)$ . When comparing two nodes with similar centrality on two different networks, on the other hand, Eqs. (3.20) and (3.21) indicate that the largest response occurs on the network with smallest generalized Kirchhoff index – except again for  $\mathcal{P}_2^\infty(k)$  and a short-time perturbation. We show below that the overall network robustness is actually given by these generalized Kirchhoff indices, which makes this observation quite counterintuitive: when perturbing two nodes of equal centrality on two different networks, the largest response is actually recorded on the overall more robust network! We will come back to this point below.

#### Averaged Global Robustness

We next assess the global robustness of synchrony in a given network, by averaging Eqs. (3.17) over an homogeneously distributed ensemble of perturbation vectors defined by  $\langle \delta P_{0,i} \delta P_{0,j} \rangle = \delta_{ij} \langle \delta P_0^2 \rangle$  [121]. Averaging Eqs. (3.17) gives, in the limit of short perturbations,  $\tau_0 \ll m/d$ ,  $(\gamma \pm \Gamma_\alpha)^{-1}$

$$\langle \mathcal{P}_1^\infty \rangle = \frac{\langle \delta P_0^2 \rangle \tau_0^2}{2d} \sum_{\alpha \geq 2} \lambda_\alpha^{-1} = \frac{\langle \delta P_0^2 \rangle \tau_0^2}{2nd} Kf_1, \quad (3.22a)$$

$$\langle \mathcal{P}_2^\infty \rangle = \frac{\langle \delta P_0^2 \rangle \tau_0^2}{2md} \frac{n-1}{n}. \quad (3.22b)$$

We see that  $\langle \mathcal{P}_1^\infty \rangle$  is given by the Kirchhoff index  $Kf_1$  which is proportional to the network's average resistance distance  $\Omega_{ij}^{(1)}$  [see Eq. (3.4)]. Similarly to the local vulnerability in this limit,  $\langle \mathcal{P}_2^\infty \rangle$  depends on the network only marginally through the number of nodes.

In the other limit  $\tau_0 \gg m/d$ ,  $(\gamma \pm \Gamma_\alpha)^{-1}$ , Eqs. (3.19) give

$$\langle \mathcal{P}_1^\infty \rangle = \langle \delta P_0^2 \rangle \tau_0 \sum_{\alpha \geq 2} \lambda_\alpha^{-2} = \frac{\langle \delta P_0^2 \rangle \tau_0}{n} Kf_2, \quad (3.23a)$$

$$\langle \mathcal{P}_2^\infty \rangle = \frac{\langle \delta P_0^2 \rangle}{d} \sum_{\alpha \geq 2} \lambda_\alpha^{-1} = \frac{\langle \delta P_0^2 \rangle}{nd} Kf_1. \quad (3.23b)$$

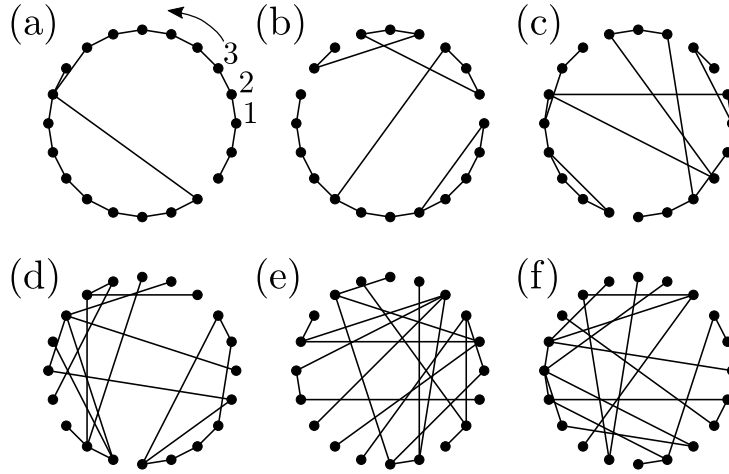


Figure 3.2 – Six networks with  $n = 20$  nodes obtained by the rewiring procedure of Ref. [126], starting from a cyclic graph and rewiring every edge of the network with a probability  $p_r = 0.15$  (a),  $p_r = 0.3$  (b),  $p_r = 0.45$  (c),  $p_r = 0.6$  (d),  $p_r = 0.75$  (e) and  $p_r = 0.9$  (f). The node numbering used in Fig. 3.3 is indicated in panel (a).

Both performance measures depend on generalized Kirchhoff indices. Quite remarkably and as for local vulnerabilities, the only average performance measure that depends on inertia is  $\langle \mathcal{P}_2^\infty \rangle$  in the short  $\tau_0$  limit.

The results of Sections 3.3.4 and 3.3.5 can be easily extended to other types of perturbations. For inertialess oscillators, Ref. [121] reached similar conclusions, that performance measures can be expressed in terms of resistance centralities and Kirchhoff indices, for several other types of perturbations. In the next Section, we numerically confirm the validity of the analytical theory presented in this Section.

## Numerical Results

### Local Vulnerabilities and Resistance Centralities

We numerically investigate local vulnerabilities by perturbing individual nodes with the quench perturbation discussed above. Our theory applies to network of any geometry with any number  $n$  of nodes. However in order to better visualize the agreement between analytical predictions and numerical results we restrict ourselves to relatively small graphs with  $n = 20$  nodes of the kind shown in Fig. 3.2.

We check Eqs. (3.17) for the model defined in Eq. (3.10) with  $b_{ij} = 1$  on the edge of the graph considered and  $a_{ij} = 0$  otherwise,  $m_i \equiv m = 1$  and  $d_i \equiv d = 1$ . We numerically time-evolve Eq. (3.10) with a fourth-order Runge-Kutta method, following a perturbation  $\delta P_i(t) = \delta P_0 \delta_{ik} \Theta(t) \Theta(\tau_0 - t)$  away from  $\mathbf{P}^{(0)} = 0$  and starting from the corresponding synchronous

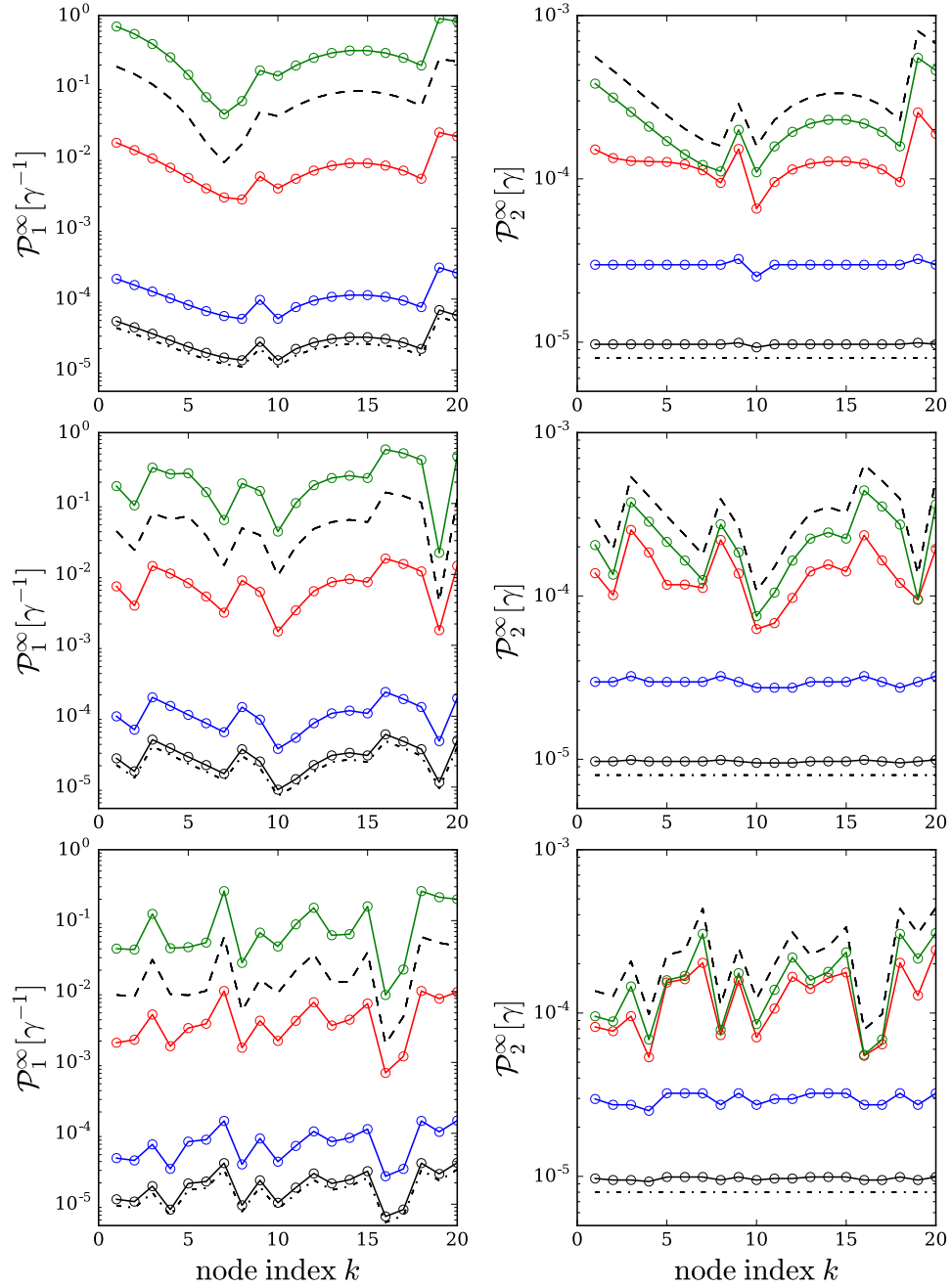


Figure 3.3 – Performances measures  $\mathcal{P}_1$  (left) and  $\mathcal{P}_2$  (right) for the graphs of Fig. 3.2a (top), Fig. 3.2c, (middle), Fig. 3.2e (bottom) and a quench perturbation of magnitude  $\delta P_0 = 0.01$  on node  $k$ . Numerical results (circles) and analytical Eqs. (3.17) (solid lines) are plotted for different durations of perturbation  $\gamma\tau_0 = 0.5$  (black), 1 (blue), 10 (red), 100 (green). The asymptotic values of short and long  $\tau_0$  given in Eqs. (3.20) (dotted line) and (3.21) (dashed line) are shown, vertically shifted by an arbitrary amount for clarity. The node numbering is given in Fig. 3.2a.

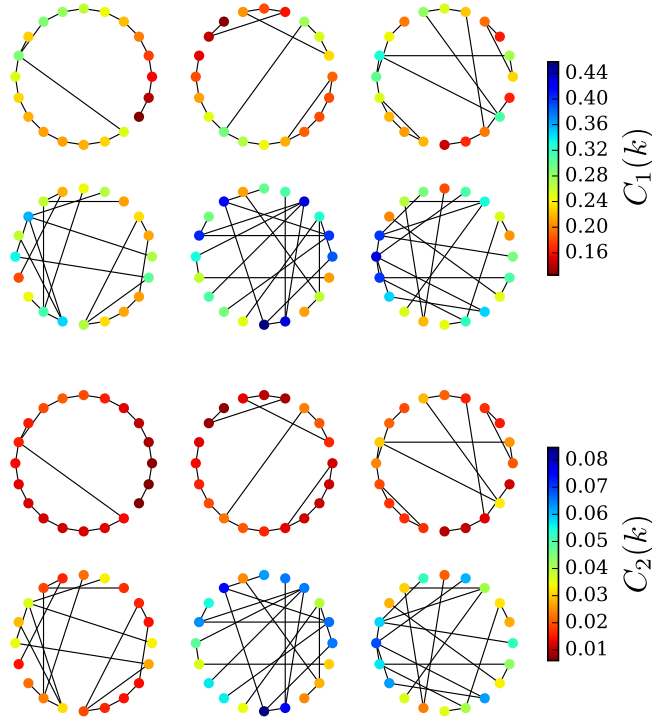


Figure 3.4 – Resistance centralities  $C_1(k)$  (top) and  $C_2(k)$  (bottom), given in Eqs. (3.3) and (3.7) respectively, for the six graphs of Fig. 3.2.

state  $\theta^{(0)} = 0$ . Fig. 3.3 shows that the theory of Eqs. (3.17) is in perfect agreement with numerical results. In particular, one clearly sees the crossover from  $[C_1^{-1}(k) - n^{-2}Kf_1]$  to  $[C_2^{-1}(k) - n^{-2}Kf_2]$  for  $\mathcal{P}_1^\infty$  (dotted to dashed lines on the left panels) and from a constant to  $[C_1^{-1}(k) - n^{-2}Kf_1]$  (dotted to dashed line on the right panels) for  $\mathcal{P}_2^\infty$ , as  $\tau_0$  increases. This fully confirms our theoretical predictions, Eqs. (3.20)-(3.21). We conclude that, generally speaking (i.e. except for  $\mathcal{P}_2^\infty$  and short perturbations), the most central nodes are the most robust. They are connected by multiple paths to the rest of the network, and when they are perturbed, the disturbance quickly diffuses across the network with small angle differences. In contrast, the most peripheral nodes such as dead ends have only few paths connecting them to the bulk of the network and the disturbance diffuses across the network with large angle differences. It has been numerically found that dead ends undermine grid stability [87], and our results shed some analytical light on that observation.

We further illustrate this strong connection between resistance centralities and response of the system. We show in Fig. 4.6 resistance centralities  $C_1(k)$  and  $C_2(k)$  for the six graphs of Fig. 3.2. One sees that  $C_1(k)$  and  $C_2(k)$  tend to become higher while going from graph (a) to (f) indicating that graphs with more rewired edges (and thus with more long-range couplings) have shorter distances between nodes and thus lower Kirchhoff indices. Interestingly, several nodes with a high centrality  $C_1(k)$  do not necessarily have a high centrality  $C_2(k)$ , and vice-versa. This is illustrated in the  $C_1(k)$  vs.  $C_2(k)$  scatterplot of Fig. 3.5. Still there is an overall

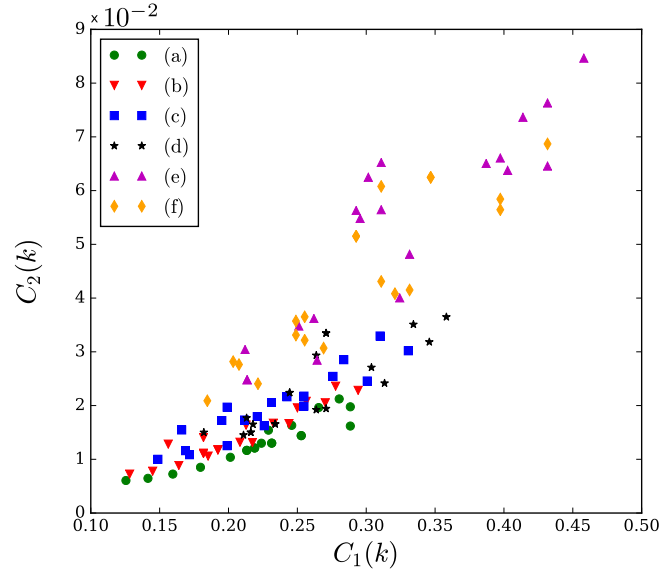


Figure 3.5 – Comparison between  $C_1(k)$  and  $C_2(k)$  for the six graphs of Fig. 3.2 (see inset).

positive correlation between  $C_1(k)$  vs.  $C_2(k)$ , quantified by a Pearson correlation parameter  $\text{cov}[C_1(k), C_2(k)] / (\text{rms}[C_1(k)] \text{rms}[C_2(k)]) = 0.87$ . We then show in Fig. 3.6 the time-evolution of angles and frequencies following a local quench perturbation on two different nodes of graph (f) with very different resistance centralities. One clearly sees that for a perturbed node with low resistance centrality (Fig. 3.6, top), angles and frequencies spread more during the perturbation than for a node with higher centrality (Fig. 3.6, bottom).

Generally speaking, networks with higher rewiring probabilities have smaller global topological indices  $Kf_1$  and  $Kf_2$  and thus smaller  $\langle \mathcal{P}_{1,2}^\infty \rangle$  according to our theory. This is confirmed numerically in the four left panels in Fig. 3.7, where we apply the same quench perturbation on nodes with resistance centralities  $C_1(k)$  close to their median value in the corresponding graph. One observes that angles and frequencies spread more and take more time to return to the initial fixed point in the graph with higher  $Kf_1$  and  $Kf_2$  (first and third rows) compared to the one with more rewired edges (second and fourth rows).

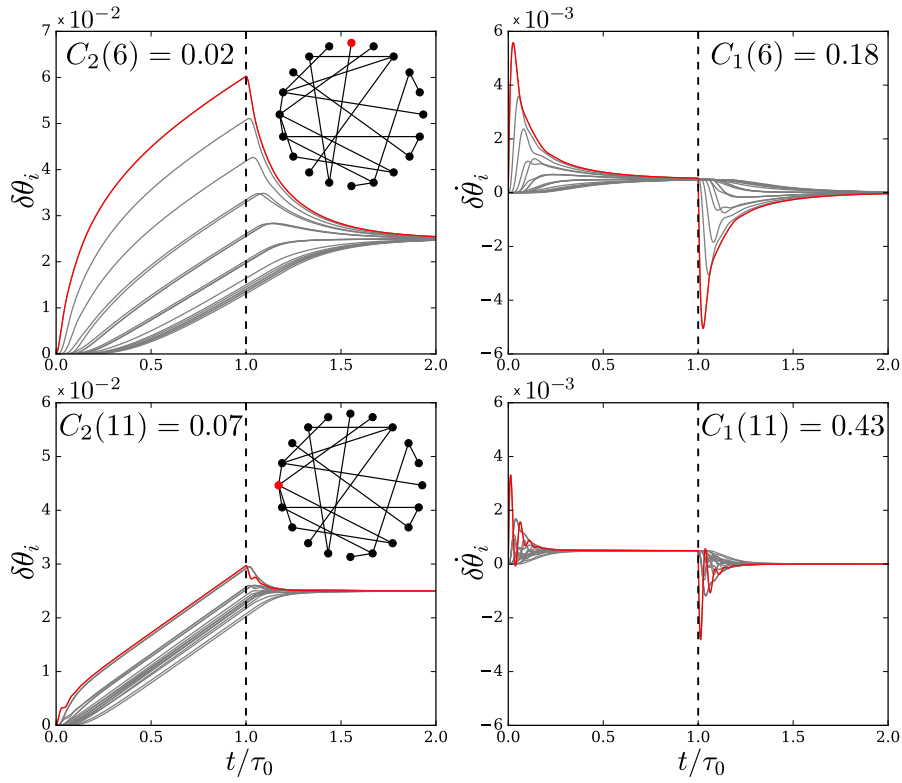


Figure 3.6 – Time-evolution of angles (left) and frequencies (right) following a quench perturbation applied on node 6 (top panels) and 11 (bottom panels) of graph (f) in Fig. 3.2 with  $\gamma\tau_0 = 50$ . The trajectory of the perturbed oscillator is shown in red. Angles and frequencies spread more when the perturbation is applied on node 6 than on node 11, in agreement with predictions of Eqs. (3.21) since node 6 has the smallest, node 11 the largest centrality in this graph.

While this is a rather general rule, it does not forbid exceptions. As a matter of fact, specific perturbations can lead to higher response in a network with lower Kirchhoff index than in a network with higher Kirchhoff index. Such an exception is illustrated in the four right panels in Fig. 3.7, where the same quench perturbation is applied on nodes with similar resistance centralities  $C_2(k)$  but belonging to graphs with very different Kirchhoff indices (see insets of Fig. 3.7). As expected from Eqs. (3.21), if two nodes on different networks have the same centralities, then, a perturbation applied on the one in the network with lower Kirchhoff index produces the largest response. Another illustration of this effect is given in Fig. 3.1, where graph (e) is more robust than graph (a) on average (dashed lines). But if we compare the response to specific local perturbations, some nodes of graph (a) are more robust than those of graph (e) (red crosses). Both the generic and the exceptional behaviors are accurately captured by our theory.

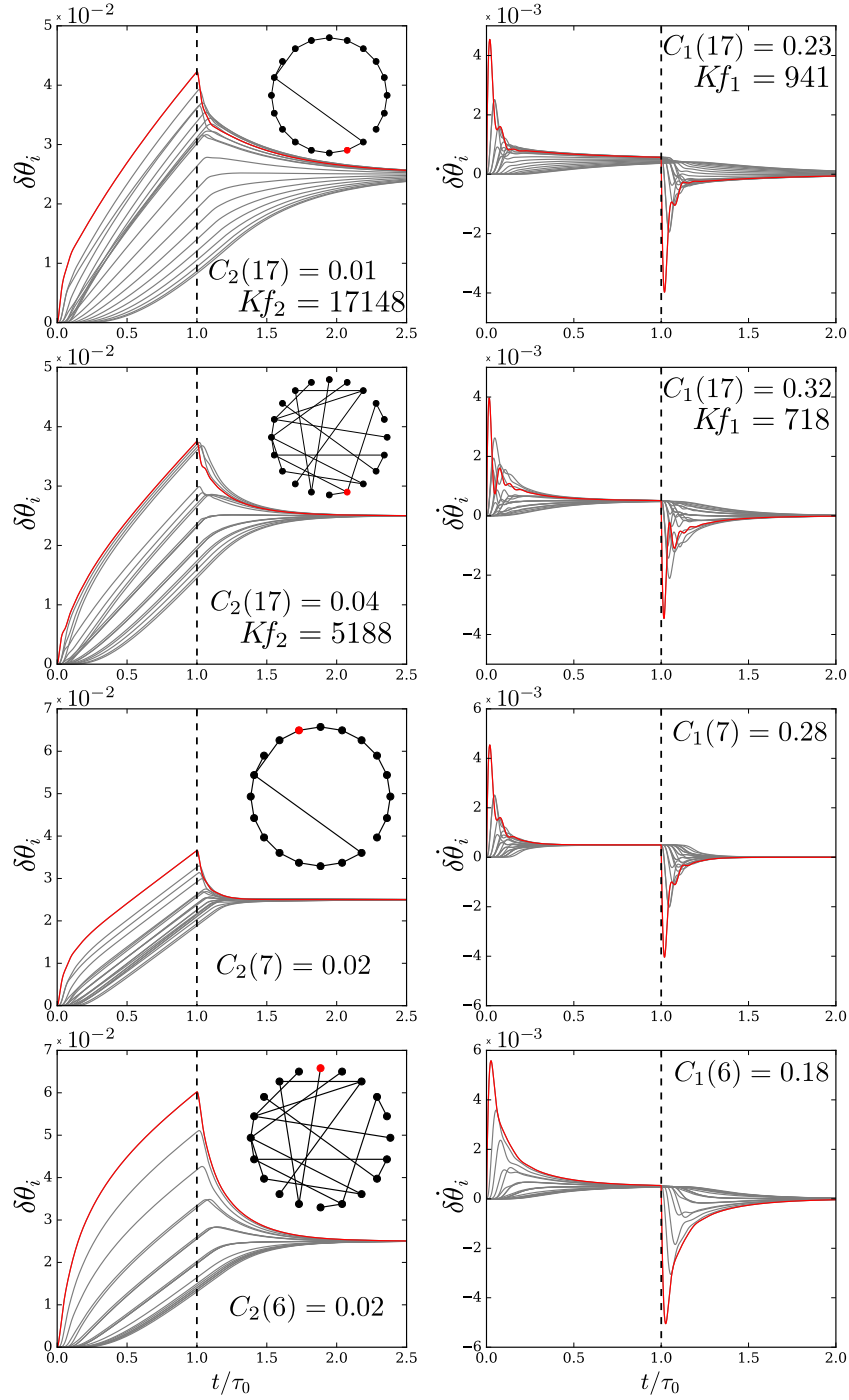


Figure 3.7 – Trajectories of angles and phases for the graphs of Fig. 3.2 with  $p_r = 0.15$  (first and third rows) and  $p_r = 0.9$  (second and fourth rows) obtained by numerically time-evolving Eq. (3.10) for the same quench perturbation with  $\gamma\tau_0 = 50$  applied on the node colored in red in the insets. In the four left panels, perturbed nodes are close to median value of  $C_2(k)$ , respectively in graph with  $p_r = 0.15$  (first and third rows) and  $p_r = 0.9$  (second and fourth rows). In the four right panels, perturbed nodes are the most (first and third rows) and least (second and fourth rows) central ones according to  $C_2(k)$ , respectively in graph with  $p_r = 0.15$  and  $p_r = 0.9$ .

### Global Robustness and Generalized Kirchhoff Indices

We next investigate global robustness by averaging performance measures over an ensemble of perturbation vectors located on a single node,  $\delta \mathbf{P}_0 = (0, \dots, \delta P_{0,k}, 0, \dots)$  with  $k = 1, \dots, n$ . Fig. 3.8 compares the resulting numerical averages  $\langle \mathcal{P}_{1,2}^\infty \rangle$  with the average of the theoretical prediction of Eqs. (3.17). Numerics and theory agree well. In particular the left panel confirms nicely the crossover between  $Kf_1$  and  $Kf_2$  predicted by Eqs. (3.22a) and (3.23a). A similar behavior is visible in the right panel, where  $\langle \mathcal{P}_2^\infty \rangle$  does not depend on the network topology for short duration of perturbation (black and blue lines and symbols) but crosses over to  $Kf_1$  as  $\tau_0$  increases, as predicted by Eqs. (3.22b) and (3.23b). We finally note that networks with high  $Kf_1$  do not necessarily have a high  $Kf_2$ , and vice-versa. This is illustrated in Fig. 3.8 where the chosen network with  $p_r = 0.15$  has a higher  $Kf_2$  but a lower  $Kf_1$  than the chosen network with  $p_r = 0.3$ . Below we analyze in more details  $Kf_{1,2}$  in randomly rewired networks.

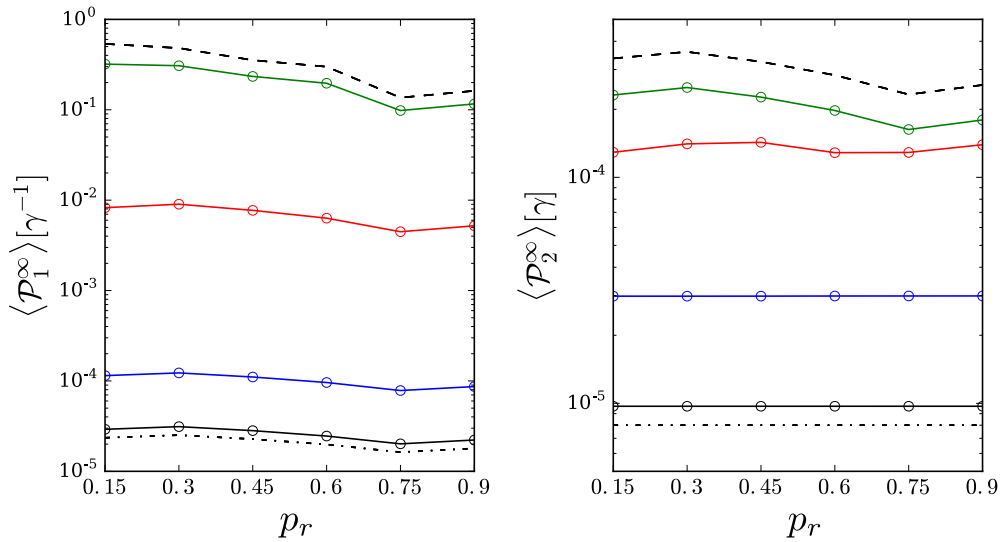


Figure 3.8 – Averaged Performances measures  $\langle \mathcal{P}_1^\infty \rangle$ ,  $\langle \mathcal{P}_2^\infty \rangle$  for the graphs of Fig. 3.2 obtained numerically (circles) and predicted analytically, Eqs. (3.17) (solid lines) for perturbations with  $\gamma\tau_0 = 0.5$  (black), 1 (blue), 10 (red), 100 (green). The asymptotic values of short and long  $\tau_0$  given in Eqs. (3.22) (dotted line) and (3.23) (dashed line) are shown, vertically shifted by an arbitrary amount for clarity.

### Generalized Kirchhoff Indices in Small-World Networks

The results obtained above relate local vulnerabilities to nodal centralities and global network robustness to generalized Kirchhoff indices. This connection is powerful: it gives a vulnerability ranking of nodes and provides robustness assessment based on well-defined, easily calculated network descriptors. To gain qualitative insight on what favors robustness in a graph, we investigate the behavior of the Kirchhoff indices for Watts-Strogatz, randomly rewired networks. Following Ref. [126], we consider initially regular, circular graphs where

nodes are coupled to their nearest, second-nearest aso. up to their  $10^{\text{th}}$  neighbors. Each edge in the corresponding coupling network is then rewired with probability  $p$ . Fig. 3.9 compares the standard measures of "nearest-neighborhood" of average geodesic distance  $l$  and clustering coefficient  $Cl$  with the generalized Kirchhoff indices  $Kf_1$  and  $Kf_2$ , as a function of  $p$ .

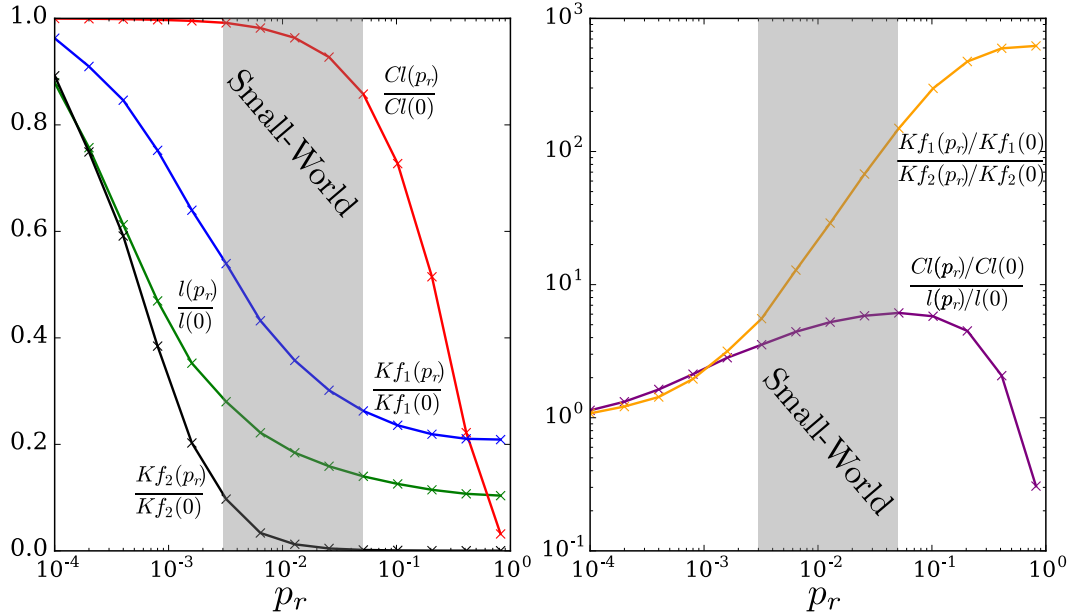


Figure 3.9 – Left panel: clustering coefficient  $Cl$ , average geodesic distance  $l$  and generalized Kirchhoff indices  $Kf_1$  and  $Kf_2$ , as a function of the rewiring probability  $p_r$  for Strogatz-Watts rewired networks [126]. Each data point corresponds to an average over 30 realizations of randomly rewired graphs, obtained from an initial cyclic graph with  $n = 1000$  nodes and nearest to  $10^{\text{th}}$ - neighbor coupling, where each edge is randomly rewired with a probability  $p_r$  (parameters chosen similar as in Ref. [126], such that the graph remains connected while rewiring and is still sparse). Right panel: ratio of the Kirchhoff indices and of clustering coefficient vs. average geodesic distance. Small-world networks are easily identified by the steepest slope of the orange line.

Both Kirchhoff indices drop, roughly following  $l$ , as  $p$  is increased, with  $Kf_2$  decreasing significantly faster than  $Kf_1$  and  $l$ . Traditionally, the "small-world" behavior occurs around  $p_r = 0.01$ , where  $l$  is significantly smaller than its initial value, while  $Cl$  has not yet changed much. In that region,  $Kf_1$  has been reduced to  $\sim 40\%$  of its initial value, while  $Kf_2$  reaches only few percents of its initial value. Accordingly, small-world networks are significantly more robust to external perturbations than regular networks, particularly when considering  $\mathcal{P}_1^\infty$  for long quenches. Only a fraction of edges need to be rewired to achieve a level of robustness comparable to that of random networks. As a side-remark, we note that the ratio of Kirchhoff indices provides for a clear identification of small-world networks, which correspond to values of  $p_r$  where  $Kf_1(p_r)/Kf_2(p_r)$  is fast increasing with  $p_r$ .

### Regular Networks

We finally comment on regular networks. In such networks, all the nodes are equivalent and therefore global robustness is equivalent to local vulnerability,  $\mathcal{P}_{1,2}^\infty(k) = \langle \mathcal{P}_{1,2}^\infty \rangle$ ,  $\forall k$ , furthermore, Kirchhoff indices can be calculated analytically. The Laplacian matrix can be diagonalized with a Fourier transform, and its spectrum is given by

$$\lambda_\alpha = 4 - 2 \cos(k_\alpha) - 2 \cos(k_\alpha q), \quad \alpha = 1, \dots, n, \quad (3.24)$$

with  $k_\alpha = 2\pi(\alpha - 1)/n$ . Kirchhoff indices Eq. (3.8) are then given by,

$$Kf_p = n \sum_{\alpha \geq 2} [4 - 2 \cos(k_\alpha) - 2 \cos(k_\alpha q)]^{-p}. \quad (3.25)$$

Fig. 3.10 shows  $Kf_1$  and  $Kf_2$  for such regular networks with  $n = 50$  nodes. When extending the coupling range  $q$ , Kirchhoff indices are generally decreasing, indicating the standard trend that longer-range couplings reduce centralities. However, for some values  $q = 10, 17, 24$  equal or close to integer divisors of  $n$ , Kirchhoff indices suddenly become larger. This is so, since then, paths made of few long-range interactions form either closed or almost closed loops (see the inset of Fig. 3.10 for  $q = 17, 24$ ), which do not reduce the geodesic distance between many pairs of nodes, compared to long range coupling with  $n/q$  not integer (e.g.  $q = 19$  in Fig. 3.10). Consequently, graphs that may appear similar, such as those with  $q = 17$  and  $q = 19$  or with  $q = 23$  and  $q = 24$  may exhibit Kirchhoff indices differing by factors of 2-4 or even more. This illustrates how assessing global robustness is hard to do from a network's general appearance and/or from arguments solely based on the existence of long-range couplings.

### Conclusion

Building up on earlier works [7, 54, 102, 93, 110, 121, 123], we have investigated the response under external perturbations of network-coupled dynamical systems initially in a stable synchronous state. We proposed to assess network robustness and identify nodal vulnerabilities through quadratic performance metrics quantifying the magnitude of the perturbation-induced transient excursion away from the synchronous state. As we reported earlier for first-order oscillators [121], we found that the response of inertiaful, second-order oscillators depends on the overlap between the perturbation vector and the eigenmodes of the weighted Laplacian. In particular, the set of nodes located on the slowest eigenmode corresponding to the smallest eigenvalue produces the largest excursions when perturbed. Considering disturbances localized on a single node we found that, oscillators which, once perturbed, induce the largest transient excursion are the ones with smallest resistance centralities. Extending the results of Ref. [121] to second-order oscillators, we found that global robustness, assessed by averaging performance measures over ergodic ensembles of perturbation vectors, is also given by generalized Kirchhoff indices. A network can then be made more robust to perturbations by minimizing its average resistance distances, for instance by introducing long-range

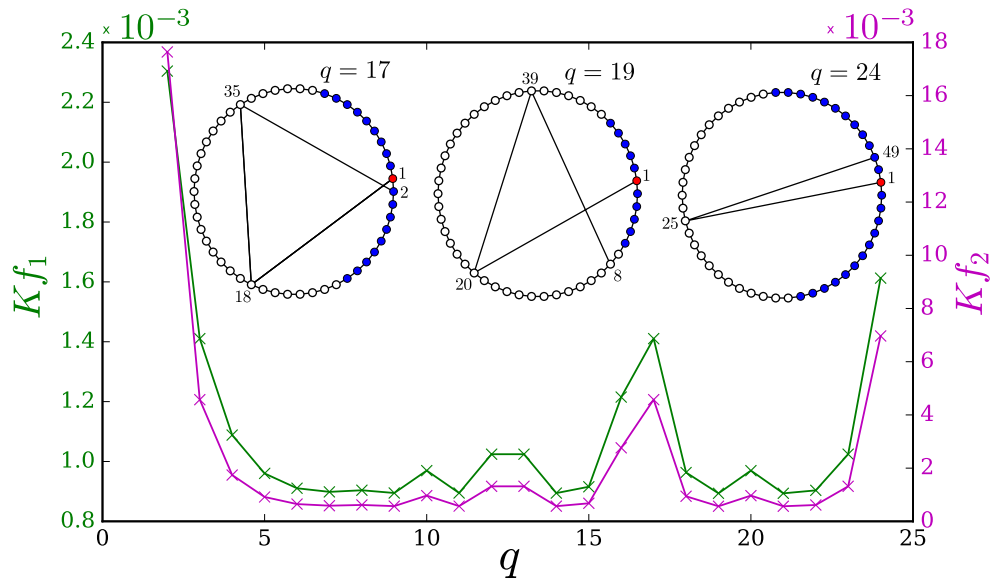


Figure 3.10 – Generalized Kirchhoff indices  $Kf_1$  (green) and  $Kf_2$  (purple) given in Eq. (3.25), for a cyclic network with  $n = 50$  nodes with nearest and  $q^{\text{th}}$ - neighbor coupling. The inset sketches the model for  $q = 17, 19$  and  $24$  and with one path involving  $q^{\text{th}}$  range coupling starting from node 1 (red). The addition of the  $q^{\text{th}}$ - neighbor coupling does not reduce geodesic distance between the reference node (red) and the set of nodes colored in blue.

edges. Quite remarkably, except for  $\mathcal{P}_2$  and short time perturbation, asymptotic behaviors of performance measures in either limit of long or short perturbations do not depend on the inertia of the oscillators.

Our findings are rather general. Together with Refs. [121, 123], they make it clear that, almost regardless of the presence of inertia, and of the type of perturbation chosen, quadratic performance measures are given by the generalized resistance distance-based centralities or, once averaged over ergodic ensembles of perturbations, by the generalized Kirchhoff indices that we introduced in Section 3.2. These local and global network characteristics therefore provide well-defined, numerically easy to calculate robustness descriptors and local vulnerability indicators.

Further studies could consider the effect of spatially correlated perturbations and go beyond the assumption of homogeneous inertia and damping. Moreover, generalized resistance centralities and Kirchhoff indices could be investigated with different network generating algorithms.



## **4 The Key Player Problem in Complex Oscillator Networks and Electric Power Grids: Resistance Centralities Identify Local Vulnerabilities**

*Chapter 4 is a preprint version of an article published in Science Advances:*  
M. Tyloo, L. Pagnier, P. Jacquod, *Science Advances* 5(11):eaaw8359 (2019) [123].

## Chapter 4. The Key Player Problem in Complex Oscillator Networks and Electric Power Grids: Resistance Centralities Identify Local Vulnerabilities

---

Identifying key players in a set of coupled individual systems is a fundamental problem in network theory [5, 19, 47]. Its origin can be traced back to social sciences and the problem led to ranking algorithms from most to least important individual systems based on graph theoretic centralities [16]. Coupled dynamical systems differ from social networks in that, first, they are characterized by degrees of freedom with a deterministic dynamics and second the coupling between individual systems is a well-defined function of those degrees of freedom. One therefore expects the resulting coupled dynamics, and not only the network topology, to also determine the key players - the most important individual dynamical systems, in a pre-defined sense. Here, we investigate synchronizable network-coupled dynamical systems such as high voltage electric power grids and coupled oscillators on complex networks. We define key players as those network nodes which, once perturbed by a local noisy disturbance, generate the largest overall transient excursion away from synchrony. A spectral decomposition of the network coupling matrix leads to an elegant, concise, yet accurate solution to this identification problem. For inertialess oscillators, or when the inertia and damping parameters are either constant or with constant ratio, we show that, when the internodal coupling matrix is Laplacian, these key players are peripheral in the sense of a centrality measure defined from effective resistance distances. For linearly coupled dynamical systems such as weakly loaded electric power grids or consensus algorithms, the nodal ranking is efficiently obtained through a single Laplacian matrix inversion, regardless of the operational synchronous state. We call the resulting ranking index *LRank*. For heavily loaded electric power grids or coupled oscillators systems closer to the transition to synchrony, nonlinearities render the nodal ranking dependent on the operational synchronous state. In this case a weighted Laplacian matrix inversion gives another ranking index, which we call *WLRank*. Quite surprisingly, we find that *LRank* provides a faithful ranking even for well developed coupling nonlinearities, corresponding to oscillator angle differences up to  $\Delta\theta \lesssim 40^\circ$  approximately. Numerical results further establish the validity of these results for more general distributions with spatially varying inertia and damping parameters.

### Introduction

Because of growing electric power demand, increasing difficulties with building new lines and the emergence of intermittent new renewable energy sources, electric power systems are more often operated closer to their maximal capacity [74, 1]. Accordingly, their operating state, its robustness against potential disturbances and its local vulnerabilities need to be assessed more frequently and precisely. Furthermore, because electricity markets become more and more integrated, it is necessary to perform these assessments over geographically larger areas. Grid reliability is commonly assessed against  $n - 1$  feasibility, transient stability and voltage stability, by which one means that a grid is considered reliable if (i) it still has an acceptable operating state after any one of its  $n$  components fails, (ii) that acceptable state is reached from the original state following the transient dynamics generated by the component failure and (iii) the new operating state is robust against further changes in operating conditions

such as changes in power productions and loads. This  $n - 1$  contingency assessment is much harder to implement in real-time for a power grid loaded close to its capacity where the differential equations governing its dynamics become nonlinear – the fast, standardly used linear approximation breaks down as the grid is more and more heavily loaded. Nonlinear assessment algorithms have significantly longer runtimes, which makes them of little use for short-time evaluations. In worst cases, they sometimes even do not converge. In short, heavily loaded grids need more frequent, more precise reliability assessments which are however harder to obtain, precisely because the loads are closer to the grid capacities.

Developing real-time procedures for  $n - 1$  contingency assessment requires new, innovative algorithms. One appealing avenue is to optimize contingency ranking [47] to try and identify a subset of  $n_s < n$  grid components containing all the potentially critical components. The  $n - 1$  contingency assessment may then focus on that subset only, with a significant gain in runtime if  $n_s \ll n$ . Identifying such a subset requires a ranking algorithm for grid components, following some well-chosen criterion. Procedures of this kind have been developed in network models for social and computer sciences, biology and other fields, in the context of the historical and fundamental problem of identifying the *key players* [5, 19, 112, 88]. They may be for instance the players who, once removed, lead to the biggest changes in the other player's activity in game theory, or to the biggest structural change in a social network. That problem has been addressed with the introduction of graph theoretic centrality measures [16, 18] which order nodes from the most "central" to the most "peripheral" – in a sense that they themselves define. A plethora of centrality indices have been introduced and discussed in the literature on network theory [16, 18], leading up to PageRank [23]. The latter ranks nodes in a network according to the stationary probability distribution of a Markov chain on the network, accordingly it gives a meaningful ranking of websites under the reasonable assumption that websurfing is a random process. Their computational efficiency makes PageRank, as well as other purely graph theoretic indicators very attractive to identify key players on complex networks. It is thus quite tempting to apply purely graph theoretic methods to identify fast and reliably key players in network-coupled dynamical systems.

Processes such as web crawling for information retrieval are essentially random diffusive walks on a complex network, with no physical conservation law beyond the conservation of probability. The situation is similar for disease [70] or rumor [20] spreading, and for community formation [52] where graph theoretic concepts of index, centrality, betweenness, coreness and so forth have been successfully applied to identify tightly-bound communities. Coupled dynamical systems such as complex supply networks [8], electric power grids [83], consensus algorithm networks [81] or more generally network-coupled oscillators [77, 2] are however fundamentally different. There, the randomness of motion on the network giving e.g. the Markov chain at the core of PageRank is replaced by a deterministic dynamics supplemented by physical conservation laws that cannot be neglected. Pure or partially extended graph theoretic methods have been applied in vulnerability investigations of electric power grids [17, 106, 59], and investigations of cascades of failures in coupled communication and electric power networks [24, 11]. They have however been partially or totally invalidated by investigations on

## Chapter 4. The Key Player Problem in Complex Oscillator Networks and Electric Power Grids: Resistance Centralities Identify Local Vulnerabilities

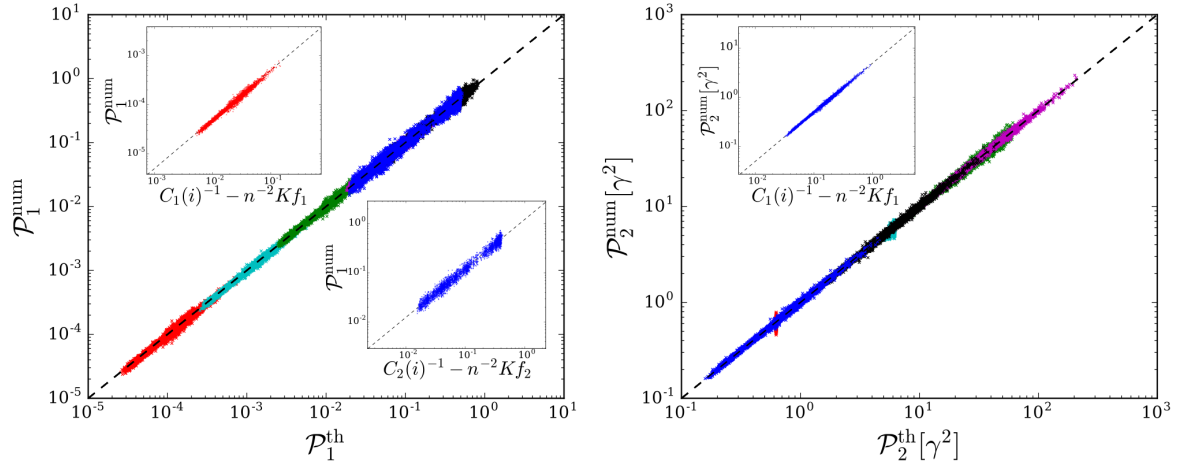


Figure 4.1 – Comparison between theoretical predictions and numerical results for both performance measures  $\mathcal{P}_1$  and  $\mathcal{P}_2$  defined in Eqs. (4.3). Each point corresponds to a noisy disturbance on a single node of the European electric power grid sketched in Fig. 4.2 (see Appendix, 4.5) and governed by Eq. (4.1) with constant inertia and damping parameters. The time-dependent disturbance  $\delta P_i(t)$  is defined by an Ornstein-Uhlenbeck noise of magnitude  $\delta P_0 = 1$  and correlation time  $\gamma\tau_0 = 4 \cdot 10^{-5}$  (red crosses),  $4 \cdot 10^{-4}$  (cyan),  $4 \cdot 10^{-3}$  (green),  $4 \cdot 10^{-2}$  (purple),  $4 \cdot 10^{-1}$  (black) and 4 (blue). Time scales are defined by the ratio of damping to inertia parameters  $\gamma = d_i/m_i = 0.4s^{-1}$  which is assumed constant with  $d_i = 0.02s$ . The insets show  $\mathcal{P}_1$  and  $\mathcal{P}_2$  as a function of the resistance distance-based graph theoretic predictions of Eqs. (4.22) valid in both limits of very large and very short noise correlation time  $\tau_0$ . Not shown is the limit of short  $\tau_0$  for  $\mathcal{P}_2$ , which gives a node-independent result, Eq. (4.22b).

more precise models of electric power transmission that take fundamental physical laws into account (in this case, Ohm's and Kirchhoff's laws) [63, 72]. It is therefore doubtful that purely topological graph theoretic descriptors are able to identify the potentially critical components in deterministic, network-coupled dynamical systems. Purely graph-theoretic approaches need to be extended to account for physical laws [17]. The influence of the dynamics on transient performance for regular graphs on  $d$ -dimensional tori has been emphasized in Ref. [7].

Here, we give an elegant solution to the key player problem for a family of deterministic, network-coupled dynamical systems related to the Kuramoto model [77, 2]. While we focus mostly on high voltage electric power grids whose swing dynamics, under the lossless line approximation, is given by a second-order version of the Kuramoto model [83, 40], we show that our approach also applies to other, generic models of network-coupled oscillators. Key players in such systems can be defined in various ways. For instance, they can be identified by an optimal geographical distribution of system parameters such as inertia, damping or natural frequencies, or alternatively as those whose removal leads to the biggest change in operating state. In this article we define key players as those nodes where a local disturbance

leads to the largest short-time transient network response. In the context of electric power grids, transient stability is the ability of the grid to maintain synchrony under relatively large disturbances such as loss or fluctuations of power generation or of a large load [76]. If under such a fault, the system remains in the vicinity of its original state, it has maintained synchrony. There are different measures to quantify the magnitude of the transient excursion, such as nadir and maximal rate of change of the network-averaged frequency [93, 55] or other dynamical quantities such as network susceptibilities [84] and the wave dynamics following disturbances [118]. Here, we quantify the total transient excursion through performance measures that are time-integrated quadratic forms in the system's degrees of freedom (see Appendix, 4.5). Transient excursions typically last ten to twenty seconds in large, continental power grids, which sets the time scales we are interested in.

Anticipating on results to come, Fig. 4.1 illustrates the excellent agreement between analytical theory and numerical calculations for such performance measures. Particularly interesting is that in both asymptotic limits of quickly and slowly decorrelating noisy disturbance, the performance measures are simply expressed in terms of the *resistance centrality* [116, 21], which is a variation of the closeness centrality [16] based on resistance distances [71]. This is shown in the insets of Fig. 4.1. Our main finding is that the resistance centrality is the relevant quantity to construct ranking algorithms in network-coupled dynamical systems.

## Results

We consider network-coupled dynamical systems defined by sets of differential equations of the form

$$m_i \ddot{\theta}_i + d_i \dot{\theta}_i = P_i - \sum_j a_{ij} \sin(\theta_i - \theta_j), \quad i = 1, \dots, n. \quad (4.1)$$

The coupled individual systems are oscillators with a compact angle degree of freedom  $\theta_i \in (-\pi, \pi]$ . Their uncoupled dynamics are determined by natural frequencies  $P_i$ <sup>1</sup>, inertia parameters  $m_i$  and damping parameters  $d_i$ . Because the degrees of freedom are compact, the coupling between oscillators needs to be a periodic function of angle differences and here we keep only its first Fourier term. The coupling between pairs of oscillators is defined on a network whose Laplacian matrix has elements  $\mathbb{L}_{ij}^{(0)} = -a_{ij}$  if  $i \neq j$  and  $\mathbb{L}_{ii}^{(0)} = \sum_{k \neq i} a_{ik}$ . Without inertia,  $m_i = 0 \forall i$ , Eq. (4.1) gives the celebrated Kuramoto model on a network with edge weights  $a_{ij} > 0, \forall i, j$  [77, 2]. With inertia on certain nodes, it is an approximate model for the swing dynamics of high voltage electric power grids in the lossless line approximation [83, 13, 40]. The latter is justified in high voltage transmission grids, where the resistance is smaller than the reactance typically by a factor of ten or more. Applied to high voltage grids, Eq. (4.1) describes the transient behavior of power grids on time scales of up to roughly ten to twenty seconds. Over such time intervals, voltage amplitudes of high voltage power grids

<sup>1</sup>We allow ourselves a small abuse of language since, strictly speaking, the natural frequency of the  $i^{\text{th}}$  oscillator would be  $P_i/d_i$ .

## Chapter 4. The Key Player Problem in Complex Oscillator Networks and Electric Power Grids: Resistance Centralities Identify Local Vulnerabilities

are almost constant, accordingly it is justified to consider only the dynamics of voltage angles [76]. In this manuscript we are interested in that transient time regime and accordingly focus on the voltage angle dynamics given by Eq. (4.1). When angle differences are small, a linear approximation  $\sin(\theta_i - \theta_j) \simeq \theta_i - \theta_j$  is justified, giving first- (without) or second-order (with inertia) consensus dynamics [81].

When the natural frequencies  $P_i$  are not too large, synchronous solutions exist that satisfy Eq. (4.1) with  $\ddot{\theta}_i = 0$  and  $\dot{\theta}_i = \omega_0, \forall i$ . Without loss of generality, one may consider Eq. (4.1) in a frame rotating with the synchronous angular frequency  $\omega_0$  in which case such states correspond to stable fixed points with  $\dot{\theta}_i = 0$ . We consider a fixed point with angle coordinates  $\boldsymbol{\theta}^{(0)} = (\theta_1^{(0)}, \dots, \theta_n^{(0)})$  corresponding to natural frequencies  $\mathbf{P}^{(0)} = (P_1^{(0)}, \dots, P_n^{(0)})$ , to which we add a time-dependent disturbance,  $P_i(t) = P_i^{(0)} + \delta P_i(t)$ . In the case of electric power grids, we will consider fixed points that are solutions to an optimal power flow problem. These solutions account for physical grid constraints such as thermal (i.e. capacity) limits of the lines and technical limitations of the power plants, as well as economic constraints following from different production costs for different power plant types (see Appendix, 4.5) [14]. Linearizing the dynamics about that solution, Eq. (4.1) becomes

$$m_i \delta \ddot{\theta}_i + d_i \delta \dot{\theta}_i = \delta P_i(t) - \sum_j a_{ij} \cos(\theta_i^{(0)} - \theta_j^{(0)}) (\delta \theta_i - \delta \theta_j), \quad i = 1, \dots, n, \quad (4.2)$$

where  $\delta \theta_i(t) = \theta_i(t) - \theta_i^{(0)}$ . This set of coupled differential equations governs the small-signal response of the system corresponding to weak disturbances. The couplings are defined by a weighted Laplacian matrix  $\mathbb{L}_{ij}(\boldsymbol{\theta}^{(0)}) = -a_{ij} \cos(\theta_i^{(0)} - \theta_j^{(0)})$  if  $i \neq j$  and  $\mathbb{L}_{ii}(\boldsymbol{\theta}^{(0)}) = \sum_k a_{ik} \cos(\theta_i^{(0)} - \theta_k^{(0)})$  which contains information on both the topology of the network and the operational state of the system. This weighted Laplacian matrix significantly differs from the network Laplacian  $\mathbb{L}^{(0)}$  when angle differences between coupled nodes are large.

We assess the nodal vulnerability of the system defined in Eq. (4.1) via the magnitude of the transient dynamics determined by Eq. (4.2) under a time-dependent disturbance  $\delta P_i(t)$ . We take the latter as an Ornstein-Uhlenbeck noise on the natural frequency of a single node, with vanishing average,  $\overline{\delta P_i(t)} = 0$ , variance  $\overline{\delta P_i^2}$  and correlation time  $\tau_0$ ,  $\overline{\delta P_i(t_1) \delta P_j(t_2)} = \delta_{ik} \delta_{jk} \overline{\delta P_0^2} \exp[-|t_1 - t_2|/\tau_0]$ . It is sequentially applied on each of the  $k = 1, \dots, n$  nodes. This noisy test disturbance is designed to investigate network properties on different time scales by varying  $\tau_0$  and identify the set of most vulnerable nodes, i.e. the key players, as the nodes where the system's response to  $\delta P_k(t)$  is largest. Besides being a probe to test nodal vulnerabilities, such noisy disturbances alternatively model fluctuating renewable energy sources in electric power grids. In this latter case, however, the correlation time  $\tau_0$  is no longer a free parameter and is typically of the order of a minute or more, i.e. larger than any dynamical time scale in the system, as we discuss below. We quantify the magnitude of the response to the disturbance with the following two performance measures [121]

$$\mathcal{P}_1 = \lim_{T \rightarrow \infty} T^{-1} \sum_i \int_0^T |\delta \theta_i(t) - \Delta(t)|^2 dt, \quad (4.3a)$$

$$\mathcal{P}_2 = \lim_{T \rightarrow \infty} T^{-1} \sum_i \int_0^T \overline{|\delta \dot{\theta}_i(t) - \dot{\Delta}(t)|^2} dt. \quad (4.3b)$$

They are similar to quadratic performance measures based on  $\mathcal{L}_2$  or  $\mathcal{H}_2$ -norms previously considered in the context of electric power grids, networks of coupled oscillators or consensus algorithms [119, 109, 110, 102, 93, 121, 31] but differ from them in two respects. First, here we subtract the averages  $\Delta(t) = n^{-1} \sum_j \delta \theta_j(t)$  and  $\dot{\Delta}(t) = n^{-1} \sum_j \delta \dot{\theta}_j(t)$  because the synchronous state does not change under a constant angle shift. Without that subtraction, artificially large performance measures may be obtained, which reflect a constant angle drift of the synchronous operational state but not a large transient excursion. Second, we divide  $\mathcal{P}_{1,2}$  by  $T$  before taking  $T \rightarrow \infty$  because we consider a noisy disturbance that is not limited in time and which would otherwise lead to diverging values of  $\mathcal{P}_{1,2}$ .

In this manuscript, we calculate  $\mathcal{P}_{1,2}$  for the network-coupled dynamical system defined in Eq. (4.1) when (i) both inertia and damping parameters are constant,  $m_i \equiv m_0$ ,  $d_i \equiv d_0$ , (ii) the inertia vanishes,  $m_i \equiv 0$ , (iii) the ratio  $\gamma \equiv d_i/m_i$  is constant, (iv) both inertia and damping vary independently. In cases (i)–(iii),  $\mathcal{P}_{1,2}$  can be analytically expressed in terms of resistance centralities that will be introduced in the next section (see Appendix, 4.5). The next paragraphs focus on case (i), following which we present numerical data for case (iv) which illustrate the general applicability of these results for not too short noise correlation time.

The performance measures  $\mathcal{P}_{1,2}$  can be computed analytically from Eq. (4.2) via Laplace transforms (see Appendix, 4.5), for homogeneous damping and inertia, i.e.  $d_i = d = \gamma m_i$ ,  $\forall i$ . In the two limits of long and short noise correlation time  $\tau_0$ , they can be expressed in terms of the resistance centrality of the node  $k$  on which the noisy disturbance acts and of graph topological indices called generalized Kirchhoff indices [71, 121]. Both quantities are based on the resistance distance, which gives the effective resistance  $\Omega_{ij}^{(1)}$  between any two nodes  $i$  and  $j$  on a fictitious electrical network where each edge is a resistor of magnitude given by the inverse edge weight in the network defined by the weighted Laplacian matrix. One obtains

$$\Omega_{ij}^{(1)}(\boldsymbol{\theta}^{(0)}) = \mathbb{L}_{ii}^\dagger(\boldsymbol{\theta}^{(0)}) + \mathbb{L}_{jj}^\dagger(\boldsymbol{\theta}^{(0)}) - \mathbb{L}_{ij}^\dagger(\boldsymbol{\theta}^{(0)}) - \mathbb{L}_{ji}^\dagger(\boldsymbol{\theta}^{(0)}), \quad (4.4)$$

where  $\mathbb{L}^\dagger$  denotes the Moore-Penrose pseudo-inverse of  $\mathbb{L}$  [71]. The resistance centrality of the  $k^{\text{th}}$  node is then defined as  $C_1(k) = [n^{-1} \sum_j \Omega_{jk}^{(1)}]^{-1}$ . It measures how central is the node  $k^{\text{th}}$  in the electrical network, in terms of its average resistance distance to all other nodes – more central nodes have smaller  $C_1(k)$ . A network descriptor, the Kirchhoff index is further defined as [71]

$$Kf_1 \equiv \sum_{i < j} \Omega_{ij}^{(1)}. \quad (4.5)$$

Generalized Kirchhoff indices  $Kf_p$  and resistance centralities  $C_p(k)$  can be defined analogously from the  $p^{\text{th}}$  power of the weighted Laplacian matrix, which is also a Laplacian matrix (see Appendix, 4.5). In terms of these quantities, the performance measures defined in Eqs. (4.3)

## Chapter 4. The Key Player Problem in Complex Oscillator Networks and Electric Power Grids: Resistance Centralities Identify Local Vulnerabilities

depend on the value of the noise correlation time  $\tau_0$  relative to the different time scales in the system. The latter are the ratios  $d/\lambda_\alpha$  of the damping coefficient  $d$  with the nonzero eigenvalues  $\lambda_\alpha$ ,  $\alpha = 2, \dots, n$ , of  $\mathbb{L}(\boldsymbol{\theta}^{(0)})$  and the inverse ratio  $\gamma^{-1} = m/d$  of damping to inertia parameters. In high voltage power grids, they are approximately given by  $d/\lambda_\alpha < 1s$  and  $m/d \cong 2.5s$ . Performance measures Eqs. (4.3) can be obtained for any correlation time  $\tau_0$  (see Appendix, 4.5). However, it is interesting to consider the specific cases where  $\tau_0$  is the smallest ( $\tau_0 \ll d/\lambda_\alpha, \gamma^{-1}$ ) or the largest ( $\tau_0 \gg d/\lambda_\alpha, \gamma^{-1}$ , appropriate for noisy power injections from new renewables) time scale in the probed system. The performance measures take in particular the asymptotic values

$$\mathcal{P}_1 = \begin{cases} (\delta P_0^2 \tau_0 / d) (C_1^{-1}(k) - n^{-2} Kf_1) , & \tau_0 \ll d/\lambda_\alpha, \gamma^{-1} \\ \delta P_0^2 (C_2^{-1}(k) - n^{-2} Kf_2) , & \tau_0 \gg d/\lambda_\alpha, \gamma^{-1} \end{cases} \quad (4.6a)$$

$$\mathcal{P}_2 = \begin{cases} (\delta P_0^2 \tau_0 / dm) (n-1)/n , & \tau_0 \ll d/\lambda_\alpha, \gamma^{-1} \\ (\delta P_0^2 / d\tau_0) (C_1^{-1}(k) - n^{-2} Kf_1) , & \tau_0 \gg d/\lambda_\alpha, \gamma^{-1} , \end{cases} \quad (4.6b)$$

in the two limits when  $\tau_0$  is the smallest or the largest time scale in the system. After averaging over the location  $k$  of the disturbed node,  $\overline{C_{1,2}^{-1}} = 2Kf_{1,2}/n^2$ , and one recovers the results of Refs. [109, 110, 121] for the global robustness of the system.

These results are remarkable : they show that the magnitude of the transient excursion under a local noisy disturbance is given by either of the generalized resistance centralities  $C_1(k)$  or  $C_2(k)$  of the perturbed node and the generalized Kirchhoff indices  $Kf_{1,2}$ . The latter are global network descriptors and are therefore fixed in a given network with fixed operational state. One concludes that perturbing the less central nodes – those with largest inverse centralities  $C_{1,2}^{-1}(k)$  – generates the largest transient excursion. In a given network, key players are therefore nodes with smallest resistance centralities. It is important to keep in mind, however, that these centralities correspond to the weighted Laplacian defined above, where internodal couplings are normalized by the cosine of voltage angle differences. Accordingly, these centralities are dependent on the initial operating state. The asymptotic analytical results of Eqs. (4.22) are corroborated by numerical results in the insets of Fig.4.1, obtained directly from Eq. (4.1), i.e. without the linearization of Eq. (4.2). The validity of the general analytical expressions for any  $\tau_0$  (see Appendix, 4.5) is further confirmed in the main panel of Fig. 4.1, and by further numerical results obtained for different networks shown in the Appendix (see 4.5).

The generalized resistance centralities and Kirchhoff indices appearing in Eqs. (4.22) depend on the operational state via the weighted Laplacian  $\mathbb{L}(\boldsymbol{\theta}^{(0)})$ . For a narrow distribution of natural frequencies  $P_i \ll \sum_j a_{ij}$ ,  $\forall i$ , angle differences between coupled nodes remain small, and the weighted Laplacian is close to the network Laplacian,  $\mathbb{L}(\boldsymbol{\theta}^{(0)}) \simeq \mathbb{L}^{(0)}$ . The resistance centralities  $C_1^{(0)}$  and  $C_2^{(0)}$  for the network Laplacian of the European electric power grid (see Appendix, 4.5) are shown in Fig. 4.3. For both centralities, the less central nodes are dominantly located in the Balkans and Spain. Additionally, for  $C_1^{(0)}$ , nodes in Denmark and Sicily are also among the most peripheral. The general pattern of these most peripheral nodes looks very similar to the

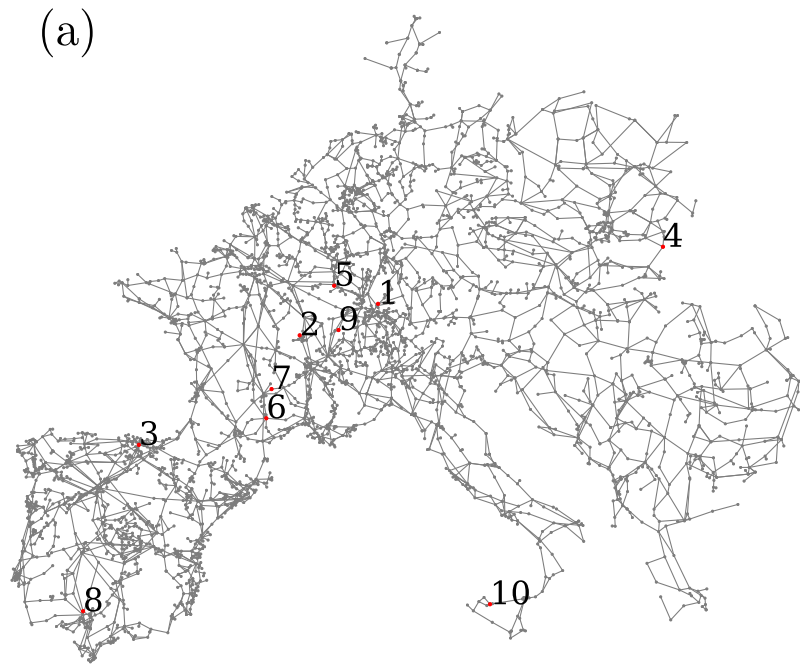


Figure 4.2 – Synchronous high voltage power grid of continental Europe. (a) Topology of the European electric power grid (see Appendix, 4.5) and location of the ten test nodes listed in Table 4.1.

pattern of most sensitive nodes numerically found in Ref. [49], and includes in particular many, but not all dead ends, which have been numerically found to undermine grid stability [87].

The asymptotic results of Eqs. (4.22), together with the numerical results of Fig. 4.1 make a strong point that nodal sensitivity to fast or slowly decorrelating noise disturbances can be predicted by generalized resistance centralities. One may wonder at this point how generalized resistance centralities differ in that prediction from other, more common centralities such as geodesic centrality, nodal degree or PageRank. Table 4.1 compares these centralities to each other and to the performance measures corresponding to slowly decorrelating noisy disturbances acting on the ten nodes shown in Fig. 4.2. As expected from Eq. (4.22),  $\mathcal{P}_1$  and  $\mathcal{P}_2$  are almost perfectly correlated with the inverse resistance centralities  $C_2^{-1}$  and  $C_1^{-1}$  respectively, but with no other centrality metrics. For the full set of nodes of the European electric power grid, we found Pearson correlation coefficients  $\rho(\mathcal{P}_1, C_2^{-1}) = 0.997$ , and  $\rho(\mathcal{P}_2, C_1^{-1}) = 0.975$  fully corroborating the prediction of Eqs. (4.22).

## Discussion

Once a one-to-one relation between the generalized resistance centralities  $C_1(k)$  and  $C_2(k)$  of the disturbed node  $k$  and the magnitude of the induced transient response is established, ranking of nodes from most to least critical is tantamount to ranking them from smallest

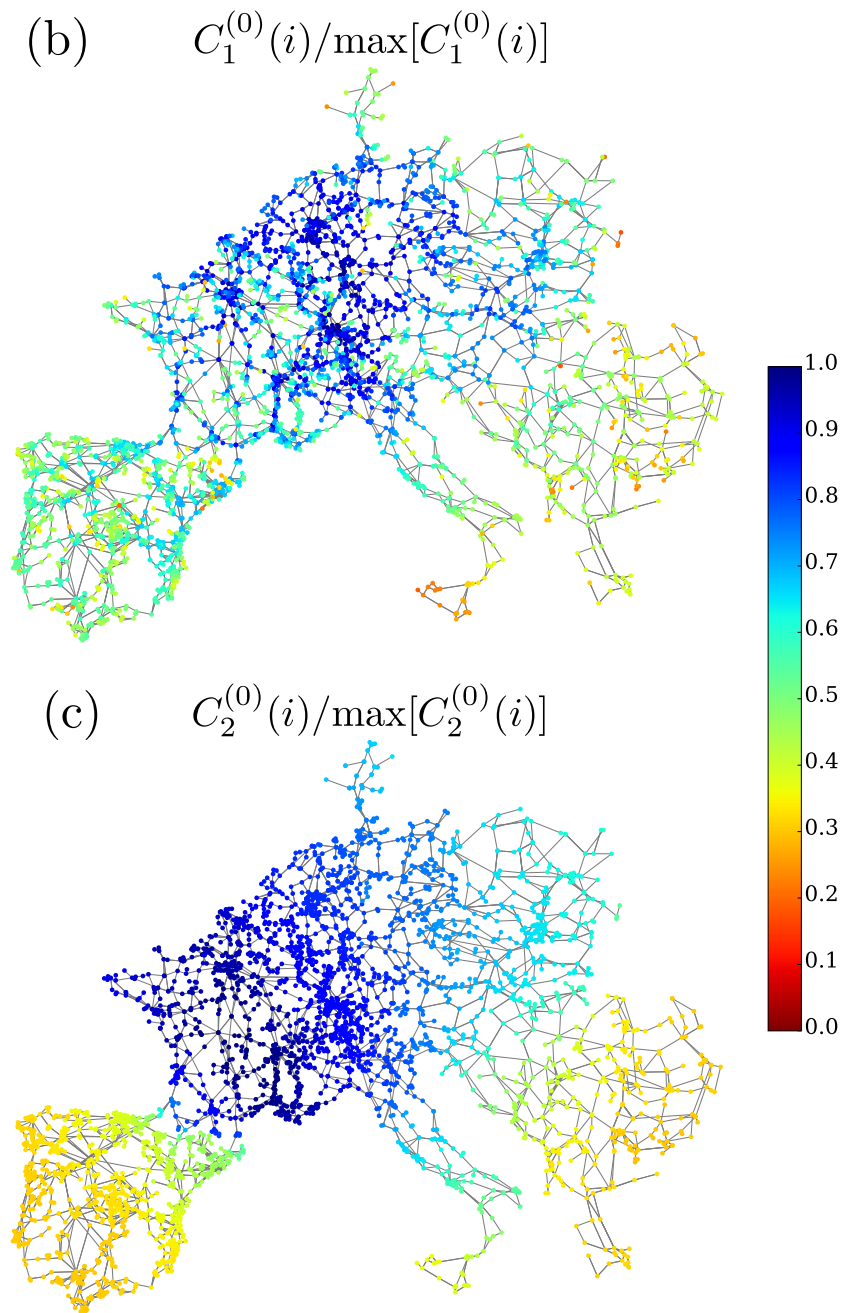


Figure 4.3 – Synchronous high voltage power grid of continental Europe. Normalized generalized resistance centralities  $C_1^{(0)}(i)$  (b), and  $C_2^{(0)}(i)$  (c) for the network Laplacian matrix of the European electric power grid.

to largest  $C_1$  or  $C_2$ . From Eqs. (4.22), which of these two centralities is relevant depends on whether one is interested (i) in the transient response under fast or slowly decorrelating noise, or (ii) in investigating transient behaviors for angles (using the performance measure  $\mathcal{P}_1$ ) or frequencies ( $\mathcal{P}_2$ ). Quite interestingly, while this gives a priori four different rankings, Eqs. (4.22)

node #	$C_{\text{geo}}$	Degree	PageRank	$C_1$	$C_2$	$\mathcal{P}_1^{\text{num}}$	$\mathcal{P}_2^{\text{num}} [\gamma^2]$
1	7.84	4	2782	31.86	5.18	0.047	0.035
2	6.8	1	199	22.45	5.68	0.021	0.118
3	5.56	10	3802	22.45	2.33	0.32	0.116
4	4.79	3	362	21.74	3.79	0.126	0.127
5	7.08	1	1217	21.74	5.34	0.026	0.125
6	4.38	6	3091	21.69	5.65	0.023	0.129
7	5.11	2	445	19.4	5.89	0.016	0.164
8	4.15	6	3648	19.38	1.83	0.453	0.172
9	5.06	1	8	10.2	5.2	0.047	0.449
10	2.72	4	3124	7.49	2.17	0.335	0.64

Table 4.1 – Centrality metrics and performance measures  $\mathcal{P}_{1,2}$  for the European electric power grid (see Appendix, 4.5) with noisy disturbances with large correlation time  $\tau_0$  applied on the nodes shown in Fig. 4.2. The performance measures  $\mathcal{P}_1$  and  $\mathcal{P}_2$  are almost perfectly correlated with the resistance centralities  $C_2$  and  $C_1$  respectively, but neither with the geodesic centrality, nor the degree, nor PageRank.

lead to only two rankings, either based on  $C_1^{-1}$  or  $C_2^{-1}$ , which can be obtained through the performance measure  $\mathcal{P}_1$  only, in either asymptotic limit of very fast (shortest time scale  $\tau_0$ ) or very slowly (largest  $\tau_0$ ) decorrelating noise. From here on, we therefore focus on the angle performance measure  $\mathcal{P}_1$  of Eq. (4.3a) and consider the two asymptotic limits in Eq. (4.22a).

We therefore define  $\text{WLRank}_1$  and  $\text{WLRank}_2$  as two rankings which order nodes from smallest to largest  $C_1$  and  $C_2$  respectively<sup>2</sup>. Smallest  $\text{WLRank}_{1,2}$  therefore identify the most vulnerable nodes in a given network. Fig. 4.4 shows that they differ very significantly. In particular a number of nodes are among the most critical according to  $\text{WLRank}_1$  but not to  $\text{WLRank}_2$  and vice-versa. This discrepancy means that nodes are not central in an absolute sense, instead, their centrality and hence how critical they are depends on details of the disturbance – in the present case, the correlation time  $\tau_0$  – and the performance measure of interest. One should therefore choose to use one or the other centrality measure, according to the network sensitivity one wants to check.

The resistance centralities in Eqs. (4.22) correspond to the network defined by the weighted Laplacian  $\mathbb{L}(\boldsymbol{\theta}^{(0)})$  defined by Eq. (4.2). They therefore depend on the unperturbed, operating state  $\boldsymbol{\theta}^{(0)}$ , consequently,  $\text{WLRank}$  depends not only on the network topology, but also, as expected, on the natural frequencies and the coupling between the nodal degrees of freedom. As mentioned above, in the strong coupling limit, angle differences between coupled nodes remain small and  $\mathbb{L}(\boldsymbol{\theta}^{(0)}) \simeq \mathbb{L}^{(0)}$ . In that limit, one therefore expects nodal ranking to be given by resistance distances corresponding to the network Laplacian  $\mathbb{L}^{(0)}$ . How long this remains true is of central interest and to answer this question we define further rankings

<sup>2</sup>When used, subscripts  $\text{LRank}_i$  and  $\text{WLRank}_i$  indicate that these are rankings obtained from the centralities  $C_i$ ,  $i = 1, 2$ .

**Chapter 4. The Key Player Problem in Complex Oscillator Networks and Electric Power Grids: Resistance Centralities Identify Local Vulnerabilities**

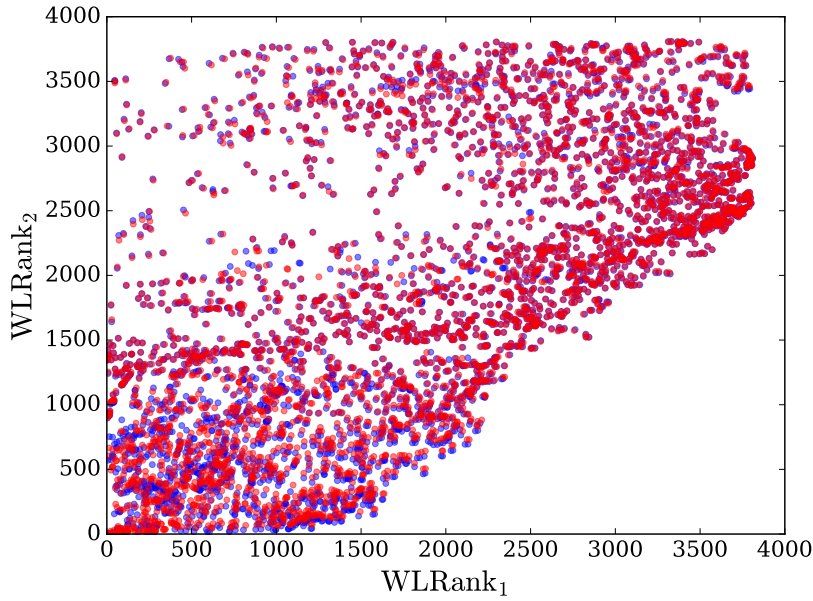


Figure 4.4 – Comparison of the two nodal rankings  $WLRank_1$  and  $WLRank_2$  obtained from the generalized resistance centralities  $C_1$  and  $C_2$  respectively for the 3809 nodes of the European electric power grid sketched in Fig. 4.2 (see Appendix, 4.5). Blue dots correspond to a moderate load during a standard winter weekday and red dots to a significantly heavier load corresponding to the exceptional November 2016 situation with a rather large consumption and twenty french nuclear reactors shut down.

$LRank_{1,2}$  as the rankings using resistance centralities  $C_{1,2}^{(0)}$  obtained from the network Laplacian  $\mathbb{L}^{(0)}$ . As long as angle differences between network-coupled nodes are not too large, the ranking  $LRank$  based on the network Laplacian matrix is almost the same as the true ranking  $WLRank$  based on the weighted Laplacian. This is shown in Fig. 4.5 for three electric power grid models and one random network of coupled oscillators. For the electric power grid models, injections/natural frequencies are limited by the standard operational constraint that the thermal limit of each power line is at most only weakly exceeded. This corresponds approximately to a maximal angle difference of  $\max(\Delta\theta) \approx 30^\circ$  between any pair of coupled nodes. Accordingly, we find that even in relatively strongly loaded power grids (corresponding for instance to the exceptional situation of the fall of 2016 when twenty french nuclear reactors were simultaneously offline; see red points in Fig. 4.5c, there is not much of a difference between  $LRank$  and  $WLRank$ . The two rankings start to differ from one another only when at least some natural frequencies become comparable with the corresponding nodal index,  $P_i \lesssim \sum_j b_{ij}$ , and angle differences become very large. This case has been investigated for an inertialess coupled oscillator system on a random rewired network with constant couplings (see Appendix, 4.5) [126]. It is shown in green in Fig. 4.5d and corresponds to  $\max(\Delta\theta) = 106^\circ$ .

In Fig. 4.6 we investigate more closely when the approximate ranking  $LRank$  starts to differ from the true ranking  $WLRank$ . To that end we used the randomly rewired model of inertialess

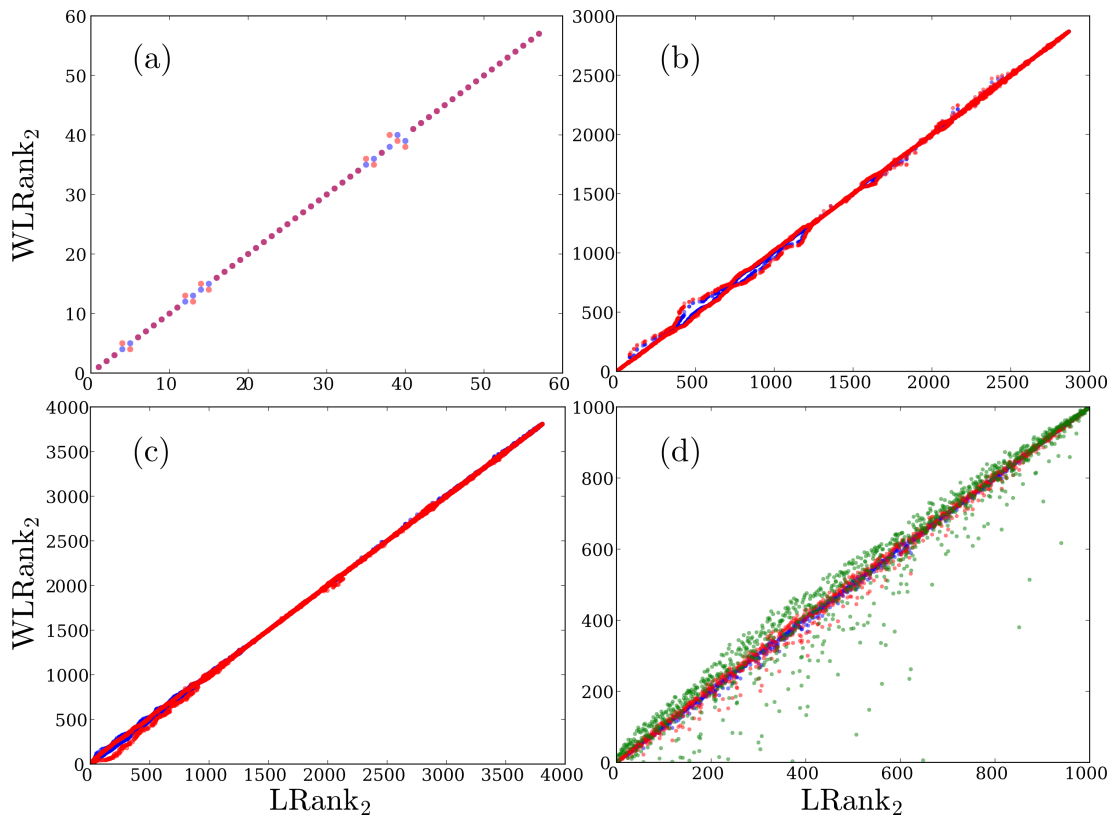


Figure 4.5 – Comparison between LRank and WLRank corresponding to  $\mathcal{P}_1$  for noisy disturbances with large correlation time  $\tau_0$ . (a–c) Electric power grid models for normally (blue) and more heavily loaded (red) operating states governed by Eq. (4.1). (a) IEEE 57 testcase where the more loaded case has injections six times larger than the moderately loaded, tabulated case [91]. (b) Pegase 2869 testcase where the more loaded case has injections 30% larger than the moderately loaded, tabulated case [134]. (c) European electric power grid model sketched in Fig. 4.2 (see Appendix, 4.5) where the moderately loaded case corresponds to a standard winter weekday and the more heavily loaded case to the November 2016 situation with twenty french nuclear reactors offline. For both cases, the operational state is obtained from an optimal power flow including physical, technological and economic constraints (see Appendix, 4.5). (d) Inertialess coupled oscillators governed by Eq. (4.1) with  $m_i = 0, \forall i$ , on a random network with 1000 nodes obtained by rewiring a cyclic graph with constant nearest and next-to-nearest neighbor coupling with probability 0.5 (see Appendix, 4.5) [126]. Natural frequencies are randomly distributed as  $P_i \in [-1.8, 1.63]$  (blue),  $P_i \in [-2.16, 1.95]$  (red) and  $P_i \in [-2.7, 2.45]$  (green), corresponding to maximal angle differences  $\max(\Delta\theta) = 31^\circ, 70^\circ$  and  $106^\circ$  respectively.

coupled oscillators of Fig. 4.5d and calculated the percentage of nodes with highest LRank<sub>2</sub> necessary to give the top 15 % ranked nodes with WLRank<sub>2</sub>. The results are plotted as a function of the maximal angle difference between directly coupled nodes. Each of the 12000 red crosses in Fig. 4.6 corresponds to one of 1000 natural frequency vectors  $\mathbf{P}^{(0)}$ , with com-

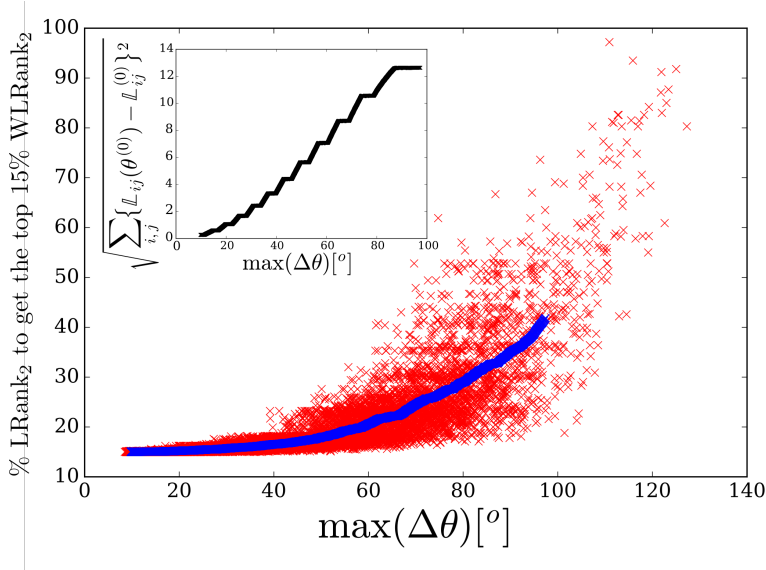


Figure 4.6 – Percentage of the nodes with highest LRank<sub>2</sub> necessary to give the top 15 % ranked nodes with WLRank<sub>2</sub> for a random network of inertialess coupled oscillators with 1000 nodes obtained by rewiring with probability 0.5 a cyclic network with constant nearest and next-to-nearest neighbor coupling (see Appendix, 4.5) [126]. Each of the 12000 red crosses corresponds to one of 1000 random natural frequency vector  $\mathbf{P}^{(0)}$  with components randomly distributed in  $[-0.5, 0.5]$  and summing to zero, multiplied by a prefactor  $\beta = 0.4, 0.6, \dots, 2.4, 2.6$ . The blue crosses correspond to running averages over 500 red crosses with consecutive values of  $\max(\Delta\theta)$ . Inset : running averages of the Frobenius distance between the matrices  $\mathbb{L}(\boldsymbol{\theta}^{(0)})$  and  $\mathbb{L}^{(0)}$ . The steps in the curve reflect discrete increments of  $\beta$ .

ponents randomly distributed in  $[-0.5, 0.5]$  and summing to zero, multiplied by a prefactor  $\beta = 0.4, 0.6, \dots, 2.4, 2.6$ . The blue crosses correspond to running averages over 500 red crosses with consecutive values of  $\max(\Delta\theta)$ . One sees that, up to almost  $\max(\Delta\theta) \simeq 40^\circ$ , the set of the 18 % of nodes with highest LRank<sub>2</sub> always includes the top 15 % ranked nodes with WLRank<sub>2</sub>. Similar results for obtaining the top 10 and 20 % ranked nodes with WLRank<sub>2</sub>, and for rankings using  $C_1$  instead of  $C_2$  are shown in the Appendix (see 4.5).

That nodal ranking remains almost the same up to angle differences of about  $40^\circ$  is quite surprising, since coupling nonlinearities are already well developed there. This is illustrated in the inset of Fig. 4.6 which plots the Frobenius distance  $\sqrt{\sum_{ij} (\mathbb{L}_{ij}(\boldsymbol{\theta}^{(0)}) - \mathbb{L}_{ij}^{(0)})^2}$  between the network Laplacian  $\mathbb{L}^{(0)}$  and the weighted Laplacian  $\mathbb{L}(\boldsymbol{\theta}^{(0)})$ . When  $\max(\Delta\theta) \simeq 40^\circ$ , the Frobenius distance has already reached about 27 % of its maximal observed value, indicating that coupling nonlinearities are already significant. Yet, obtaining a desired set of the  $n_s$  most critical nodes for any configuration with  $\max(\Delta\theta) \lesssim 40^\circ$ , including cases with nonnegligible nonlinearities, is achieved with a single matrix inversion of the network Laplacian  $\mathbb{L}^{(0)}$ , while considering a slightly extended set of  $n_s + \delta n_s$  nodes with highest LRank,  $\delta n_s / n_s \ll 1$ . This is a

moderate price to pay, compared to the price of calculating WLRank for each configuration, which each time requires inverting the weighted Laplacian matrix  $\mathbb{L}(\boldsymbol{\theta}^{(0)})$ . That latter procedure would be too-time consuming for real-time assessment of large networks.

So far we have assumed constant inertia and damping parameters, which led us to the analytical expressions given in Eqs. (4.22) for the performance measures. Analytical results can further be obtained for inertialess systems with  $m_i = 0$  as well as in the case of homogeneous damping to inertia ratio,  $d_i/m_i \equiv \gamma$ . In this latter case the ranking is again given by a resistance centrality, but this time related to the inertia-weighted matrix  $\mathbf{M}^{-1/2} \mathbb{L} \mathbf{M}^{-1/2}$  with  $\mathbf{M}$  the diagonal matrix whose  $i^{\text{th}}$  diagonal entry is given by  $m_i$  (see Appendix, 4.5), but not in the case of independently varying  $m_i$  and  $d_i$ . We therefore finally address this more general case using a purely numerical approach. This question is especially important for electric power grids where only nodes connected to rotating machines (such as conventional power plants) have inertia, and consumer nodes have significantly smaller damping parameters [13]. Time scales in electric power grids have typical values  $m_i/d_i \in [1, 3]s$  and  $d_i/\lambda_\alpha \lesssim 1s$ , and accordingly we focus on the regime of large noise correlation time  $\tau_0 \gg m_i/d_i, d_i/\lambda_\alpha$ , which is appropriate for persisting power fluctuations such as those arising from renewable energy sources. Fig. 4.7 shows results corresponding to inertia and damping parameters fluctuating randomly from node to node by up to 40 %. The ranking obtained from a full numerical calculation is compared to the ranking obtained from a direct calculation of the centrality of the weighted Laplacian  $\mathbb{L}_{ij}(\boldsymbol{\theta}^{(0)})$ , corresponding to the long correlation time asymptotic limit of Eqs. (4.22). One sees that the centrality-based ranking is close to the true, numerically obtained ranking, even in this case of strongly fluctuating inertia and damping parameters. This extends the validity of Eqs. (4.22) for large  $\tau_0$  in a much wider range of parameters than their derivation would suggest.

## Conclusion

We have formulated a key player problem in deterministic, network-coupled dynamical systems. The formulation is based on the dynamical response to a nodal additive disturbance of the initial problem, and the most critical nodes – the key players – are defined as those where the response to the disturbance is largest. While this manuscript focused on (i) noisy Ornstein-Uhlenbeck disturbances, (ii) network-coupled systems on undirected graphs, in particular with symmetric couplings  $a_{ij} = a_{ji}$  in Eq. (4.1), and (iii) performance measures of the transient response that are quadratic forms in the system's degrees of freedom, the method is not restricted to such cases. First, it can be used to deal with different disturbances and in the Appendix (see 4.5), we calculate  $\mathcal{P}_{1,2}$  for a box disturbance  $\delta P_i(t) = \delta_{ik} \delta P_0 \Theta(t) \Theta(\tau_0 - t)$  with the Heaviside function  $\Theta(t)$ . Remarkably, this disturbance gives the same ranking as the Ornstein-Uhlenbeck noise disturbance considered above. Second, asymmetric couplings occurring e.g. in directed graphs [36], in Kuramoto models with frustration [2] or in electric power grids with Ohmic dissipation [83] can also be considered. In this case, the internodal coupling is given by asymmetric real matrices instead of symmetric Laplacian matrices. How-

## Chapter 4. The Key Player Problem in Complex Oscillator Networks and Electric Power Grids: Resistance Centralities Identify Local Vulnerabilities

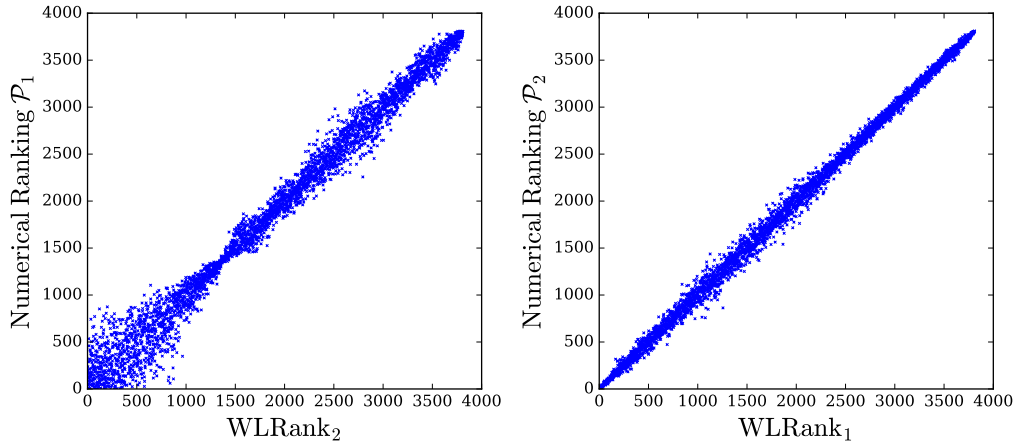


Figure 4.7 – (Left) Numerically obtained ranking based on the performance measure  $\mathcal{P}_1$  plotted against the ranking  $\text{WLRank}_2$  based on the centrality  $C_2$  and (Right) numerically obtained ranking based on the performance measure  $\mathcal{P}_2$  plotted against the ranking  $\text{WLRank}_1$  based on the centrality  $C_1$ . Each point is an average over 40 different noisy disturbances on a single node of the European electric power grid sketched in Fig. 4.2, with independently fluctuating damping and inertia coefficients,  $d_i = d_0 + \delta d_i$  and  $m_i = m_0 + \delta m_i$  with  $\delta m_i / m_0, \delta d_i / d_0 \in [-0.4, 0.4]$  and  $\gamma = d_0 / m_0 = 0.4 \text{ s}^{-1}$ . The noise correlation time is given by  $\gamma \tau_0 = 4$ .

ever, the definition of the resistance distance, Eq. (4.4), remains valid even if  $\mathbb{L}$  is replaced by an asymmetric matrix  $\mathbb{A}$ , in that it still gives  $\Omega_{ii}^{(1)} = 0$ ,  $\Omega_{ij}^{(1)} \geq 0$ , and  $\Omega_{ij}^{(1)} \leq \Omega_{ik}^{(1)} + \Omega_{kj}^{(1)}$ ,  $\forall i, j, k$  as long as the synchronous fixed point considered remains stable. Third, nonquadratic performance measures can in principle be considered within the spectral decomposition used in this article. One may think of average frequency nadir and rate of change of frequency, which are linear performance measures [93, 55]. It is at present unclear whether these quantities can be analytically related to the location of disturbances via resistance or other centralities.

We gave an elegant answer to this key player problem : ranking nodes from most to least critical is tantamount to ranking nodes from least to most central in the sense of resistance centralities. Depending on how the problem is formulated – mostly on details of the disturbance as well as on how the magnitude of the transient response is measured – different centralities have to be considered, giving different rankings. The key player problem in deterministic systems is therefore not uniquely defined and its formulation must be tailored to reflect the most relevant dynamical properties one wants to evaluate. Averaged rankings, reflecting several such properties simultaneously could also be considered. Finally we found numerically that resistance centralities are still accurate to identify the most critical nodes even when nodal dynamical parameters (damping and inertia) are not homogeneous.

The results shown in Fig. 4.7 are rather surprising, and further inspection of our analytical results, Eqs. (4.22) as well as Eq. (4.20b) suggest that an inertia dependence could emerge in the opposite limit of short correlation time  $\tau_0 \ll m_i / d_i, d_i / \lambda_\alpha$ . This point deserves further

investigations. It would be furthermore interesting to extend our investigations to cases of distributions of inertia and damping parameters corresponding to realistic electric power grids. Work along those lines is in progress.

## Appendix

### Calculation of the Performance Measures

We give some details of the calculation of the performance measures, Eqs. (4.3). These calculations generalize to second-order swing equations the results obtained for the first-order Kuramoto model in Ref. [121]. Starting from Eq. (4.1), we consider a stable fixed-point solution  $\boldsymbol{\theta}^{(0)} = (\theta_1^{(0)}, \dots, \theta_n^{(0)})$  with unperturbed natural frequencies  $\mathbf{P}^{(0)}$ . We subject this state to a time-dependent disturbance  $\mathbf{P}(t) = \mathbf{P}^{(0)} + \delta\mathbf{P}(t)$ , which makes angles become time-dependent,  $\boldsymbol{\theta}(t) = \boldsymbol{\theta}^{(0)} + \delta\boldsymbol{\theta}(t)$ . Linearizing the dynamics defined by Eq. (4.1) about  $\boldsymbol{\theta}^{(0)}$  and under the assumption that  $d_i/m_i = \gamma, \forall i$ , one obtains

$$\delta\ddot{\boldsymbol{\theta}} + \gamma\delta\dot{\boldsymbol{\theta}} = \mathbf{M}^{-1/2}\delta\mathbf{P} - \mathbf{M}^{-1/2}\mathbb{L}(\boldsymbol{\theta}^{(0)})\mathbf{M}^{-1/2}\delta\bar{\boldsymbol{\theta}}, \quad (4.7)$$

where we introduced matrices with elements  $D_{ij} = \delta_{ij}d_i = \gamma M_{ij}$  and new angle coordinates  $\delta\bar{\boldsymbol{\theta}} = \mathbf{M}^{1/2}\delta\boldsymbol{\theta}$ . The weighted Laplacian matrix  $\mathbb{L}(\boldsymbol{\theta}^{(0)})$  is defined as

$$\mathbb{L}_{ij} = \begin{cases} -a_{ij} \cos(\theta_i^{(0)} - \theta_j^{(0)}), & i \neq j, \\ \sum_k a_{ik} \cos(\theta_i^{(0)} - \theta_k^{(0)}), & i = j. \end{cases} \quad (4.8)$$

This Laplacian is minus the stability matrix of the linearized dynamics about a stable synchronous state. It is therefore positive semidefinite, with its largest eigenvalue  $\lambda_1 = 0$  corresponding to a constant eigenvector  $\mathbf{u}_1 = (1, 1, \dots, 1)/\sqrt{n}$ , and  $\lambda_\alpha > 0, \alpha = 2, 3, \dots, n$ . We define the matrix  $\mathbb{L}^M = \mathbf{M}^{-1/2}\mathbb{L}\mathbf{M}^{-1/2}$  with eigenvectors  $\mathbf{u}_\alpha^M$  and eigenvalues  $\lambda_\alpha^M$ , for  $\alpha = 1, 2, \dots, n$ . To calculate the response of the system to  $\delta\mathbf{P}(t)$ , we expand angle deviations over the eigenstates  $\mathbf{u}_\alpha^M$  of  $\mathbb{L}^M$ ,  $\delta\bar{\boldsymbol{\theta}}(t) = \sum_\alpha c_\alpha(t) \mathbf{u}_\alpha^M$ . Eq. (4.7) becomes

$$\ddot{c}_\alpha(t) + \gamma\dot{c}_\alpha(t) = \mathbf{M}^{-1/2}\delta\mathbf{P}(t) \cdot \mathbf{u}_\alpha^M - \lambda_\alpha^M c_\alpha(t). \quad (4.9)$$

The disturbance starts at  $t = 0$  and therefore  $\delta\bar{\boldsymbol{\theta}}(0) = 0$  and  $\delta\dot{\bar{\boldsymbol{\theta}}}(0) = 0$ . Performing a Laplace transform on Eq. (4.9), one gets

$$s^2 c_\alpha(s) + \gamma s c_\alpha(s) = \lambda_\alpha^M c_\alpha(s) + (\mathbf{M}^{-1/2}\delta\mathbf{P} \cdot \mathbf{u}_\alpha^M)(s), \quad (4.10)$$

where  $c_\alpha(s) = \int_0^t e^{-st'} c_\alpha(t') dt'$  and  $(\mathbf{M}^{-1/2}\delta\mathbf{P} \cdot \mathbf{u}_\alpha^M)(s) = \int_0^t e^{-st'} \mathbf{M}^{-1/2}\delta\mathbf{P}(t') \cdot \mathbf{u}_\alpha^M dt'$ . Finally one obtains the Laplace transformed expansion coefficients of the angles over the eigenbasis of  $\mathbf{u}_\alpha^M$  of  $\mathbb{L}^M$ ,

$$c_\alpha(s) = (\mathbf{M}^{-1/2}\delta\mathbf{P} \cdot \mathbf{u}_\alpha^M)(s) / \left( s - \frac{-\gamma + \Gamma_\alpha}{2} \right) \left( s + \frac{\gamma + \Gamma_\alpha}{2} \right), \quad (4.11)$$

with  $\Gamma_\alpha = \sqrt{\gamma^2 - 4\lambda_\alpha^M}$ . Applying an inverse Laplace transform leads to,

$$c_\alpha(t) = e^{-\frac{\gamma - \Gamma_\alpha}{2}t} \int_0^t e^{\Gamma_\alpha t'} \int_0^{t'} \mathbf{M}^{-1/2}\delta\mathbf{P}(t'') \cdot \mathbf{u}_\alpha^M e^{\frac{\gamma - \Gamma_\alpha}{2}t''} dt'' dt'. \quad (4.12)$$

The time-dependence of angle and frequency degrees of freedom is then given by,

$$\delta\boldsymbol{\theta}(t) = \mathbf{M}^{-1/2}\delta\bar{\boldsymbol{\theta}}(t) = \sum_{\alpha} c_{\alpha}(t)\mathbf{M}^{-1/2}\mathbf{u}_{\alpha}^M, \quad (4.13)$$

$$\delta\dot{\boldsymbol{\theta}}(t) = \mathbf{M}^{-1/2}\delta\dot{\bar{\boldsymbol{\theta}}}(t) = \sum_{\alpha} \dot{c}_{\alpha}(t)\mathbf{M}^{-1/2}\mathbf{u}_{\alpha}^M. \quad (4.14)$$

The variances  $p_1(t)$  and  $p_2(t)$  of the angle and frequency deviations read,

$$p_1(t) = \delta\boldsymbol{\theta}^2(t) = \sum_{\alpha,\beta} c_{\alpha}(t)c_{\beta}(t)\mathbf{u}_{\beta}^{M\top}\mathbf{M}^{-1}\mathbf{u}_{\alpha}^M, \quad (4.15)$$

$$p_2(t) = \delta\dot{\boldsymbol{\theta}}^2(t) = \sum_{\alpha,\beta} \dot{c}_{\alpha}(t)\dot{c}_{\beta}(t)\mathbf{u}_{\beta}^{M\top}\mathbf{M}^{-1}\mathbf{u}_{\alpha}^M. \quad (4.16)$$

When  $d_i = d = \gamma m_i \forall i$ , both matrices  $\mathbb{L}$  and  $\mathbb{L}^M$  have the same eigenvectors and  $\lambda_{\alpha}^M = \lambda_{\alpha}/m$ . Below we consider noisy disturbances sequentially for the homogeneous case,  $m_i = m$ ,  $d_i = d$ , inertialess case,  $m_i = 0$  and constant ratio case,  $d_i/m_i = \gamma$ .

### Correlated Noisy disturbances

#### Homogeneous Case

We assume homogeneous inertia and damping factor, respectively  $m_i = m$  and  $d_i = d$ , for the next calculations. In the case of stochastic disturbances that persist in time, we average the  $p_i$ 's as follows,

$$\mathcal{P}_i = \lim_{T \rightarrow \infty} T^{-1} \int_0^T \overline{p_i(t)} dt, \quad i = 1, 2, \quad (4.17)$$

where  $\overline{p_i(t)}$  indicates an average taken over the ensemble defined by e.g. the moments of the stochastic disturbance. We consider Ornstein-Uhlenbeck correlated noise on a single node,  $k$ , with zero mean  $\overline{\delta P_k(t)} = 0$  and second moment  $\overline{\delta P_i(t_1)\delta P_j(t_2)} = \delta_{ik}\delta_{jk}\delta P_0^2 \exp[-|t_1 - t_2|/\tau_0]$ , correlated over a typical time scale  $\tau_0$ . We have,

$$\mathcal{P}_1 = \lim_{T \rightarrow \infty} T^{-1} \sum_{\alpha \geq 2} \int_0^T \overline{c_{\alpha}^2(t)} dt \quad (4.18)$$

$$\begin{aligned} &= \lim_{T \rightarrow \infty} T^{-1} \sum_{\alpha \geq 2} \int_0^T e^{-(\gamma + \Gamma_{\alpha})t} \int_0^t \int_0^t e^{\Gamma_{\alpha}(t'_1 + t'_2)} \times \\ &\quad \int_0^{t'_1} \int_0^{t'_2} \sum_{i,j} \frac{u_{\alpha,i}u_{\alpha,j}}{m} \overline{\delta P_i(t''_1)\delta P_j(t''_2)} e^{\frac{\gamma - \Gamma_{\alpha}}{2}(t''_1 + t''_2)} dt dt'_1 dt'_2 dt''_1 dt''_2. \end{aligned} \quad (4.19)$$

## Chapter 4. The Key Player Problem in Complex Oscillator Networks and Electric Power Grids: Resistance Centralities Identify Local Vulnerabilities

---

For homogeneous damping and inertia one has  $\Gamma_\alpha = \sqrt{\gamma^2 - 4\lambda_\alpha/m}$ . The integrals can be performed straightforwardly and one obtains

$$\mathcal{P}_1 = \delta P_0^2 \sum_{\alpha \geq 2} \frac{u_{\alpha,k}^2(\tau_0 + m/d)}{\lambda_\alpha(\lambda_\alpha \tau_0 + d + m\tau_0^{-1})}, \quad (4.20a)$$

$$\mathcal{P}_2 = \delta P_0^2 \sum_{\alpha \geq 2} \frac{u_{\alpha,k}^2}{d(\lambda_\alpha \tau_0 + d + m\tau_0^{-1})}. \quad (4.20b)$$

Taking the two limits  $\lambda_\alpha \tau_0 \gg d$ ,  $\lambda_\alpha \tau_0^2 \gg m$  and  $\lambda_\alpha \tau_0 \ll d$ ,  $\lambda_\alpha \tau_0^2 \ll m$ , Eqs. (6a,b) of the main text are then easily obtained.

### *Inertialess case*

The performance measures for Kuramoto oscillators are obtained from Eqs. (4.20) with  $m = 0$  [39]

$$\mathcal{P}_1 = \delta P_0^2 \sum_{\alpha \geq 2} \frac{u_{\alpha,k}^2 \tau_0}{\lambda_\alpha(\lambda_\alpha \tau_0 + d)}, \quad (4.21a)$$

$$\mathcal{P}_2 = \delta P_0^2 \sum_{\alpha \geq 2} \frac{u_{\alpha,k}^2}{d(\lambda_\alpha \tau_0 + d)}. \quad (4.21b)$$

The asymptotics are then obtained by taking the asymptotic limits of large/small  $\tau_0$  only after setting  $m = 0$ . One obtains,

$$\mathcal{P}_1 = \begin{cases} (\delta P_0^2 \tau_0 / d)(C_1^{-1}(k) - n^{-2} Kf_1), & \lambda_\alpha \tau_0 \ll 1, \\ \delta P_0^2 (C_2^{-1}(k) - n^{-2} Kf_2), & \lambda_\alpha \tau_0 \gg d, \end{cases} \quad (4.22a)$$

$$\mathcal{P}_2 = \begin{cases} (\delta P_0^2 \tau_0 / d)(n-1)/n, & \lambda_\alpha \tau_0 \ll 1, \\ (\delta P_0^2 / d \tau_0)(C_1^{-1}(k) - n^{-2} Kf_1), & \lambda_\alpha \tau_0 \gg d, \end{cases} \quad (4.22b)$$

where we use the generalized resistance centralities  $C_{1,2}(i)$  and Kirchhoff indices  $Kf_{1,2}$  discussed in Section 4.5.2 below.

### *Constant inertia to damping ratio*

The cases of varying  $m_i$  and  $d_i$  can be further treated analytically, provided the ratio  $d_i/m_i = \gamma$  remains constant. The price to pay is to include inertia coefficients in the performance measures and consider

$$\mathcal{P}_1 = \lim_{T \rightarrow \infty} T^{-1} \sum_i m_i \int_0^T \frac{1}{|\delta\theta_i(t) - \Delta(t)|^2} dt, \quad (4.23a)$$

$$\mathcal{P}_2 = \lim_{T \rightarrow \infty} T^{-1} \sum_i m_i \int_0^T \frac{1}{|\delta\dot{\theta}_i(t) - \dot{\Delta}(t)|^2} dt. \quad (4.23b)$$

Note that this is not a fundamental redefinition, since all previously obtained results in the case of constant inertia and damping can be multiplied by  $m_i \equiv m$  for comparison with results

about to be presented. Performance measures are then obtained in a similar way as for the homogeneous case. They read,

$$\mathcal{P}_1 = \frac{\delta P_0^2}{m_k} \sum_{\alpha \geq 2} \frac{u_{\alpha,k}^{M^2} (\tau_0 \gamma + 1)}{\gamma \lambda_\alpha^M (\lambda_\alpha^M \tau_0 + \gamma + \tau_0^{-1})}, \quad (4.24a)$$

$$\mathcal{P}_2 = \frac{\delta P_0^2}{m_k} \sum_{\alpha \geq 2} \frac{u_{\alpha,k}^{M^2}}{\gamma (\lambda_\alpha^M \tau_0 + \gamma + \tau_0^{-1})}. \quad (4.24b)$$

Here,  $\lambda_\alpha^M, \mathbf{u}_\alpha^M$  are respectively the eigenvalues and eigenvectors of the matrix  $\mathbf{M}^{-1/2} \mathbb{L} \mathbf{M}^{-1/2}$ . Similar expressions were obtained for other performance measures such as kinetic energy, primary control effort or line dissipation [119, 109, 110, 31]. In both limits  $\tau_0 \ll \gamma^{-1}, \lambda_\alpha^{M^{-1/2}}$  and  $\tau_0 \gg \gamma^{-1}, \lambda_\alpha^{M^{-1/2}}$  performance measures  $\mathcal{P}_1, \mathcal{P}_2$  can be expressed in terms of resistance centralities related to  $\mathbf{M}^{-1/2} \mathbb{L} \mathbf{M}^{-1/2}$  (see Eq. (4.32) with  $\mathbb{L}' = \mathbf{M}^{-1/2} \mathbb{L} \mathbf{M}^{-1/2}$ ) and the inertia  $m_k$  of the perturbed node.

### Box disturbances

The same kind of computation as for the noisy disturbance can be done with a box disturbance acting on node  $k$ , i.e.  $\delta P_i(t) = \delta_{ik} \delta P_0 \Theta(t) \Theta(\tau_0 - t)$  with the Heaviside step function  $\Theta(t) = 0$  for  $t < 0$  and  $\Theta(t) = 1$  for  $t \geq 1$ . As the perturbation is limited in time, we consider the performance measures,

$$\mathcal{P}_1^\infty = \sum_i \int_0^\infty |\delta \theta_i - \Delta(t)|^2 dt, \quad (4.25)$$

$$\mathcal{P}_2^\infty = \sum_i \int_0^\infty |\delta \dot{\theta}_i - \dot{\Delta}(t)|^2 dt, \quad (4.26)$$

instead of (4.17). For uniform inertia and damping one obtains,

$$\mathcal{P}_1^\infty = \frac{\delta P_0^2 m}{8\gamma} \sum_{\alpha \geq 2} \frac{u_{\alpha,k}^2}{\Gamma_\alpha \lambda_\alpha^3} \left[ 2\Gamma_\alpha (4\gamma \tau_0 \lambda_\alpha / m - 3\gamma^2 - \Gamma_\alpha^2) + (\gamma + \Gamma_\alpha)^3 e^{-\tau_0 \frac{(\gamma - \Gamma_\alpha)}{2}} - (\gamma - \Gamma_\alpha)^3 e^{-\tau_0 \frac{(\gamma + \Gamma_\alpha)}{2}} \right],$$

$$\mathcal{P}_2^\infty = \frac{\delta P_0^2}{2d} \sum_{\alpha \geq 2} \frac{u_{\alpha,k}^2}{\Gamma_\alpha \lambda_\alpha} \left[ 2\Gamma_\alpha - (\gamma + \Gamma_\alpha) e^{-\frac{\tau_0(\gamma - \Gamma_\alpha)}{2}} + (\gamma - \Gamma_\alpha) e^{-\frac{\tau_0(\gamma + \Gamma_\alpha)}{2}} \right],$$

with  $\Gamma_\alpha = \sqrt{\gamma^2 - 4\lambda_\alpha / m}$ . The two asymptotic limits of large and small  $\tau_0$  are given by,

$$\mathcal{P}_1^\infty = \begin{cases} (\delta P_0^2 \tau_0^2 / 2d) (C_1^{-1}(k) - n^{-2} K f_1), & (\gamma \pm \Gamma_\alpha) \tau_0 \ll 1, \\ \delta P_0^2 \tau_0 (C_2^{-1}(k) - n^{-2} K f_2), & (\gamma \pm \Gamma_\alpha) \tau_0 \gg 1 \text{ and } \lambda_\alpha \tau_0 / d \gg 1, \end{cases} \quad (4.27a)$$

$$\mathcal{P}_2^\infty = \begin{cases} (\delta P_0^2 \tau_0^2 / 2md) (n-1)/n, & (\gamma \pm \Gamma_\alpha) \tau_0 \ll 1, \\ (\delta P_0^2 / d) (C_1^{-1}(k) - n^{-2} K f_1), & (\gamma \pm \Gamma_\alpha) \tau_0 \gg 1, \end{cases} \quad (4.27b)$$

which are also given by resistance centralities and Kirchhoff indices.

### Resistance Distances, Centralities and Kirchhoff Indices

The resistance centralities  $C_1$  and  $C_2$  can be expressed as functions of the distribution of resistance distances  $\Omega_{ij}^{(1)}$ , between any pairs of nodes  $(i, j)$  of the network. The Laplacian matrix  $\mathbb{L}$  of the network has one zero eigenvalue associated to the constant eigenvector  $u_{1,i} = 1/\sqrt{n}$ , its pseudoinverse  $\mathbb{L}^\dagger$  is defined by [71],

$$\mathbb{L}\mathbb{L}^\dagger = \mathbb{L}^\dagger\mathbb{L} = \mathbb{1} - \mathbf{u}_1\mathbf{u}_1^\top, \quad (4.28)$$

from which the resistance distance between nodes  $i$  and  $j$  is expressed as,

$$\Omega_{ij}^{(1)} = \mathbb{L}^\dagger_{ii} + \mathbb{L}^\dagger_{jj} - \mathbb{L}^\dagger_{ij} - \mathbb{L}^\dagger_{ji}. \quad (4.29)$$

Using the eigenvectors of  $\mathbb{L}$  we can rewrite Eq. (4.29) as [39],

$$\Omega_{ij}^{(1)} = \sum_{\alpha \geq 2} \frac{(u_{\alpha,i} - u_{\alpha,j})^2}{\lambda_\alpha}. \quad (4.30)$$

The resistance distance is a graph metric in the sense that : i)  $\Omega_{ii}^{(1)} = 0, \forall i$ , ii)  $\Omega_{ij}^{(1)} \geq 0, \forall i, j$ , and iii)  $\Omega_{ij}^{(1)} + \Omega_{jk}^{(1)} \geq \Omega_{ik}^{(1)}, \forall i, j, k$  (triangle inequality) [71]. The Kirchhoff index of a network is obtained from the resistance distances by summing over all pairs of nodes [71],

$$Kf_1 = \sum_{i < j} \Omega_{ij}^{(1)} = n \sum_{\alpha \geq 2} \lambda_\alpha^{-1}. \quad (4.31)$$

The Kirchhoff index is, up to a normalization factor, the mean resistance distance over the whole graph.

We generalize this definition of the resistance distance for matrices that are powers of the original Laplacian matrix,  $\mathbb{L}' = \mathbb{L}^p$  and thus  $[\mathbb{L}']^\dagger = [\mathbb{L}^p + \mathbf{u}_1\mathbf{u}_1^\top]^{-1}$ . One has

$$\Omega_{ij}^{(p)} = [\mathbb{L}']^\dagger_{ii} + [\mathbb{L}']^\dagger_{jj} - [\mathbb{L}']^\dagger_{ij} - [\mathbb{L}']^\dagger_{ji}. \quad (4.32)$$

The eigenvectors of  $\mathbb{L}'$  are the same as those of  $\mathbb{L}$ . Thus we have,

$$\Omega_{ij}^{(p)} = \sum_{\alpha \geq 2} \frac{(u_{\alpha,i} - u_{\alpha,j})^2}{\lambda_\alpha^p}. \quad (4.33)$$

We still have to check that the generalized resistance distances  $\Omega_{ij}^{(p)}$  have the three properties of a graph metric. We remark that  $\Omega_{ij}^{(p)}$  corresponds to the resistance distance between nodes  $i$  and  $j$  in a new graph whose Laplacian is  $\mathbb{L}' = \mathbb{L}^p$ . Therefore it is sufficient to show that  $\mathbb{L}'$  is also a Laplacian matrix. to that end we demonstrate that the product of two Laplacian matrices  $\mathcal{A}$  and  $\mathcal{B}$  is still a Laplacian matrix. For a Laplacian matrix  $\mathcal{A}$  one has (i)  $\sum_i \mathcal{A}_{ij} = 0$ , (ii)  $\mathcal{A}_{ii} = -\sum_{j \neq i} \mathcal{A}_{ij}$ . From these generic properties of Laplacian matrices, matrix elements of

the product  $\mathcal{A}\mathcal{B}$  satisfy

$$\sum_j [\mathcal{A}\mathcal{B}]_{ij} = \sum_{j,k} \mathcal{A}_{ik} \mathcal{B}_{kj} = 0, \quad (4.34)$$

$$\sum_{j \neq i} [\mathcal{A}\mathcal{B}]_{ij} = \sum_j [\mathcal{A}\mathcal{B}]_{ij} - [\mathcal{A}\mathcal{B}]_{ii} = -[\mathcal{A}\mathcal{B}]_{ii}. \quad (4.35)$$

We conclude that the product  $\mathcal{A}\mathcal{B}$  is also a Laplacian matrix, and therefore, the generalized resistance distances  $\Omega_{ij}^{(p)}$  have the three properties of a graph metric. With the generalized resistance distances, we can define generalized Kirchhoff indices [121],

$$Kf_p = \sum_{i < j} \Omega_{ij}^{(p)} = n \sum_{\alpha \geq 2} \lambda_\alpha^{-p}. \quad (4.36)$$

The relation between the resistive centrality  $C_1(i)$  and the resistance distance is obtained from Eqs. (4.30) and (4.31),

$$C_1(i) = \left[ n^{-1} \sum_j \Omega_{ij}^{(1)} \right]^{-1} = \left[ \sum_{\alpha \geq 2} \frac{u_{\alpha,i}^2}{\lambda_\alpha} + n^{-2} Kf_1 \right]^{-1}. \quad (4.37)$$

The expression for  $C_2(i)$  involves higher moments of the distribution of resistance distances. We obtain

$$C_2(i) = \sum_j \Omega_{ij}^{(1)2} - n C_1^{-2}(i) + 2 \sum_j \Omega_{ij}^{(1)} C_1^{-1}(j) - 4 C_1^{-1}(i) n^{-1} Kf_1 - 3 \sum_j C_1^{-2}(j) + 12 n^{-3} Kf_1^2.$$

### Numerical Comparison of LRank with WLRank

In Fig.5 of the main text, we calculated the percentage of nodes with highest LRank<sub>2</sub> necessary to give the top 15 % ranked nodes with WLRank<sub>2</sub>. The conclusions drawn from these data are generic – they are valid for different percentages than 15% and for LRank<sub>1</sub> vs. WLRank<sub>1</sub>. This is illustrated in Fig. 4.8, which shows similar results for the percentage of nodes with highest LRank<sub>1,2</sub> that include the top 10% and 20% ranked nodes with WLRank<sub>1,2</sub>.

**Chapter 4. The Key Player Problem in Complex Oscillator Networks and Electric Power Grids: Resistance Centralities Identify Local Vulnerabilities**

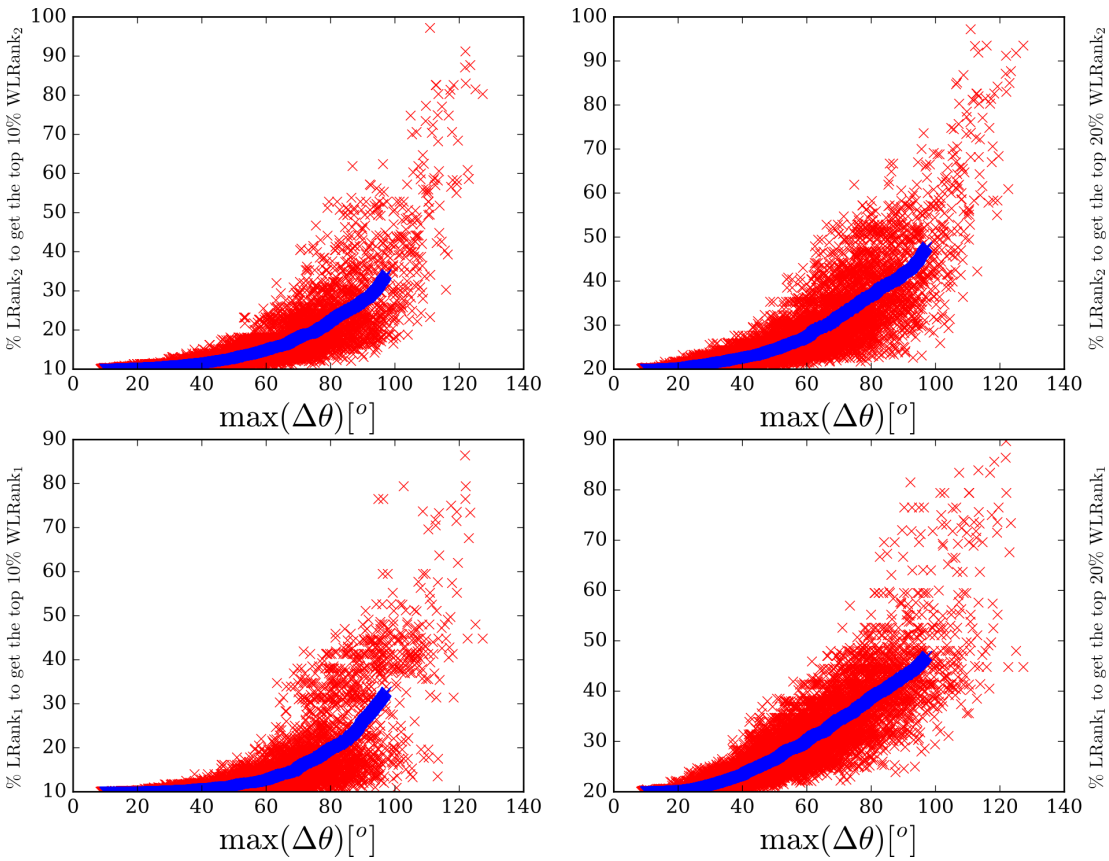


Figure 4.8 – Percentage of the nodes with highest  $LRank_{1,2}$  necessary to give the top 10 % (left), 20% (right) ranked nodes with  $WLRank_{1,2}$  for a random network of inertialess coupled oscillators with 1000 nodes obtained by rewiring with probability 0.5 a cyclic graph with constant nearest and next-to-nearest neighbor coupling (see Appendix, 4.5). Each of the 12000 red crosses corresponds to one of 1000 random natural frequency vector  $\mathbf{P}^{(0)}$  with components randomly distributed in  $[-0.5, 0.5]$  and summing to zero, multiplied by a prefactor  $\beta = 0.4, 0.6, \dots 2.6$ . The blue crosses correspond to running averages over 500 red crosses with consecutive values of  $\max(\Delta\theta)$ .

# **5 Noise-Induced Desynchronization and Stochastic Escape from Equilibrium in Complex Networks**

*Chapter 5 is a postprint version of an article published as:*

M. Tyloo, R. Delabays, P. Jacquod, *Physical Review E*, 99(6):062213 (2019) [122].

## Chapter 5. Noise-Induced Desynchronization and Stochastic Escape from Equilibrium in Complex Networks

---

Complex physical systems are unavoidably subjected to external environments not accounted for in the set of differential equations that models them. The resulting perturbations are standardly represented by noise terms. If these terms are large enough, they can push the system from an initial stable equilibrium point, over a nearby saddle point, outside of the basin of attraction of the stable point. Except in some specific cases, the distance between these two points is not known analytically. Focusing on Kuramoto-like models and under simple assumptions on this distance, we derive conditions under which such noise terms perturb the dynamics strongly enough that they lead to stochastic escape from the initial basin of attraction. We numerically confirm the validity of that criterion for coupled oscillators on four very different complex networks. We find in particular that, quite counterintuitively, systems with inertia leave their initial basin faster than or at the same time as systems without inertia, except for strong white-noise perturbations.

### Introduction

Complex physical systems are mathematically modelled as dynamical systems. Equilibrium and steady states, if they exist, are determined and characterized by fixed points and limit cycles/tori of the corresponding differential equations [92]. For deterministic dynamical systems, the latter equations should be complemented by stochastic terms to account for unavoidable perturbations from unaccountable environmental degrees of freedom [124]. A central question of broad interest is to determine the magnitude and statistical properties of the relevant stochastic terms that could lead to the loss of equilibrium or induce transitions between different local equilibria. Some physically important situations where such stochastic escape phenomena may occur are electric power grids with high penetration of fluctuating renewable energy sources [82, 4, 107], superconducting rings [53] and Josephson junction arrays [64] subjected to noisy magnetic fields, as well as neuronal systems subjected to synaptic, ion-channel, neurotransmitter or membrane potential noise [22, 80].

Despite decades of investigations, theoretical studies of problems related to stochastic escape are generally extensions of the pioneering work of Kramers [75], which relates chemical reaction rates to action integrals between different potential minima. The problem is analytically tractable in low dimensions only (see also Ref. [41]), and several recent works considered noise-induced large fluctuations in the dynamical behavior of higher-dimensional network-coupled systems through the numerical determination of action minimizing paths [38, 107, 60, 61]. A better analytical understanding of the interplay of noise characteristics with the network topology is clearly desirable.

For some noisy coupled dynamical systems, escapes from a basin of attraction can be related to noise characteristics and to the topology of the interaction network. For sufficiently weak, bounded noise, fluctuations are small and there is no stochastic escape [79]. Noise makes the system fluctuate about its equilibrium, and typical deviation amplitudes can be evaluated from a linearized dynamics about the equilibrium [7, 121, 57]. The situation becomes fundamentally

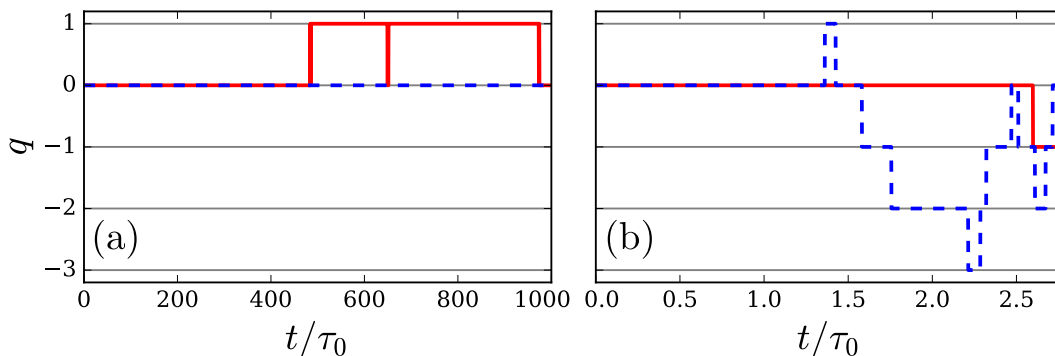


Figure 5.1 – Time evolution of the winding number  $q$  for Eq.(5.1) on a single-cycle network with  $n = 83$  nodes,  $m = 0$  (red lines) and  $\frac{m}{d} / \frac{d}{\lambda_2} = 10/175$  (blue dashed lines). (a) Noise with short correlation time  $\lambda_2 \tau_0 / d = 5.7 \cdot 10^{-4}$ . (b) Noise with longer correlation time  $\lambda_2 \tau_0 / d = 0.03$ .

different for stronger noise. For Kuramoto-like models, Eq. (5.1), with additive Ornstein-Uhlenbeck noise, this is illustrated in Fig. 5.1, which shows the time-evolution of the winding number  $q$  (defined in Sec. 5.4), characterizing different equilibrium fixed points. Changes in  $q$  indicate that the system visits other basins of attraction, surrounding different equilibrium states. Below we use  $q$  to detect transition from one basin to another. Depending on the oscillators' inertia and the noise amplitude and correlation time, this happens more or less quickly and for longer or shorter periods of time. Due to the high dimensionality of the state space and the nonlinear coupling between oscillators, the exact shape and size of the basins are impossible to capture [128, 86, 35], consequently, the escape time from one basin is hard to predict. For the Kuramoto model with cyclic interactions, DeVille [38] showed that the escape time scales as the exponential of the potential barrier height between the initial and final equilibrium states. In the spirit of Kramers [75], Hindes and Schwartz [60, 61] further relate the escape time to the numerically computed action on the action-minimizing trajectory between the two equilibria. In higher dimensions it is hard to see how these approaches could give analytical estimates other than in specific situations.

In this paper we propose a resolutely different approach to stochastic escape from stable equilibria in complex, network-coupled dynamical systems, incorporating noise characteristics as well as network dynamics and topology. We focus on synchronous fixed points of Kuramoto-like models [i.e.,  $\dot{\theta}_i(t) = \dot{\theta}_j(t)$ ,  $\forall i, j, t$ ], but stress that the approach is applicable to more general systems. We subject the initial, synchronous state to additive Ornstein-Uhlenbeck noise. Linearizing the dynamics about the synchronous state, we calculate the standard deviation of the noise-induced fluctuations about that state. The linearized dynamics is no longer accurate when the standard deviation exceeds some threshold distance  $D_c$ . Clearly,  $D_c$  is bounded from above by the distance  $\Delta$  between the stable synchronous state and the closest saddle point to the next basin of attraction. We postulate that  $D_c$  is parametrically proportional to  $\Delta$ . This postulate allows us to derive a criterion for stochastic escape based on the distance  $\Delta$  between the initial stable synchronous fixed point and the nearest saddle point and not as in Kramers' and other approaches [75, 38, 107, 60, 61] on their potential height

## Chapter 5. Noise-Induced Desynchronization and Stochastic Escape from Equilibrium in Complex Networks

---

difference. We validate numerically our postulate that  $D_c \sim \Delta$  for four, very different networks and furthermore show that it gives precise estimates for the first stochastic escape time. We note that similar linearization procedures have been used in a different context in Ref. [101] to predict transitions in an evolutionary ecology model.

The paper is organized as follows. In section 5.2, we introduce our model of coupled oscillators and give analytical expressions for the response induced by noisy perturbations. Section 5.3 describes our criterion for stochastic escapes, and section 5.4 illustrates numerically our theory. Our conclusions are given in section 5.5.

### The Model

We consider generic, Kuramoto-like models of nonlinearly coupled oscillators on complex graphs defined by the differential equations [77]

$$m\ddot{\theta}_i + d\dot{\theta}_i = P_i - \sum_j a_{ij} \sin(\theta_i - \theta_j). \quad (5.1)$$

Oscillators with inertia  $m$  and damping parameter  $d$  are described by compact angle coordinates  $\theta_i \in (-\pi, \pi)$  and natural frequencies  $P_i \in \mathbb{R}$ . They are located on nodes  $i = 1, \dots, n$  of a connected coupling network defined by the adjacency matrix,  $a_{ij} \geq 0$ . Without loss of generality, we consider  $\sum_i P_i = 0$ , which is equivalent to considering the system in a rotating frame, because Eq. (5.1) is invariant under  $\theta_i(t) \rightarrow \theta_i(t) + \Omega t$ ,  $P_i \rightarrow P_i + d\Omega$ . For bounded distributions of natural frequencies on small enough intervals, synchronous states exist with  $\dot{\theta}_i \equiv 0$ ,  $\forall i$ .

We consider a stable synchronous state  $\boldsymbol{\theta}^{(0)} = (\theta_1^{(0)}, \dots, \theta_n^{(0)})$  corresponding to natural frequencies  $\mathbf{P}^{(0)}$ . We subject this state to a time-dependent perturbation  $\mathbf{P}(t) = \mathbf{P}^{(0)} + \delta\mathbf{P}(t)$ . Linearizing the dynamics defined by Eq. (5.1) with  $\boldsymbol{\theta}(t) = \boldsymbol{\theta}^{(0)} + \delta\boldsymbol{\theta}(t)$ , one obtains

$$m\delta\ddot{\boldsymbol{\theta}} + d\delta\dot{\boldsymbol{\theta}} \approx \delta\mathbf{P} - \mathbb{L}(\{\theta_i^{(0)}\})\delta\boldsymbol{\theta}, \quad (5.2)$$

with the weighted Laplacian  $\mathbb{L}(\{\theta_i^{(0)}\})$  defined by

$$\mathbb{L}_{ij} = \begin{cases} -a_{ij} \cos(\theta_i^{(0)} - \theta_j^{(0)}), & i \neq j, \\ \sum_k a_{ik} \cos(\theta_i^{(0)} - \theta_k^{(0)}), & i = j. \end{cases} \quad (5.3)$$

This matrix is positive semidefinite, with a single eigenvalue  $\lambda_1 = 0$  and associated eigenvector  $\mathbf{u}_1 = (1, 1, 1, \dots, 1)/\sqrt{n}$ , while  $\lambda_\alpha > 0$ ,  $\alpha = 2, 3, \dots, n$ .

The dynamics of Eq. (5.2) is characterized by different times scales. The first one characterizes the noisy perturbations. We consider spatially uncorrelated noise with vanishing average and

Ornstein-Uhlenbeck correlator

$$\langle \delta P_i(t_1) \delta P_j(t_2) \rangle = \delta_{ij} \delta P_0^2 \exp[-|t_1 - t_2|/\tau_0]. \quad (5.4)$$

Thus, the perturbation is characterized by its variance,  $\delta P_0^2$  and its correlation time,  $\tau_0 > 0$ . The second time scale is  $m/d$ . It gives the typical time over which local excitations are damped by  $d$ , neglecting the network dynamics. Finally, one has a set of time scales  $d/\lambda_\alpha$ ,  $\alpha = 2, \dots, n$ , each of them defined by the ratio of the damping parameter and an eigenvalue of the Laplacian. For  $m/d > d/4\lambda_\alpha$  these are related to oscillation time scales of the Laplacian modes, while for  $m/d < d/4\lambda_\alpha$  they relate to network-dynamical corrections to the damping time scale. We consider  $\tau_0$  as a tunable parameter allowing us to explore different regimes depending on its relation with  $m/d$  and  $d/\lambda_\alpha$ .

We measure the distance between the state of the system and the initial synchronous state as the square root of the variance  $\langle \delta \boldsymbol{\theta}^2(t) \rangle = \sum_i \langle [\delta \theta_i(t) - \overline{\delta \theta}(t)]^2 \rangle$  with  $\overline{\delta \theta}(t) = n^{-1} \sum_i \delta \theta_i(t)$  and brackets indicating an average over different realizations of noise with the same first two moments. It appropriately gives the standard deviation of the angle deviations in the subspace orthogonal to  $\mathbf{u}_1$ , because displacements in that subspace do not change the state. To calculate  $\langle \delta \boldsymbol{\theta}^2(t) \rangle$ , we expand angle deviations over the eigenbasis of  $\mathbb{L}$  and solve Eq. (5.2) for the coefficients of that expansion [123, Appendix 5.6.1]. We obtain the long-time limit

$$\lim_{t \rightarrow \infty} \langle \delta \boldsymbol{\theta}^2(t) \rangle = \delta P_0^2 \sum_{\alpha \geq 2} \frac{\tau_0 + m/d}{\lambda_\alpha (\lambda_\alpha \tau_0 + d + m/\tau_0)}. \quad (5.5)$$

In the two limits of long and short  $\tau_0$ , one has

$$\lim_{t \rightarrow \infty} \langle \delta \boldsymbol{\theta}^2(t) \rangle \simeq \begin{cases} \frac{\delta P_0^2 \tau_0}{nd} Kf_1, & \tau_0 \ll \frac{d}{\lambda_\alpha}, \frac{m}{d}, \\ \frac{\delta P_0^2}{n} Kf_2, & \tau_0 \gg \frac{d}{\lambda_\alpha}, \frac{m}{d}, \end{cases} \quad (5.6)$$

with  $Kf_p = n \sum_{\alpha \geq 2} \lambda_\alpha^{-p}$  [71, 121]. Interestingly, none of these asymptotics depend on inertia.

## Escape from the basin

The dynamics of Eq. (5.1) is described by a vector function  $\boldsymbol{\theta}(t)$  following the gradient of the potential

$$\mathcal{V}(\boldsymbol{\theta}, t) = \sum_{i=1}^n P_i(t) \theta_i - \sum_{i,j} a_{ij} [1 - \cos(\theta_i - \theta_j)], \quad (5.7)$$

starting from  $\boldsymbol{\theta}(t=0) = \boldsymbol{\theta}^{(0)}$ . When the noisy perturbation tilts this potential strongly enough,  $\boldsymbol{\theta}$  can escape the basin of attraction of  $\boldsymbol{\theta}^{(0)}$ . DeVille showed that, for not too large  $\delta P_0$ , the system almost surely escapes the basin in a neighborhood of a saddle point with a unique

## Chapter 5. Noise-Induced Desynchronization and Stochastic Escape from Equilibrium in Complex Networks

---

unstable direction, which we call 1-saddle [38]. Comparing the typical distance between  $\theta$  and  $\theta^{(0)}$  of Eq. (5.5) with the distance  $\Delta$  between  $\theta^{(0)}$  and its closest 1-saddle  $\varphi$  gives us a parametric condition for noise-induced stochastic escape

$$\delta P_0^2 \sum_{\alpha \geq 2} \frac{\tau_0 + m/d}{\lambda_\alpha (\lambda_\alpha \tau_0 + d + m/\tau_0)} \leq \Delta^2. \quad (5.8)$$

Our task is therefore to identify the position of the 1-saddles. This is in general no trivial task because the geometry of basins of attraction in such high-dimensional problems is impossible to fully capture. For single-cycle networks with identical frequencies, 1-saddles can be identified analytically [38, 35]. For more general networks, we give in Appendix 5.6.4 a numerical algorithm which locates 1-saddles  $\varphi$  and constructs the distribution of their distance to  $\theta^{(0)}$ .

### Numerical simulations

We first check Eq. (5.8) against numerical simulations of the Kuramoto model of Eq. (5.1) with  $m = 0$ . We consider four different networks (see Appendix 5.6.3) with constant couplings  $b_0 = 1$  and identical frequencies, which are a single-cycle network with nearest-neighbor coupling, a single-cycle with nearest- and 3<sup>rd</sup>-neighbor coupling, a model of the UK transmission network and a realization of a small-world network [126]. At each node, natural frequencies are perturbed by spatially uncorrelated Gaussian noisy sequences  $\delta P_i(t)$  satisfying Eq. (5.4). We integrate the dynamics of Eq. (5.1), using a 4<sup>th</sup>-order Runge-Kutta method, during an observation time  $T_{\text{obs}}$ , and check for a stochastic escape at every time step. Our method for detecting such occurrences is based on Refs. [40, 34, 85] which showed that on meshed networks, different fixed-point solutions of Eq. (5.1) correspond to different vectors of winding numbers  $\mathbf{q}$ . While winding around a cycle of a meshed network, the sum of angle differences is an integer multiple of  $2\pi$ . This integer is the winding number  $q$  on the corresponding cycle of the interaction graph. Such winding numbers can be defined on each cycle of the network and form together a winding vector  $\mathbf{q}$ . Refs. [38, 61] observed that transitions between different such equilibrium states occur by phase slips of few oscillators, and we show in Appendix 5.6.2 that these slips can be detected by recording the time evolution of  $\mathbf{q}$ , as illustrated on Fig. 5.1. We therefore detect desynchronizing events through variations of winding numbers. For each set of noise parameters  $\delta P_0$  and  $\tau_0$  we perform several calculations corresponding to different noise realizations. Fig. 5.2 shows the fraction  $\mathbb{P}$  of runs that remain in the initial basin for  $t \leq T_{\text{obs}}$ . The parameter space is sharply divided into (a) the red region (denoted  $U$  for "unstable") where all runs left the basin of attraction before  $T_{\text{obs}}$ , (b) the blue region (denoted  $S$  for "stable"), where none of the runs left the initial basin of attraction and (c) a rather narrow intermediate region between  $U$  and  $S$  where some runs left and some runs stayed in the initial basin.

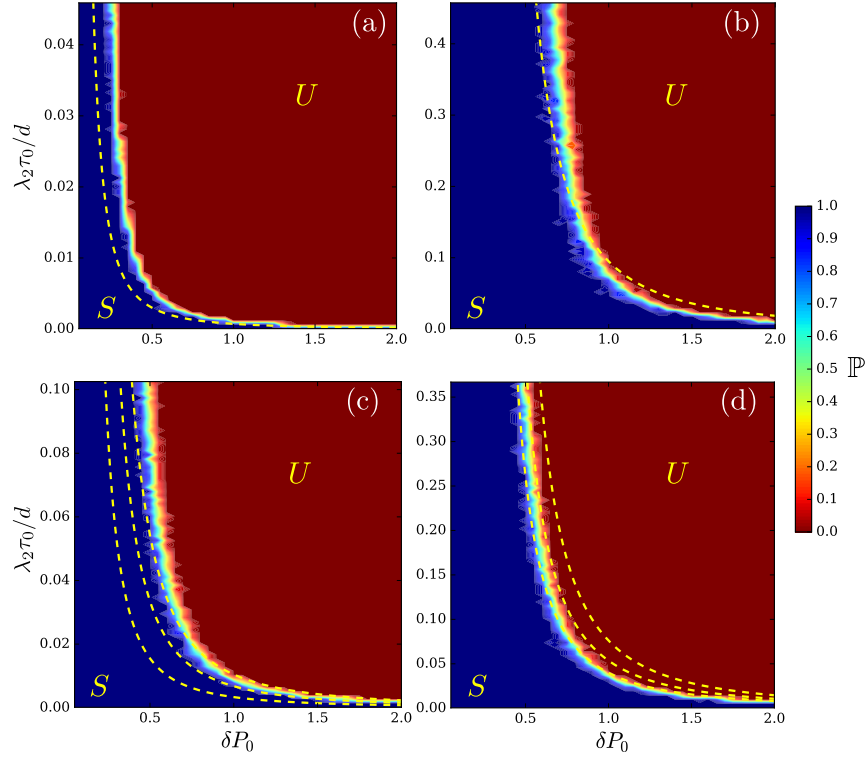


Figure 5.2 – Color-coded survival probability  $\mathbb{P}$  for Eq. (5.1) with  $m = 0$ . (a) Single-cycle network with  $n = 83$  and nearest-neighbor coupling; (b) single-cycle network with  $n = 83$ , nearest- and 3<sup>rd</sup>-neighbor coupling; (c) UK transmission network with  $n = 120$ ; (d) small-world network with  $n = 200$  nodes. Yellow dashed lines give the boundary of the region of validity of the inequality in Eq. (5.8) with  $m = 0$  and  $\Delta$  obtained analytically for panel (a) and numerically for panels (b-d). Observation times  $T_{\text{obs}}$  correspond to comparable dimensionless parameters  $\lambda_2 T_{\text{obs}} / d = 143$  (a), 143 (b), 130 (c) and 115 (d).

It is quite remarkable that the intermediate region (c) is qualitatively if not quantitatively identified by Eq. (5.8) with a network-dependent  $\Delta$ . As discussed above,  $\Delta$  is given by a typical distance between the initial stable fixed point  $\theta^{(0)}$  and the nearest saddle point  $\varphi$  roughly giving the smallest linear size of the basin of attraction. For the single-cycle network, all 1-saddles are located at the same distance from  $\theta^{(0)}$ , which can be obtained analytically [38]. For the other three networks, many, though likely not all 1-saddles are identified numerically. The detailed methods for finding 1-saddles are given in Appendix 5.6.4. For the single-cycle network with nearest- and 3<sup>rd</sup>-neighbor coupling, the distance  $\Delta$  from  $\theta^{(0)}$  only takes a few different values of which we only consider the most representative. For the UK and small-world networks, on the other hand, we find a distribution of  $\Delta \in [\Delta_{\text{min}}, \Delta_{\text{max}}]$ , which is likely due to the complexity of those meshed networks. The yellow dashed lines in Fig. 5.2 then indicate our theoretical prediction Eq. (5.8) for the obtained value  $\Delta$  for the two single-cycle networks and for values of  $\Delta$  corresponding to the 25<sup>th</sup>, the 50<sup>th</sup> and the 75<sup>th</sup> percentiles of the distribution of  $\Delta$  for the UK and small-world networks. In all cases, the shape of the

## Chapter 5. Noise-Induced Desynchronization and Stochastic Escape from Equilibrium in Complex Networks

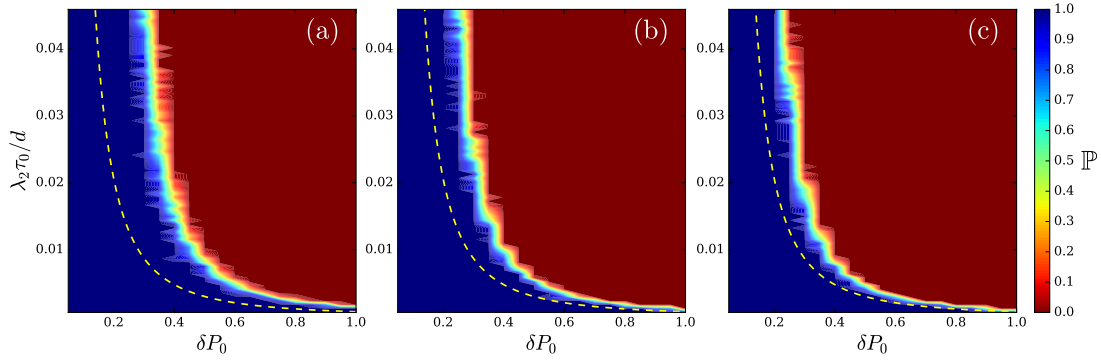


Figure 5.3 – Color-coded survival probability  $\mathbb{P}$  for Eq. (5.1) with  $m = 0$  for a single-cycle network with  $n = 83$  and nearest-neighbor coupling;  $\lambda_2 T_{\text{obs}}/d = 14.3$  (a), 143 (b), 569 (c). The yellow dashed line give the boundary of the region of validity of the inequality in Eq. (5.8) with  $m = 0$  and  $\Delta$  obtained analytically.

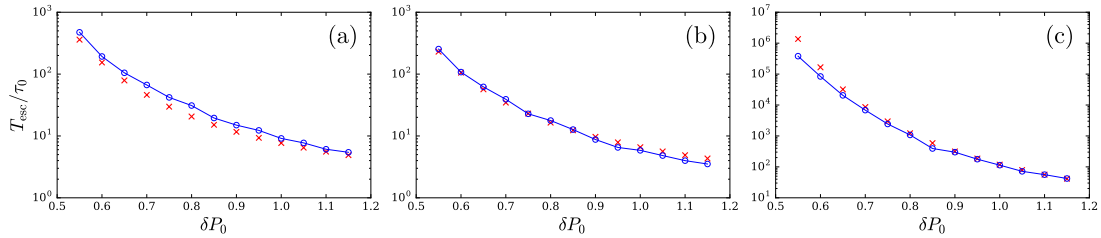


Figure 5.4 – Escape time  $T_{\text{esc}}$  from the initial basin of attraction vs. noise amplitude,  $\delta P_0$ , for cycle networks with  $n = 83$  (a),  $n = 249$  (b), and for the UK transmission network (c). The noise correlation time corresponds to  $\lambda_2 \tau_0/d = 8.6 \cdot 10^{-3}$  (a),  $\lambda_2 \tau_0/d = 9.6 \cdot 10^{-4}$  (b) and  $\lambda_2 \tau_0/d = 0.02$  (c). Blue circles are averages over 40 realizations of noise. Red crosses correspond to Eq. (5.9), with  $\beta \cong 5/8$  (a-b) and  $\beta \cong 2/5$  (c).

boundary is well predicted. For the more complex UK transmission network, Fig. 5.2(c), there is a horizontal shift between theory and numerics, presumably due to stronger anisotropies of the basins of attraction in this more complex network, effectively requiring a larger  $T_{\text{obs}}$ .

In the case of bounded noise, we expect an inertialess system to remain in its initial basin for weak enough noise [79]. However, the noise considered in our case is Gaussian and arbitrarily large excursion will occur if one waits long enough. As a matter of fact, we found that increasing  $T_{\text{obs}}$  shifts the boundary between stable and unstable regions to lower  $\delta P_0$ . We evaluated the influence of the observation time by reproducing Fig. 5.2(a) with different  $T_{\text{obs}}$ . This is shown in Fig. 5.3 where we performed simulations for the cycle, increasing the observation time. Fig. 5.3 shows the fraction of simulations that stay in the initial basin of attraction after an observation time satisfying  $\lambda_2 T_{\text{obs}}/d = 14.2$  [Fig. 5.3(a)], 142.4 [Fig. 5.3(b)], 569 [Fig. 5.3(c)], for a cycle network with  $n = 83$  nodes. As  $T_{\text{obs}}$  increases exponentially, we observe the boundary between regions  $U$  and  $S$  drifting to the left due to the escape time that is superexponential as  $\delta P_0$  decreases.

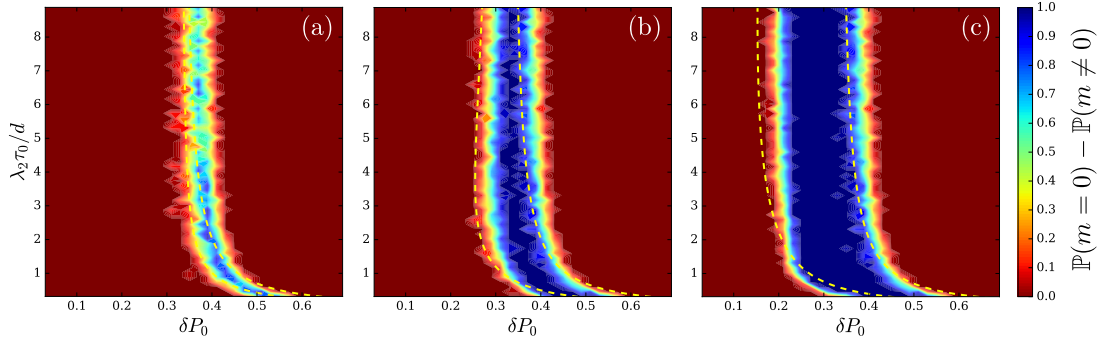


Figure 5.5 – Color-coded difference in survival probability  $\mathbb{P}$  with and without inertia for a single-cycle network with  $n = 83$  with nearest- and 3<sup>rd</sup>-neighbor coupling obtained from 20 realizations of noise; (a)  $\frac{m}{d} / \frac{d}{\lambda_2} = 0.25/0.35$ , (b) 2.5/0.35 and (c) 25/0.35. The yellow dashed lines give the boundary of the region of validity of the inequality in Eq. (5.8), as discussed in the main text.

Fig. 5.4 further shows the stochastic escape time as a function of  $\delta P_0$ . A superexponential behavior is observed which can be understood as follows. The noise generates a distribution of angle deviations which we expect to be Gaussian with a variance given by Eq. (5.5). The escape time is then inversely proportional to the probability to have such a deviation exceeding  $\Delta$ , i.e.

$$T_{\text{esc}} \propto \left[ 2 \int_{\beta\Delta}^{\infty} P(\overline{\delta\theta}) d(\overline{\delta\theta}) \right]^{-1} \quad (5.9)$$

with a free parameter  $\beta$  of order 1. Fig. 5.4 validates this argument using a Gaussian distribution of single-angle deviation  $P(\overline{\delta\theta})$  with variance  $\langle \delta\theta^2(t) \rangle / n$ , see Eq. (5.5). We have found, but do not show, that  $T_{\text{esc}}$  diverges at a finite value of  $\delta P_0$  for a box-distributed, bounded noise.

We finally consider Eq. (5.1) with nonzero inertia. We focus on the single-cycle network with nearest- and 3<sup>rd</sup>-neighbor coupling, and tune the inertia parameter  $m$  to explore different regimes defined by the different time scales of Eq. (5.1). Fig. 5.5 shows the difference in survival probabilities with and without inertia in the regimes (a)  $d/\lambda_\alpha \gtrsim m/d$ , (b)  $d/\lambda_\alpha \lesssim m/d$  and (c)  $d/\lambda_\alpha \ll m/d$ . Deep in the stable (unstable) regions, both inertialess and inertiaful models have  $\mathbb{P} = 1$  ( $\mathbb{P} = 0$ ) and the difference  $\mathbb{P}(m=0) - \mathbb{P}(m) = 0$ . Somehow counterintuitively, however, there is an intermediate region where the presence of inertia facilitates stochastic escape compared to the inertialess case,  $\mathbb{P}(m=0) - \mathbb{P}(m) > 0$ . The boundary of that region are in excellent agreement with the prediction of Eq. (5.8), giving the two dashed yellow lines for  $m=0$  and  $m \neq 0$ .

For large  $\tau_0$ , the faster escape of the system with finite inertia is easily understood. With long correlation time, the noise tends to push the system in the same direction for long sequences. This is sufficient to have the inertiaful system accumulate a significant kinetic energy. The system keeps then moving, even if, after some time, the noise starts pushing the other way and allows it to move above a saddle point with inertia, whereas the inertialess system is

## Chapter 5. Noise-Induced Desynchronization and Stochastic Escape from Equilibrium in Complex Networks

---

immediately stopped by noise reversal.

For smaller  $\tau_0$ , on the other hand, inertia resists short sequences of pushes in rapidly varying directions and accordingly, we found that inertia stabilizes the system in that case (see Appendix 5.6.5). This is not predicted by Eq. (5.8) and is probably due to contributions beyond our linear response theory, because discrepancies appear for values of  $\delta P_0$  comparable to the coupling strength  $a_0$ . The influence of inertia on stochastic escapes is perhaps best illustrated in Fig. 5.1, where the presence of inertia stabilizes the system under short-correlated noise [panel (a)] but leads to more frequent stochastic escapes for long-correlated noise [panel (b)].

### Conclusion

We have constructed a novel approach to stochastic escape. We compare a spectral calculation of typical sizes of stochastic excursions about synchronous equilibrium states with an evaluation of the distance between this synchronous equilibrium state and 1-saddles. This method provides analytical results with a single, model-dependent free parameter of order one [ $\beta$  in Eq. (5.9)]. It gives remarkably accurate estimates for stochastic escape times, as is illustrated in Fig. 5.4. Even if, in this work, we considered networks of coupled oscillators, our method can be applied to any dynamical system where some stable fixed points and 1-saddles are available, and the linearization of the dynamics in a neighborhood of the considered fixed point is possible. The distance  $\Delta$  between stable fixed points and 1-saddles, and the eigenvalues of the linearization of the dynamical system are the main ingredients of Eq. (5.8), which determine regions where escape is unlikely in reasonable time.

In the context of coupled oscillators, we interestingly observed that the presence of inertia leads to faster, more frequent escapes for long noise coherence times, while the effect is reversed for short noise coherence times. This is illustrated in Fig. 5.1. Further studies should consider the effect of spatially correlated noise and non-Gaussian, long-tailed noise distributions [57].

### Appendix

#### Details of Calculations for the variance of the angle displacements

We give some details of the calculation that leads to Eq. (5.5). Expanding the angle deviations over the eigenmodes of the Laplacian Eq. (5.3), i.e.,  $\delta\boldsymbol{\theta}(t) = \sum_{\alpha} c_{\alpha}(t) \mathbf{u}_{\alpha}$ , Eq. (5.2) becomes,

$$m \ddot{c}_{\alpha}(t) + d \dot{c}_{\alpha}(t) = \delta\mathbf{P}(t) \cdot \mathbf{u}_{\alpha} - \lambda_{\alpha} c_{\alpha}(t), \quad \alpha = 2, \dots, n. \quad (5.10)$$

With the help of a Laplace transform, the solution of Eq. (5.10) is given by

$$c_\alpha(t) = m^{-1} e^{-\frac{d/m-\Gamma_\alpha}{2} t} \int_0^t e^{\Gamma_\alpha t'} \int_0^{t'} \delta \mathbf{P}(t'') \cdot \mathbf{u}_\alpha e^{\frac{d/m-\Gamma_\alpha}{2} t''} dt'' dt', \quad (5.11)$$

with  $\Gamma_\alpha = \sqrt{(d/m)^2 - 4\lambda_\alpha/m}$ . Taking advantage of the orthogonality between eigenmodes of the Laplacian we have,

$$\langle \delta \theta^2(t) \rangle \equiv \sum_i \langle [\delta \theta_i(t) - \delta \bar{\theta}(t)]^2 \rangle = \sum_{\alpha \geq 2} \langle c_\alpha^2(t) \rangle, \quad (5.12)$$

with  $\delta \bar{\theta}(t) = n^{-1} \sum_i \delta \theta_i(t)$ . Inserting Eq. (5.10) into Eq. (5.12), using the time correlator of  $\delta \mathbf{P}$  Eq. (5.4), and finally taking the long time limit one obtains, after some algebra, Eq. (5.5).

### Method to determine escape times

Various methods can be used to determine, at any iteration step of the simulation, if the system under consideration has escaped its initial basin of attraction. We compared three of them, which we detail here.

**Method 1.** As stated above, stable equilibria of Eq. (5.17) can be unambiguously distinguished by their winding vector  $\mathbf{q}$ . The method that we used for the numerical simulations proceeds as:

1. At each time step, compute  $\mathbf{q}$ ;
2. If  $\mathbf{q} \neq \mathbf{q}^{(0)}$  the winding vector of the initial basin of attraction, check if the system is still in the initial basin. To do so, simulate the dynamics without noise, taking the current state of the system as initial conditions. Once synchrony is reached, compute the winding vector  $\mathbf{q}^{(1)}$ ;
3. If  $\mathbf{q}^{(1)} \neq \mathbf{q}^{(0)}$ , then the system was out of the initial basin. Otherwise, if  $\mathbf{q}^{(1)} = \mathbf{q}^{(0)}$ , the system was still in the basin and thus the simulation can move to the next time step.

**Method 2.** This method is based on DeVille's observation [38] that escapes from basins of attraction occur on a short time interval and can be identified by a fast slip of a small group of angles. It proceeds as:

1. At each time step, check if some angles made a large excursion, i.e.,  $\|\boldsymbol{\theta}(t) - \boldsymbol{\theta}^{(0)}\|_\infty > 2\pi$ ;
2. If so, then simulate the dynamics without noise, taking the current state of the system as initial conditions, until it synchronizes to the state  $\boldsymbol{\theta}^{(1)}$ ;
3. If  $\boldsymbol{\theta}^{(1)} \neq \boldsymbol{\theta}^{(0)}$ , then the system was out of the initial basin. Otherwise, if  $\boldsymbol{\theta}^{(1)} = \boldsymbol{\theta}^{(0)}$ , the system was still in the basin and thus the simulation can move to the next time step.

## Chapter 5. Noise-Induced Desynchronization and Stochastic Escape from Equilibrium in Complex Networks

Simulation	Method	$q^{(1)}$	No. iterations
1	1	-1	400
	2	-1	400
	3	-1	400
2	1	-1	685
	2	-1	685
	3	-1	685
3	1	-1	558
	2	-1	558
	3	-1	550
4	1	1	1609
	2	1	1609
	3	-1	950
5	1	-1	1664
	2	-1	1664
	3	-1	1249
6	1	1	1887
	2	1	1887
	3	-1	1151

Table 5.1 – Final winding number  $q^{(1)}$  and number of iterations before the escape for  $m = 0$  (simulations 1-3) and finite inertia (simulations 4-6). Each triplet is obtained by integrating Eq. (5.1) with the same noise sequence.

**Method 3.** Finally, we tested the method in which we check at every time step whether the system returns to the initial basin or not. This method guarantees to find the best estimate of the escape time, at least for the Kuramoto model ( $m = 0$ ), but is very time-consuming.

Table 5.1 compares escape times and final winding numbers for a single-cycle of  $n = 83$  nodes. For the Kuramoto model ( $m = 0$ ) the three methods give very similar results. For the case with inertia, the first two give larger escape times compared to the last method. We explain this as follows. When the noise is removed, the system may have accumulated some kinetic energy that will drive it out of the basin of attraction. And this can happen before the winding number changes or a large angle excursion occurs. Furthermore, if the perturbation was still active, it could have pushed the system back towards the stable fixed point before it leaves the basin of attraction, increasing the escape time.

### The four networks

We briefly describe the networks used for the numerical simulations.

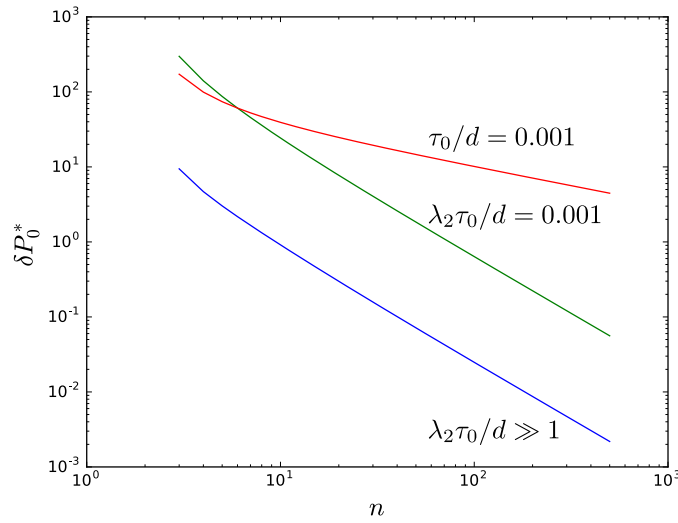


Figure 5.6 – Maximum value  $\delta P_0^*$  of the noise amplitude obtained from Eqs. (5.14), (5.15) for large (blue) and short (green, red) time correlation,  $\tau_0$ , as a function of the size of the cyclic network  $n$ . For the red curve, we consider a constant ratio  $\tau_0/d = 0.001$ . For the green curve we consider a constant ratio  $\lambda_2 \tau_0/d = 0.001$  where  $\lambda_2 = 2 - 2 \cos(2\pi/n)$  depends on the size of the network.

### Cycle with nearest neighbors coupling

We consider a cycle network of size  $n$ , with identical natural frequencies. The eigenvalues of its weighted Laplacian, Eq. (5.3), can be obtained analytically,

$$\lambda_\alpha = \cos(\delta)[2 - 2 \cos(k_\alpha)], \quad \alpha = 1, \dots, n, \quad (5.13)$$

where  $\delta$  is the angle difference between neighboring sites (which are identical at a stable equilibrium [33]) and  $k_\alpha = 2\pi(\alpha - 1)n^{-1}$ . For  $n = 83$  we have  $\lambda_\alpha \in [0, 4 \cos(\delta)]$  and  $\lambda_2 = 0.0057$ .

Eq. (5.6) can be explicitly calculated for cyclic networks as functions of the number of nodes  $n$

$$\delta P_0^2 \leq \frac{\pi^2 d n}{\tau_0 (n-2)^2}, \quad \tau_0 \ll d/\lambda_\alpha, m/d, \quad (5.14)$$

$$\delta P_0^2 \leq \frac{60\pi^2 n}{(n-2)^2(n^2+11)}, \quad \tau_0 \gg d/\lambda_\alpha, m/d. \quad (5.15)$$

Fig. 5.6 shows the maximum values of  $\delta P_0$  satisfying Eqs. (5.14), (5.15). One remarks that, while increasing the size of the cycle, the stable region gets smaller and even vanishes for  $n \rightarrow \infty$  similarly to fluctuations that destroy long-range order in 1 dimensional locally interacting quantum magnets [51].

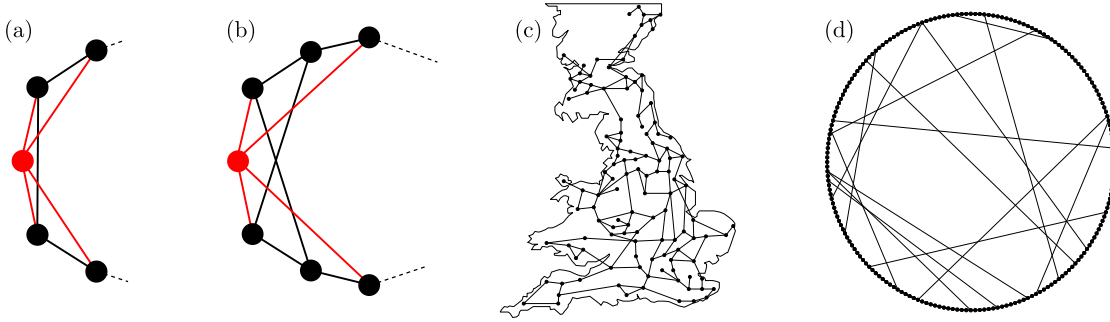


Figure 5.7 – (a) Illustration of the connections of a vertex to its first and second neighbors on a cycle. (b) Illustration of the connections of a vertex to its nearest- and 3<sup>rd</sup>-neighbors on a cycle. (c) Illustration of the UK network with  $n = 120$  vertices and  $m = 165$  edges. (d) Illustration of our small world network with  $n = 200$  vertices. Its relative clustering coefficient is  $C(\mathcal{G}_p)/C(\mathcal{G}_0) \approx 0.89$  and its relative characteristic path length is  $L(\mathcal{G}_p)/L(\mathcal{G}_0) \approx 0.32$ .

### Cycle with nearest- and 3<sup>rd</sup>-neighbors coupling

We consider a cycle network of size  $n$ , where each vertex is connected to its nearest- and 3<sup>rd</sup>-neighbors [see Fig. 5.7(b)]. With identical natural frequencies, the eigenvalues of its weighted Laplacian, Eq. (5.3), can be obtained analytically,

$$\lambda_\alpha = \cos(\delta)[4 - 2 \cos(k_\alpha) - 2 \cos(3k_\alpha)], \quad \alpha = 1, \dots, n, \quad (5.16)$$

where  $\delta$  is the angle difference between neighboring sites (which are identical at a stable steady-state [33]) and  $k_\alpha = 2\pi(\alpha - 1)n^{-1}$ . For  $n = 83$  we have  $\lambda_\alpha \in [0, 8 \cos(\delta)]$  and  $\lambda_2 = 0.057$ .

### UK transmission grid

Model of the electrical transmission grid of UK depicted in Fig. 5.7(c). It is composed of 120 nodes and 165 edges making 44 cycles. During the numerical simulations, to check whether the system has left the initial basin of attraction or not, we check the winding number on each cycle, i.e., the winding vector  $\mathbf{q} = (q_1, \dots, q_{44})$ . The second eigenvalue of its Laplacian matrix is  $\lambda_2 \approx 0.013$ .

### Small world

A small world network is constructed from an initial network, where some edges are randomly rewired (see [126]). In our case, the initial network  $\mathcal{G}_0$  is a cycle with  $n = 200$  vertices and where each vertex is connected to its first and second neighbors [see Fig. 5.7(a)]. Each edge  $(i, j)$  is then replaced with probability  $p = 0.05$  by the edge  $(i, k)$ , where  $k$  is chosen at random among the vertices not already connected to  $i$ . The network obtained  $\mathcal{G}_p$  is illustrated in Fig. 5.7(d). It is a small world as it has a large relative clustering coefficient  $C(\mathcal{G}_p)/C(\mathcal{G}_0) \approx 0.89$  and a small relative characteristic path length  $L(\mathcal{G}_p)/L(\mathcal{G}_0) \approx 0.32$  (see [126] for more details). The second

eigenvalue of its Laplacian matrix is  $\lambda_2 \approx 0.046$ .

### Finding 1-saddles

We detail our methods for finding 1-saddles (equilibria with a unique unstable direction) of the dynamical system

$$m_i \ddot{\theta}_i + d_i \dot{\theta}_i = P_i^{(0)} + \delta P_i(t) - \sum_j a_{ij} \sin(\theta_i - \theta_j), \quad (5.17)$$

with  $i = 1, \dots, n$ , for arbitrary coupling graph.

### Cycle Networks

For cycle networks with nearest neighbor coupling and identical natural frequencies, the distance between the stable equilibrium  $\boldsymbol{\theta}^{(0)} = (0, \dots, 0)$ , and the 1-saddle  $\boldsymbol{\varphi}$ , can be computed analytically as [35]

$$\Delta^2 = \|\boldsymbol{\theta}^{(0)} - \boldsymbol{\varphi}\|_2^2 = \frac{n(n^2 - 1)}{12(n - 2)^2} \pi^2. \quad (5.18)$$

### General Networks

For general networks, the anisotropy of the basins of attraction renders the 1-saddles complicated to identify analytically. We propose a numerical method to locate 1-saddles, which is based on two results of DeVille [38]:

- Escapes from basins of attraction almost always occur in a neighborhood of a 1-saddle of the potential

$$\mathcal{V}(\boldsymbol{\theta}) = \sum_{i=1}^n P_i^{(0)} \theta_i - \sum_{i < j} a_{ij} [1 - \cos(\theta_i - \theta_j)]; \quad (5.19)$$

- Transitions from a basin to another occur on a short time interval compared to the time the system remains in a basin of attraction.

We numerically integrate Eq. (5.17), where  $\delta P_i$  is a noise with small variance, and keep track of the angles in order to identify iterations where the system is close to a 1-saddle. As observed in [38], when the system is driven (by the noise) to another basin of attraction, its trajectory goes close to a 1-saddle, and this can be seen in the time-evolution of the angles as a fast jump of a set of angles of amplitude  $2\pi$  (see Fig. 5.8). The state  $\boldsymbol{\varphi}^{(0)}$  of the system in the middle of this jump will be a candidate for a 1-saddle. This state is probably not exactly a 1-saddle, but

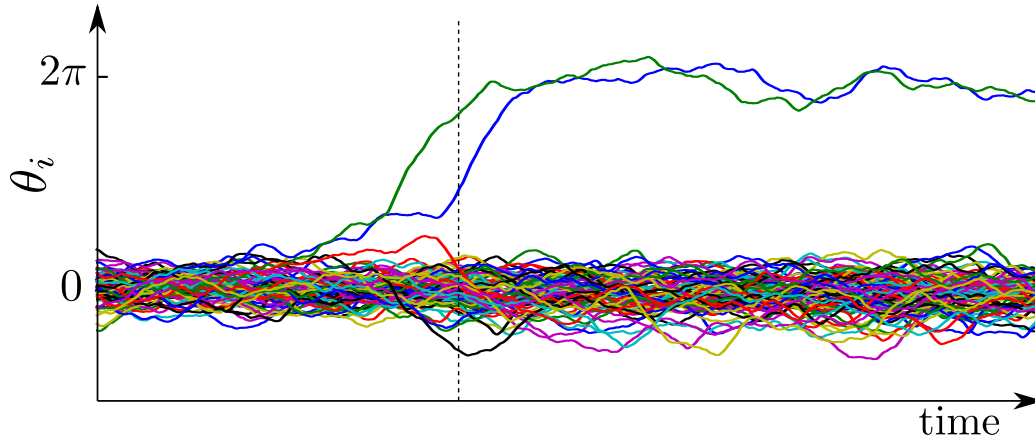


Figure 5.8 – Example of the time evolution of the 120 angles of the UK network [Fig. 5.7(c)]. We clearly see two angles jumping from a value close to 0 to a value close to  $2\pi$ . The state of the system at the time given by the vertical dashed line is our candidate for a 1-saddle  $\varphi$ .

according to [38], it should be close to one. We then solve the steady-state equations

$$P_i^{(0)} = \sum_j a_{ij} \sin(\theta_i - \theta_j), \quad i = 1, \dots, n, \quad (5.20)$$

using a Newton-Raphson method with initial conditions  $\varphi^{(0)}$ . This gives an equilibrium  $\varphi^*$  of Eq. (5.17), which we expect to be close to  $\theta^{(0)}$ . Computing the eigenvalues of the Jacobian of Eq. (5.17), the equilibrium  $\varphi^*$  is a  $p$ -saddle if and only if it has  $p$  positive eigenvalues. Note that one eigenvalue is always zero due to invariance of Eqs. (5.17) and (5.19) under a constant shift of all angles.

Running this simulation for a long enough time, we identified:

- 284 1-saddles for the cycle with nearest- and 3<sup>rd</sup>-neighbor. The distribution of their distance to the stable equilibrium  $\theta^{(0)}$  is given in Fig. 5.9(a). Looking more into details, we observe that each value in Fig. 5.9(a) corresponds to a unique 1-saddle, up to an index shift or the angles' sign reversal. The 1-saddles with the two smallest norm,  $\varphi^{(1)}$  and  $\varphi^{(2)}$ , are represented in Fig. 5.10. The first one [Fig. 5.10(a)] has the smallest 2-norm, but its configuration with  $n - 1$  equal angles and one angle  $\pi$  apart from all others is, in our opinion, unlikely to occur. As we consider noisy perturbation at all nodes, a configuration with a single large angle excursion and no excursion for all other nodes seems less likely than a configuration where all angles are slightly displaced from their neighbors. We performed our study using  $\varphi^{(2)}$  as 1-saddle for the cycle with nearest- and 3<sup>rd</sup>-neighbor.

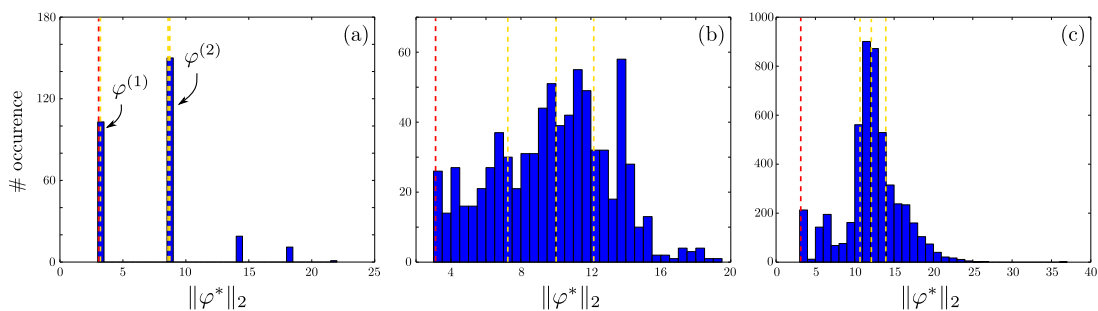


Figure 5.9 – Histograms of the 2-norm distance from the fixed point of the set of 1-saddles found numerically for the cycle with 3<sup>rd</sup>-neighbor (a), the UK network (b), and the small world network (c). We found: (a) 284 1-saddles for the cycle with 3<sup>rd</sup>-neighbor, with smallest 2-norm  $n_{\min} \approx 3.12$ , and quartiles of the 2-norms ( $Q_1, Q_2, Q_3 \approx (3.12, 8.61, 8.61)$ ); (b) 788 1-saddles for the UK network, with smallest 2-norm  $n_{\min} \approx 3.13$ , and quartiles of the 2-norms ( $Q_1, Q_2, Q_3 \approx (7.24, 10.02, 12.17)$ ); and (c) 4956 1-saddles for the small-world network, with smallest 2-norm  $n_{\min} \approx 3.13$ , and quartiles of the 2-norms ( $Q_1, Q_2, Q_3 \approx (10.74, 12.13, 13.95)$ ). The yellow dashed lines indicate the three quartiles  $Q_1, Q_2$ , and  $Q_3$ , and the red dashed lines indicate the norm of the closest 1-saddle.

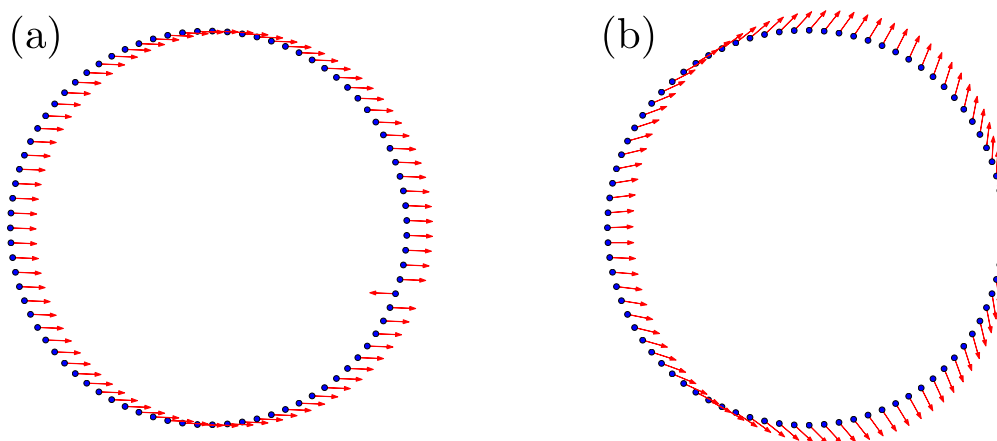


Figure 5.10 – The two 1-saddles,  $\boldsymbol{\varphi}^{(1)}$  and  $\boldsymbol{\varphi}^{(2)}$ , with smallest 2-norm, for the cycle network, with nearest- and 3<sup>rd</sup>-neighbors. (a)  $\boldsymbol{\varphi}^{(1)}$ : all angles are equal, except one which is  $\pi$  apart from all others. The 2-norm of this 1-saddles is  $\sim 3.12$ . (b)  $\boldsymbol{\varphi}^{(2)}$ : all angles are slightly displaced compared to their neighbors. The 2-norm of this 1-saddle is  $\sim 8.61$ . This configuration is, in our opinion, more likely to occur under noisy perturbations applied to all nodes.

- 788 1-saddles for the UK network, whose distribution of the distances to the stable equilibrium is given in Fig. 5.9(b). Distances cover a large range of value, due to the anisotropy of the basin of attraction;
- 4956 1-saddles for the small-world network. The distribution of the distances to  $\boldsymbol{\theta}^{(0)}$  is given in Fig. 5.9(c). Most of the 1-saddles are at similar distance.

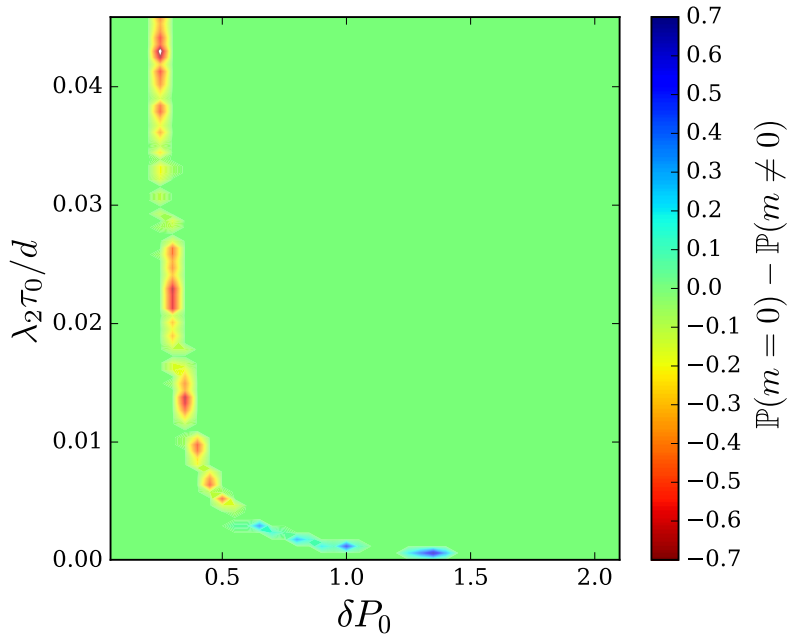


Figure 5.11 – Color plot of the difference of fraction of trajectories that stay in the initial basin of attraction with finite inertia compared to  $m = 0$  for a cycle network of  $n = 83$  nodes. Time scales are  $\frac{m}{d} / \frac{d}{\lambda_2} = 10/175$ .

### Linearization Breakdown

We showed that, according to our theory, inertia always destabilizes the system compared to the inertialess case. However, for the cycle network, we found that for small  $\tau_0$  and large  $\delta P_0$ , inertia stabilizes the system, as illustrated on Fig. 5.11. The blue area where inertia stabilized the system is not predicted by our theory, Eq. (5.8). This can be explained by the breakdown of the linear approximation. Indeed, the blue region on Fig. 5.11 starts for value of the order of the coupling  $\delta P_0 \cong a_0 \equiv 1$ .

## 6 Overall Conclusion and Outlook

Many graph theoretic metrics have been defined over the years to identify most important nodes in a network or to compare different networks. Most of these metrics have been constructed considering only networks' structures decoupled from any deterministic dynamics. In order to correctly identify vulnerabilities of coupled dynamical systems, these complex network metrics need to be extended to account for physical conservation laws governing such systems. We achieved such extension to assess vulnerabilities of complex synchronous networks. We quantified their transient responses to weak external perturbations and directly connected them to newly defined distances that include both the topology of the coupling network and the dynamical features of the synchronous states. These new distances are generalization of the resistance distance originally introduced in Ref. [71], to powers of the weighted Laplacian of the system. Both global robustness and local vulnerabilities are efficiently and accurately assessed using resistance distances. Indeed, on the one hand, by considering the magnitude of transient excursion of ensemble averaged perturbations, we directly connected global robustness of oscillatory networks to generalized Kirchhoff indices. The latter are intuitively interpreted as the sum of all resistance distances in the network and are easily obtained from the eigenvalues of the weighted Laplacian of the system. To improve the overall robustness of an oscillatory network, one should minimize its Kirchhoff indices. On the other hand, we straightforwardly related magnitude of the transient following specific local perturbations to generalized resistance centralities. We constructed these latter as closeness centralities using resistance distances. Moreover they are easily expressed in term of the eigenvectors and eigenvalues of the weighted Laplacian of the system and Kirchhoff indices. Most vulnerable elements, leading to largest excursion, are then the least central according to resistance centralities. With Kirchhoff indices and resistance centralities respectively as global and local network descriptors, we have defined an efficient and intuitive framework to evaluate vulnerabilities of complex synchronous networks. Additionally, we found that, for second order oscillators, inertia does not affect much transient excursions. The formalism we developed is rather general and therefore may also be useful to analyze other types of dynamical systems. Current work under preparation focuses on the extension of the above results to oscillators with non-homogeneous dynamical parameters namely inertia

## Chapter 6. Overall Conclusion and Outlook

---

and damping coefficients. In that case, distances similar to resistance distances can still be defined but this time out of a rescaled Laplacian  $\mathbf{D}^{-1/2}\mathbb{L}\mathbf{D}^{-1/2}$  where  $\mathbf{D}$  is the diagonal matrix of damping coefficients.

We then considered robustness of coupled oscillators against larger perturbations that can potentially drive the system through a transition to another stable fixed point. More precisely we investigated couple oscillators subjected to noise and found a simple heuristic criterion to predict escape from the initial basin of attraction. Using linear response and little knowledge about the structure of the basin of attraction, we obtained estimates for the survival probability and first escape time as function of the noise characteristics and eigenvalues of the weighted Laplacian of the system. The latter estimates were surprisingly well validated by numerical simulations. Moreover, we showed that, most of the time, increasing the inertia of oscillators tends to facilitate transitions between fixed points. Interestingly, the heuristic criterion used is rather general and thus may be applied to other dynamical systems.

In summary, we have investigated fragility of coupled oscillators systems from both their small-signal responses and the potential transitions they may undergo due to larger perturbations. In both cases we have defined frameworks allowing to assess and predict efficiently vulnerabilities.

Possible extensions of the results presented in this thesis should include topological perturbation such as edge removals. We recently made some progresses in that direction calculating the rate of change of frequency–second time derivative of angles– following an edge removal [37]. Another direction of research building on presented results is about network inference and disturbance location. As network response can be directly connected to a complex network metric, namely resistance distances, by measuring the response of the system subject to noise or to some known input signal, one may be able to infer the connectivity of the system. Current works on that topic are under preparation. Note also that the results obtained for coupled oscillators can be adapted to investigate consensus algorithms and opinion dynamics [12].

# Acknowledgements

First I would like to thank Philippe for his supervision of my work, the freedom I received during the last 3 years to go to conferences and visit research groups around the world and finally and most importantly for giving me the culture of efficient and highly competitive scientific research. I also thank Frédéric M for the official supervision of the thesis. Thanks to Enrique Mallada, Mauricio Barahona and Paolo De Los Rios for serving in the jury of the defense.

Many thanks to my colleagues and now friends from the office in Sion. To Tommaso for all the discussions we had commuting between Lausanne and Sion, or waiting for trains... To David T, Laurent and Robin for all the relevant discussions related to work in a broad sense we had. A special thank to Robin for the discoveries we made at LANL about science and margs and the nice road trip from one LA to another...

Then to all my friends from HEI alphabetically ordered: André, Baljeet, David M, Didier, Glory, Koen, Sébastien, Tharsan, Vincent and Frédéric A: Thank you for all the exciting debates about F1 or higher quality of wine coming from Vaud compared to Valais we had at the cafeteria or building G or even in the train and also for giving me reasons beyond work to commute 90,000km per year.

I also would like to thank my friend and colleague from Berlin, Fabian for the international collaboration we built in Catania, at Newtonstraße and in any Berliner pub.

Finally I thank my old friends and my family for constant support and for whom I should probably have taken more time these last years.

*St-Prex, January 6, 2020*

Melvyn



# Bibliography

- [1] *Analytic research foundations for the next-generation electric grid*. National Academies of Sciences, Engineering, and Medicine and others, National Academies Press, 2016.
- [2] J. A. Acebrón, L. L. Bonilla, C. J. Pérez Vicente, F. Ritort, and R. Spigler. The *Kuramoto* model: A simple paradigm for synchronization phenomena. *Rev. Mod. Phys.*, 77(1):137, 2005.
- [3] A. Arenas, A. Díaz-Guilera, J. Kurths, Y. Moreno, and C. Zhou. Synchronization in complex networks. *Phys. Rep.*, 469(3):93–153, 2008.
- [4] S. Auer, F. Hellmann, M. Krause, and J. Kurths. Stability of synchrony against local intermittent fluctuations in tree-like power grids. *Chaos*, 27:127003, 2017.
- [5] C. Ballester, A. Calvó-Armengol, and Y. Zenou. Who's who in networks. wanted: The key player. *Econometrica*, 74(5):1403–1417, 2006.
- [6] B. Bamieh and D. F. Gayme. The price of synchrony: Resistive losses due to phase synchronization in power networks. *American Control Conference*, pages 5815–5820, June 2013. ISSN 0743-1619.
- [7] B. Bamieh, M. R. Jovanovic, P. Mitra, and S. Patterson. Coherence in Large-Scale Networks: Dimension-Dependent Limitations of Local Feedback. *IEEE Trans. Autom. Control*, 57(9):2235–2249, 2012.
- [8] M. K. Banda, M. Herty, and A. Klar. Gas flow in pipeline networks. *NHM*, 1(1):41–56, 2006.
- [9] A.-L. Barabási. *Network science*. Cambridge University Press, Cambridge, England, 2016.
- [10] M. Barahona and L. M. Pecora. Synchronization in small-world systems. *Phys. Rev. Lett.*, 89:054101, Jul 2002.
- [11] A. Bashan, Y. Berezin, S. V. Buldyrev, and S. Havlin. The extreme vulnerability of interdependent spatially embedded networks. *Nat. Phys.*, 9(10):667, 2013.
- [12] F. Baumann, I. Sokolov, and M. Tyloo. The role of active leaders in opinion formation on social networks. *arXiv preprint arXiv:1910.01897*, 2019.

## Bibliography

---

- [13] A. R. Bergen and D. J. Hill. *IEEE Transaction on Power Apparatus and Systems*, PAS-100: 25, 1981.
- [14] A. R. Bergen and V. Vittal. *Power Systems Analysis*. Prentice Hall, 2000.
- [15] C. Böde, I. A. Kovács, M. S. Szalay, R. Palotai, T. Korcsmáros, and P. Csermely. Network analysis of protein dynamics. *Febs Letters*, 581(15):2776–2782, 2007.
- [16] P. Boldi and S. Vigna. Axioms for centrality. *Internet Mathematics*, 10:222, 2014.
- [17] E. Bompard, E. Pons, and D. Wu. Analysis of the structural vulnerability of the interconnected power grid of continental europe with the integrated power system and unified power system based on extended topological approach. *International Transactions on Electrical Energy Systems*, 23(5):620–637, 2013.
- [18] P. Bonacich. Power and centrality: A family of measures. *American journal of sociology*, 92(5):1170–1182, 1987.
- [19] S. Borgatti. Identifying sets of key players in a social network. *Comput. Math. Organiz. Theor.*, 12:21, 2006.
- [20] J. Borge-Holthoefer and Y. Moreno. Absence of influential spreaders in rumor dynamics. *Phys. Rev. E*, 85(2):026116, 2012.
- [21] U. Brandes and D. Fleischer. Centrality measures based on current flow. In *Annual symposium on theoretical aspects of computer science*, pages 533–544. Springer, 2005.
- [22] H. A. Braun, H. Wissing, K. Schäfer, and M. C. Hirsch. Oscillation and noise determine signal transduction in shark multimodal sensory cells. *Nature*, 367:270, 1994.
- [23] S. Brin and L. Page. The anatomy of a large-scale hypertextual web search engine. *Computer networks and ISDN systems*, 30(1-7):107–117, 1998.
- [24] S. V. Buldyrev, R. Parshani, G. Paul, H. E. Stanley, and S. Havlin. Catastrophic cascade of failures in interdependent networks. *Nature*, 464(7291):1025, 2010.
- [25] G. Caldarelli, A. Capocci, P. De Los Rios, and M. A. Munoz. Scale-free networks from varying vertex intrinsic fitness. *Phys. Rev. Lett.*, 89(25):258702, 2002.
- [26] M. Chavez, D.-U. Hwang, A. Amann, H. G. E. Hentschel, and S. Boccaletti. Synchronization is enhanced in weighted complex networks. *Phys. Rev. Lett.*, 94:218701, Jun 2005.
- [27] T. Coletta and P. Jacquod. Linear stability and the braess paradox in coupled-oscillator networks and electric power grids. *Phys. Rev. E*, 93(3), 2016. ISSN 2470-0045, 2470-0053.
- [28] T. Coletta and P. Jacquod. Resistance distance criterion for optimal slack bus selection. *arXiv:1711.10348*, 2017.

- 
- [29] T. Coletta and P. Jacquod. Performance measures in electric power networks under line contingencies. *IEEE Transactions on Control of Network Systems*, pages 1–1, 2019.
- [30] T. Coletta, R. Delabays, I. Adagideli, and P. Jacquod. Topologically protected loop flows in high voltage AC power grids. *New J. Phys.*, 18(10):103042, 2016. ISSN 1367-2630.
- [31] T. Coletta, B. Bamieh, and P. Jacquod. Transient performance of electric power networks under colored noise. In *2018 IEEE Conference on Decision and Control (CDC)*, pages 6163–6167. IEEE, 2018.
- [32] G. Deffuant, D. Neau, F. Amblard, and G. Weisbuch. Mixing beliefs among interacting agents. *Advances in Complex Systems*, 3(01n04):87–98, 2000.
- [33] R. Delabays, T. Coletta, and P. Jacquod. Multistability of phase-locking and topological winding numbers in locally coupled Kuramoto models on single-loop networks. *J. Math. Phys.*, 57(3):032701, 2016.
- [34] R. Delabays, T. Coletta, and P. Jacquod. Multistability of phase-locking in equal-frequency kuramoto models on planar graphs. *J. Math. Phys.*, 58(3):032703, 2017.
- [35] R. Delabays, M. Tyloo, and P. Jacquod. The size of the sync basin revisited. *Chaos*, 27(10):103109, 2017.
- [36] R. Delabays, P. Jacquod, and F. Dörfler. The kuramoto model on oriented and signed graphs. *SIAM Journal on Applied Dynamical Systems*, 18(1):458–480, 2019.
- [37] R. Delabays, M. Tyloo, and P. Jacquod. Rate of change of frequency under line contingencies in high voltage electric power networks with uncertainties. *Chaos*, 29(10):103130, 2019.
- [38] L. DeVille. Transitions amongst synchronous solutions in the stochastic kuramoto model. *Nonlinearity*, 25(5):1473–1494, 2012. ISSN 0951-7715, 1361-6544.
- [39] F. Dörfler and F. Bullo. On the critical coupling strength for kuramoto oscillators. *Proc. of the 2011 IEEE ACC*, 2011.
- [40] F. Dörfler, M. Chertkov, and F. Bullo. Synchronization in complex oscillator networks and smart grids. *Proc. Natl. Acad. Sci.*, 110(6):2005–2010, 2013.
- [41] M. I. Dykman. Large fluctuations and fluctuational transitions in systems driven by colored gaussian noise: A high-frequency noise. *Phys. Rev. A*, 42:2020–2029, Aug 1990.
- [42] G. B. Ermentrout. The behavior of rings of coupled oscillators. *J. Math. Biol.*, 22(1): 55–74, 1985.
- [43] G. B. Ermentrout. An adaptive model for synchrony in the firefly *Pteroptyx malaccae*. *J. Math. Biol.*, 29(6):571–585, 1991.

## Bibliography

---

- [44] E. Estrada and N. Hatano. Communicability in complex networks. *Phys. Rev. E*, 77(3): 036111, 2008.
- [45] E. Estrada, M. Fox, D. J. Higham, and G.-L. Oppo. *Network science: complexity in nature and technology*. Springer Science & Business Media, 2010.
- [46] M. Fiedler. Algebraic connectivity of graphs. *Czechoslovak Mathematical Journal*, 23(2): 298–305, 1973.
- [47] S. Fliscounakis, P. Panciatici, F. Capitanescu, and L. Wehenkel. Contingency ranking with respect to overloads in very large power systems taking into account uncertainty, preventive, and corrective actions. *IEEE Transactions on Power Systems*, 28(4):4909–4917, 2013.
- [48] R. F. Fox, I. R. Gatland, R. Roy, and G. Vemuri. Fast, accurate algorithm for numerical simulation of exponentially correlated colored noise. *Phys. Rev. A*, 38:5938–5940, Dec 1988.
- [49] L. V. Gambuzza, A. Buscarino, L. Fortuna, M. Porfiri, and M. Frasca. Analysis of dynamical robustness to noise in power grids. *IEEE Journal on Emerging and Selected topics in Circuits and Systems*, 7(3):413–421, 2017.
- [50] A. Ganesh, L. Massoulié, and D. Towsley. The effect of network topology on the spread of epidemics. In *Proceedings IEEE 24th Annual Joint Conference of the IEEE Computer and Communications Societies.*, volume 2, pages 1455–1466. IEEE, 2005.
- [51] T. Giamarchi. *Quantum Physics in One Dimension*. Oxford University Press, 2004. ISBN 9780198525004.
- [52] M. Girvan and M. E. Newman. Community structure in social and biological networks. *Proc. Natl. Acad. Sci.*, 99(12):7821–7826, 2002.
- [53] C. E. Gough, M. S. Colclough, E. M. Forgan, R. G. Jordan, M. Keene, C. M. Muirhead, A. I. M. Rae, N. Thomas, J. S. Abell, and S. Sutton. Flux quantization in a high- $t_c$  superconductor. *Nature*, 326:855, 1987.
- [54] T. W. Grunberg and D. F. Gayme. Performance measures for linear oscillator networks over arbitrary graphs. *IEEE Transactions on Control of Network Systems*, 5(1):456–468, March 2018. ISSN 2325-5870.
- [55] L. Guo, C. Zhao, and S. H. Low. Graph laplacian spectrum and primary frequency regulation. *IEEE Conference on Decision and Control*, pages 158–165, 2018.
- [56] I. Gutman and B. Mohar. The quasi-wiener and the kirchhoff indices coincide. *Journal of Chemical Information and Computer Sciences*, 36(5):982–985, 1996.
- [57] H. Haehne, K. Schmietendorf, S. Tamrakar, J. Peinke, and S. Kettemann. Propagation of wind-power-induced fluctuations in power grids. *Phys. Rev. E*, 99(5):050301, 2019.

- 
- [58] H. Haken. Some aspects of synergetics. In H. Haken, editor, *Synergetics*, pages 2–17, Berlin, Heidelberg, 1977. Springer Berlin Heidelberg. ISBN 978-3-642-66784-8.
- [59] K. N. Hasan, R. Preece, and J. V. Milanović. Priority ranking of critical uncertainties affecting small-disturbance stability using sensitivity analysis techniques. *IEEE Transactions on Power Systems*, 32(4):2629–2639, 2017.
- [60] J. Hindes and I. B. Schwartz. Epidemic extinction and control in heterogeneous networks. *Phys. Rev. Lett.*, 117:028302, 2016.
- [61] J. Hindes and I. B. Schwartz. Rare slips in fluctuating synchronized oscillator networks. *Chaos*, 28(7):071106, 2018.
- [62] J. Hindes, P. Jacquod, and I. B. Schwartz. Network desynchronization by non-gaussian fluctuations. *arXiv:1904.12174*, 2019.
- [63] P. Hines, E. Cotilla-Sanchez, and S. Blumsack. Do topological models provide good information about electricity infrastructure vulnerability? *Chaos*, 20:033122, 2010.
- [64] E. Il'ichev and A. N. Omelyanchouk. Magnetic flux noise in the three-josephson-junction superconducting ring. *Low Temp. Phys.*, 34:413, 2008.
- [65] R. A. Ims and H. P. Andreassen. Spatial synchronization of vole population dynamics by predatory birds. *Nature*, 408(6809):194, 2000.
- [66] A. Jadbabaie, J. Lin, and A. S. Morse. Coordination of groups of mobile autonomous agents using nearest neighbor rules. *Departmental Papers (ESE)*, page 29, 2003.
- [67] A. Jadbabaie, N. Motee, and M. Barahona. On the stability of the kuramoto model of coupled nonlinear oscillators. *American Control Conference*, pages 4296–4301, 2004.
- [68] N. Janssens and A. Kamagate. Loop flows in a ring AC power system. *Int. J. Elect. Power Energy Syst.*, 25(8):591 – 597, 2003.
- [69] S. Kettemann. Delocalization of disturbances and the stability of ac electricity grids. *Phys. Rev. E*, 94:062311, Dec 2016.
- [70] M. Kitsak, L. K. Gallos, S. Havlin, F. Liljeros, L. Muchnik, H. E. Stanley, and H. A. Makse. Identification of influential spreaders in complex networks. *Nat. Phys.*, 6(11):888, 2010.
- [71] D. J. Klein and M. Randić. Resistance distance. *J. Math. Chem.*, 12(1):81–95, 1993.
- [72] M. Korkali, J. G. Veneman, B. F. Tivnan, J. P. Bagrow, and P. D. Hines. Reducing cascading failure risk by increasing infrastructure network interdependence. *Scientific reports*, 7: 44499, 2017.
- [73] A. J. Korsak. On the question of uniqueness of stable load-flow solutions. *IEEE Trans. Power App. Syst.*, PAS-91(3):1093–1100, 1972.

## Bibliography

---

- [74] D. Kramer. Models poised to boost grid efficiency. *Physics today*, 69(9):25, 2016.
- [75] H. Kramers. Brownian motion in a field of force and the diffusion model of chemical reactions. *Physica*, 7(4):284 – 304, 1940. ISSN 0031-8914.
- [76] P. Kundur, N. J. Balu, and M. G. Lauby. *Power system stability and control*, volume 7. McGraw-hill New York, 1994.
- [77] Y. Kuramoto. Self-entrainment of a population of coupled non-linear oscillators. In H. Araki, editor, *Lecture Notes in Physics 39, International Symposium on Mathematical Problems in Theoretical Physics*, Berlin, 1975. Springer. ISBN 978-3-540-37509-8.
- [78] Y. Kuramoto. *Chemical Oscillations, Waves and Turbulence*, volume 19 of *Springer Series in Synergetics*. Springer Berlin Heidelberg, 1984. ISBN 978-3-642-69691-6.
- [79] D. Lee, L. Aolaritei, T. L. Vu, and K. Turitsyn. Robustness against disturbances in power systems under frequency constraints. *arXiv:1803.00817*, 2018.
- [80] Y. Liu, R. Cai, and J. Duan. Lévy noise induced escape in the morris–lecar model. *Physica A: Statistical Mechanics and its Applications*, 531:121785, 2019. ISSN 0378-4371.
- [81] N. A. Lynch. *Distributed Algorithms*, Morgan Kaufmann Publishers, volume 1. 1996.
- [82] J. Machowski, J. W. Bialek, and J. R. Bumby. *Power System Dynamics*. Wiley, Chichester, U.K, 2nd edition, 2008. ISBN 978-0-470-72558-0.
- [83] J. Machowski, J. Bialek, and J. Bumby. *Power system dynamics: stability and control*. John Wiley & Sons, 2011.
- [84] D. Manik, M. Rohden, H. Ronellenfitsch, X. Zhang, S. Hallerberg, D. Witthaut, and M. Timme. Network susceptibilities: Theory and applications. *Phys. Rev. E*, 95:012319, Jan 2017.
- [85] D. Manik, M. Timme, and D. Witthaut. Cycle flows and multistability in oscillatory networks. *Chaos*, 27(8):083123, 2017.
- [86] P. J. Menck, J. Heitzig, N. Marwan, and J. Kurths. How basin stability complements the linear-stability paradigm. *Nat. Phys.*, 9:89, 2013.
- [87] P. J. Menck, J. Heitzig, J. Kurths, and H. J. Schellnhuber. How dead ends undermine power grid stability. *Nat. Commun.*, 5:3969, 2014.
- [88] J. M. Montoya, S. L. Pimm, and R. V. Solé. Ecological networks and their fragility. *Nature*, 442(7100):259, 2006.
- [89] A. E. Motter, C. Zhou, and J. Kurths. Network synchronization, diffusion, and the paradox of heterogeneity. *Phys. Rev. E*, 71:016116, Jan 2005.

- 
- [90] N. O’Clery, Y. Yuan, G.-B. Stan, and M. Barahona. Observability and coarse graining of consensus dynamics through the external equitable partition. *Phys. Rev. E*, 88:042805, Oct 2013.
- [91] U. of Washington Electrical Engineering. Power systems test case archive available online at [www2.ee.washington.edu/research/pstca](http://www2.ee.washington.edu/research/pstca). *IEEE Trans. Cybern.*, 1993.
- [92] E. Ott. *Chaos in Dynamical Systems*. Cambridge University Press, 2 edition, 2002.
- [93] F. Paganini and E. Mallada. Global performance metrics for synchronization of heterogeneously rated power systems: The role of machine models and inertia. *55th Annual Allerton Conference on Communication, Control, and Computing*, pages 324–331, 2017.
- [94] L. Pagnier and P. Jacquod. Inertia location and slow network modes determine disturbance propagation in large-scale power grids. *PLoS ONE*, 14(3):1–17, 03 2019.
- [95] R. Pastor-Satorras and A. Vespignani. Epidemic spreading in scale-free networks. *Phys. Rev. Lett.*, 86(14):3200, 2001.
- [96] S. Patterson and B. Bamieh. Leader selection for optimal network coherence. *Proc. of the 49<sup>th</sup> IEEE CDC*, 2010.
- [97] S. Patterson and B. Bamieh. Interaction-driven opinion dynamics in online social networks. In *Proceedings of the First Workshop on Social Media Analytics*, pages 98–105. ACM, 2010.
- [98] S. D. Pauls and D. Remondini. Measures of centrality based on the spectrum of the laplacian. *Phys. Rev. E*, 85:066127, Jun 2012.
- [99] L. M. Pecora and T. L. Carroll. Master stability functions for synchronized coupled systems. *Phys. Rev. Lett.*, 80(10):2109, 1998.
- [100] A. Pikovsky, M. Rosenblum, and J. Kurths. *Synchronization: a universal concept in nonlinear sciences*. Cambridge university press, 2003.
- [101] D. Piovani, J. Grujić, and H. J. Jensen. Linear stability theory as an early warning sign for transitions in high dimensional complex systems. *Journal of Physics A: Mathematical and Theoretical*, 49(29):295102, jun 2016.
- [102] B. K. Poolla, S. Bolognani, and F. Dörfler. Optimal Placement of Virtual Inertia in Power Grids. *IEEE Transaction Automatic Control*, 62(12):6209–6220, 2017.
- [103] W. Ren, K. L. Moore, and Y. Chen. High-order and model reference consensus algorithms in cooperative control of multivehicle systems. *Journal of Dynamic Systems, Measurement, and Control*, 129(5):678–688, 2007.
- [104] F. A. Rodrigues, T. K. D. Peron, P. Ji, and J. Kurths. The kuramoto model in complex networks. *Physics Reports*, 610:1 – 98, 2016. ISSN 0370-1573.

## Bibliography

---

- [105] E. Rosa Jr, E. Ott, and M. H. Hess. Transition to phase synchronization of chaos. *Phys. Rev. Lett.*, 80(8):1642, 1998.
- [106] J. L. Sanchez Torres. *Vulnérabilité, interdépendance et analyse des risques des postes sources et des modes d'exploitation décentralisés des réseaux électriques*. PhD thesis, Grenoble, 2013.
- [107] B. Schäfer, M. Matthiae, X. Zhang, M. Rohden, M. Timme, and D. Witthaut. Escape routes, weak links, and desynchronization in fluctuation-driven networks. *Phys. Rev. E*, 95:060203(R), Jun 2017.
- [108] P. Schultz, F. Hellmann, K. N. Webster, and J. Kurths. Bounding the first exit from the basin: Independence times and finite-time basin stability. *Chaos*, 28(4):043102, 2018.
- [109] M. Siami and N. Motee. Systemic measures for performance and robustness of large-scale interconnected dynamical networks. In *53rd IEEE Conference on Decision and Control*, pages 5119–5124. IEEE, 2014.
- [110] M. Siami and N. Motee. Fundamental limits and tradeoffs on disturbance propagation in linear dynamical networks. *IEEE Transactions on Automatic Control*, 61(12):4055–4062, Dec 2016. ISSN 0018-9286.
- [111] P. S. Skardal, D. Taylor, and J. Sun. Optimal synchronization of complex networks. *Phys. Rev. Lett.*, 113(14):144101, 2014.
- [112] R. V. Sole and M. Montoya. Complexity and fragility in ecological networks. *Proceedings of the Royal Society of London. Series B: Biological Sciences*, 268(1480):2039–2045, 2001.
- [113] S. Soltan, D. Mazauric, and G. Zussman. Analysis of failures in power grids. *IEEE Transactions on Control of Network Systems*, 4(2):288–300, June 2017. ISSN 2325-5870.
- [114] D. A. Spielman and S.-H. Teng. Spectral partitioning works: Planar graphs and finite element meshes. In *Proceedings of 37th Conference on Foundations of Computer Science*, pages 96–105. IEEE, 1996.
- [115] T. Stankovski, T. Pereira, P. V. E. McClintock, and A. Stefanovska. Coupling functions: Universal insights into dynamical interaction mechanisms. *Rev. Mod. Phys.*, 89:045001, Nov 2017.
- [116] K. Stephenson and M. Zelen. Rethinking centrality: Methods and examples. *Social networks*, 11(1):1–37, 1989.
- [117] S. H. Strogatz. *Sync: The Emerging Science of Spontaneous Order*. Penguin Press Science Series. Penguin Adult, 2004. ISBN 0786887214.
- [118] S. Tamrakar, M. Conrath, and S. Kettemann. Propagation of disturbances in ac electricity grids. *Scientific reports*, 8(1):6459, 2018.

- 
- [119] E. Tegling, B. Bamieh, and D. F. Gayme. The price of synchrony: Evaluating the resistive losses in synchronizing power networks. *IEEE Transactions on Control of Network Systems*, 2(3):254–266, 2015.
- [120] M. Tyloo and P. Jacquod. Global robustness versus local vulnerabilities in complex synchronous networks. *Phys. Rev. E*, 100(3):032303, 2019.
- [121] M. Tyloo, T. Coletta, and P. Jacquod. Robustness of Synchrony in Complex Networks and Generalized Kirchhoff Indices. *Phys. Rev. Lett.*, 120(8):084101, 2018.
- [122] M. Tyloo, R. Delabays, and P. Jacquod. Noise-induced desynchronization and stochastic escape from equilibrium in complex networks. *Phys. Rev. E*, 99(6):062213, Jun 2019.
- [123] M. Tyloo, L. Pagnier, and P. Jacquod. The key player problem in complex oscillator networks and electric power grids: Resistance centralities identify local vulnerabilities. *Science Advances*, 5(11):eaaw8359, 2019.
- [124] N. G. van Kampen. Stochastic differential equations. *Phys. Rep.*, 24(3):171, 1976.
- [125] A. Voros. *Advanced Studies in Pure Mathematics Vol. 21*. edited by N. Kurokawa and T. Sunada (Kinokuniya, Tokyo, 1992), pp. 327–358., 1992.
- [126] D. J. Watts and S. H. Strogatz. Collective dynamics of "small-world" networks. *Nature*, 393(6684):440–442, 1998.
- [127] K. Wiesenfeld, P. Colet, and S. H. Strogatz. Frequency locking in Josephson arrays: Connection with the Kuramoto model. *Phys. Rev. E*, 57(2):1563–1569, 1998.
- [128] D. A. Wiley, S. H. Strogatz, and M. Girvan. The size of the sync basin. *Chaos*, 16(1):015103, 2006.
- [129] J. Wolter, B. Lünsmann, X. Zhang, M. Schröder, and M. Timme. Quantifying transient spreading dynamics on networks. *Chaos*, 28(6):063122, 2018.
- [130] W. Xiao and I. Gutman. Resistance distance and laplacian spectrum. *Theoretical Chemistry Accounts*, 110(4):284–289, Nov 2003. ISSN 1432-2234.
- [131] X. Zhang, S. Hallerberg, M. Matthiae, D. Witthaut, and M. Timme. unpublished.
- [132] C. Zhou, A. E. Motter, and J. Kurths. Universality in the synchronization of weighted random networks. *Phys. Rev. Lett.*, 96:034101, Jan 2006.
- [133] H.-Y. Zhu, D. J. Klein, and I. Lukovits. Extensions of the wiener number. *Journal of Chemical Information and Computer Sciences*, 36(3):420–428, 1996.
- [134] R. D. Zimmerman, C. E. Murillo-Sánchez, and R. J. Thomas. Matpower: Steady-state operations, planning, and analysis tools for power systems research and education. *IEEE Transactions on power systems*, 26(1):12–19, 2010.



# Melvyn Tyloo

## Education

- Oct. 2016– **PhD student in Physics at EDPY**, *Swiss Federal Institute of Technology in Lausanne - EPFL*.  
Studying synchrony in dynamical systems under the supervision of Prof. Ph. Jacquod.
- 2014–2016 **Master of Science in Physics**, *Swiss Federal Institute of Technology in Lausanne - EPFL*.  
Specialisation in theoretical physics (RQFT, Relativity and Cosmology, Statistical, Solid-state physics, Doctoral quantum class, Information Theory). Completed 96/90 ETCS.  
Master thesis at the Chair of Condensed Matter Theory at EPFL supervised by Prof. F. Mila : Quantum Monte Carlo simulation of  $SU(N)$  antiferromagnetic Heisenberg chain in the fully symmetric/antisymmetric representations (including the full implementation).
- 2011–2014 **Bachelor of Science in Physics**, *Swiss Federal Institute of Technology in Lausanne - EPFL*.  
Emphasis on theoretical courses (Statistical, Solid-state, Quantum, Computational, Plasma physics).
- 2008–2011 **Swiss Maturity**, *Gymnase de Morges, Marcellin*.  
Advanced Mathematics, Physics and Applied Mathematics.

## Conference Contributions, Invited Talks, Group Visits

### 2019

- Oct. 17 Institute of Physics, Humboldt University, Berlin. Group seminar.
- Sep. 6-11 Statistical Physics and Nonlinear Dynamics & Stochastic Processes Group, Humboldt University, Berlin. Visiting researcher.
- Sep. 2-6 Dynamics Days Europe 2019, Rostock, Germany. Talk in the Power Grid minisymposium.
- Aug. 26-27 Johns Hopkins University, Baltimore, MD, USA. Visiting researcher and group seminar.
- Jul.-Aug. Los Alamos National Laboratory (LANL), Theory Division T-5, Los Alamos, NM, USA. Invited researcher.
- Feb. 3-8 Future Electric Power Systems and the Energy Transition, 2nd International conference in Champéry, Switzerland. Talk.
- Jan. 14 National Renewable Energy Laboratory (NREL), Golden CO, USA. Brown Bag Talk.
- Jan. 7-11 2019 Grid Science Winter School & Conference, Santa Fe NM, USA. Poster.

### 2018

- Oct. 15-19 International School on Informatics and Dynamics in Complex Networks, University of Catania, Italy. Talk. **Winner of the Best Presentation Award**.
- Sep. 3-7 Dynamics Days Europe 2018, Loughborough, England.
- Jan. 29-31 661. WE-Heraeus-Seminar: Nonlinear Dynamics, Optimization and Control of Distributed Energy Systems, Physikzentrum Bad Honnef, Germany. Poster.

### 2017

- Feb. 5-9 Future Electric Power Systems and the Energy Transition, International conference in Champéry, Switzerland. Poster.

---

## Publications and Preprints

### Submitted

Oct. 2019 F. Baumann, I. M. Sokolov, **M. Tyloo**, *The Role of Active Leaders in Opinion Formation on Social Networks*, arXiv:1910.01897 (2019).

### Published

Nov. 2019 **M. Tyloo**, L. Pagnier, P. Jacquod, *The Key Player Problem in Complex Oscillator Networks and Electric Power Grids: Resistance Centralities Identify Local Vulnerabilities*, *Science Advances* **5** (11), eaaw8359 (2019).

Jun. 2019 R. Delabays, **M. Tyloo**, P. Jacquod, *Rate of change of frequency under line contingencies in high voltage electric power networks with uncertainties*, *Chaos* **29**, 103130 (2019).

Sep. 2019 **M. Tyloo**, P. Jacquod, *Global Robustness vs. Local Vulnerabilities in Complex Synchronous Networks*, *Phys. Rev. E* **100**, 032303 (2019).

Jun. 2019 **M. Tyloo**, R. Delabays, P. Jacquod, *Noise-Induced Desynchronization and Stochastic Escape from Equilibrium in Complex Networks*, *Phys. Rev. E* **99**, 062213 (2019).

Feb. 2018 **M. Tyloo**, T. Coletta, P. Jacquod, *Robustness of Synchrony in Complex Networks and Generalized Kirchhoff Indices*, *Phys. Rev. Lett.* **120**, 084101 (2018).

Oct. 2017 R. Delabays, **M. Tyloo**, P. Jacquod, *The Size of the Sync Basin Revisited*, *Chaos* **27**, 103109 (2017).

---

## Research Interests

Coupled dynamical systems, complex networks, coupled oscillators, network inference, opinion dynamics.

---

## Doctoral Courses

Nov.–Dec. 2016 *Low dimensional interacting systems*, Professor A. Tselik (CUSO), 1 ECTS, written exam.

Sep.–Dec. 2016 *Introduction to Frustrated Magnetism*, Professor F. Mila (EPFL), 2 ECTS, oral exam.

Jun. 2017 *Interfaces in disordered media : the standard model and beyond*, Professor A. Rosso (EPFL), 1 ECTS, oral exam.

---

## Professional Experience

**Tutoring** 3 years of physics, maths, chemistry, probability and programming courses given to bachelor, master and doctoral students at EPFL and UNIL.

**Substitute lecturer** At the HES-SO Valais/Wallis for the course of general physics.

---

## Languages

**French** Mother tongue

**English** Advanced level, C1 (European standard tested at EPFL)

**German** Upper intermediate, B1